

國立臺灣大學材料科學與工程學系暨研究所

碩士論文

Department of Material Science and Engineering

College of Engineering

National Taiwan University

Master Thesis

壓電超音波元件聲阻匹配層之材料設計與性能分析

Design and characterization of acoustic matching layers for
piezoelectric ultrasonic transducers



指導教授：謝宗霖 博士

Advisor: Tzong-Lin Jay Shieh, Ph.D.

中華民國 96 年 7 月

July, 2007



國立臺灣大學碩士學位論文

口試委員會審定書

論文中文題目：壓電超音波元件聲阻匹配層之材料設計與
性能分析

論文英文題目：Design and characterization of acoustic
matching layers for piezoelectric ultrasonic
transducers

本論文係柯忠廷君(R94527002)在國立臺灣大學材料
科學與工程學系、所完成之碩士學位論文，於民國 96 年 07
月 16 日承下列考試委員審查通過及口試及格，特此證明

口試委員：

謝宗霖

謝宗霖

(指導教授)

陳俊杉

陳俊杉

陳文翔

陳文翔

系主任、所長

廖文彬

廖文彬

(簽名)



致謝

在台大已經是第六年了，時光匆匆飛逝而過。尤其是碩士這兩年，雖然快的不可思議，卻也過的扎扎实實的，似忽塞滿了兩年裡的每一刻時間。學了很多東西，實驗上的或是踏入社會前的知識，都讓人感覺這些日子總算沒有浪費。

首先，要感謝我的指導教授 謝宗霖 教授，提供我們一個很好的學習環境，循循善誘並且細心指導我們，經過這兩年的磨練，對「實驗」二字的體會又更上一層樓。還有 HIFU Group 的教授們，同時也是我的碩士口試教授，陳俊杉教授與陳文翔醫生，在實驗與論文上的指導與協助，讓我的實驗更順利也更嚴謹，同時也學習到更多 HIFU 的知識。已畢業的學長姊，國璋、弘翔學長和月華學姊，碩一的時候，實驗上或是心情上，都是給你們照顧的。實驗室的俊名學長、阿樺、貞好、名揚、叔叔、郁華、還有俊賢，隔壁實驗室的養樂多、駝駝、孟凱，跟你們一起學習，感覺很開心，讓所有的壓力得以紓解。

然後，就是我的大學好友了。百勵、小顏、莊少、棒棒、土碩、澎澎、建州、還有家嘉，很高興大學畢業後，還可以跟大家多相處兩年，相信這兩年來大家應該都學到很多，希望未來有機會還可以一起讀書工作。

最後，我要謝謝我的父母、蕙吟表姊、憲信、棋能表哥和妹妹，在這兩年來對我的支持與陪伴。





摘要

在高能聚焦超音波的領域，鋯鈦酸鉛被應用成為一種新穎的聲阻匹配層。此層鋯鈦酸鉛匹配層可將原本超音波探頭之寬頻率分佈過濾成某些特定頻率之峰值，且沒有降低該頻率峰值相對於原始探頭強度之強度。這個現象可歸納為鋯鈦酸鉛之壓電性質與機械性質，並且，在本論文裡設計一系列之實驗，藉由改變鋯鈦酸鉛匹配層之壓電性質，例如有無極化與表面電荷特性，來更深一步探討鋯鈦酸鉛匹配層之性質。

傳統之聲阻匹配層，例如陶瓷高分子複合材料，也在本篇論文裡探討。利用三種不同的陶瓷粉末混合環氧樹脂形成聲阻匹配層，並且探討三種陶瓷高分子複合材料之超音波匹配性質。在這三種陶瓷高分子複合材料內，氧化鋯粉末混合環氧樹脂之複合材料的超音波能量衰減係數與聲阻匹配值為最適當之選擇數值。因此，將氧化鋯環氧樹脂之複合材料應用於一個實驗室自製的高能聚焦超音波探頭上，藉由實驗去探討其聲阻匹配效果。此實驗藉由水診器量測並分析探頭之聲波強度分佈，且藉由豬肉之活體實驗印證此聲阻匹配層之效能。

最後，在本論文裡還探討孔洞陶瓷材料與孔洞陶瓷填充環氧樹脂之複合材料的性質，利用其低超音波能量衰減係數與可調式聲波聲阻值，是一個有潛力應用於匹配超音波探頭與水或是人體血管之材料。

關鍵字：聲阻匹配層、濾波、高能聚焦超音波、複合材料、孔洞陶瓷



Abstract

A novel active matching layer made of lead zirconate titanate (PZT) plate has been developed as an “impedance matching layer” for high-intensity focused ultrasound (HIFU) applications. The PZT matching layer redistributes the frequency spectrum of an original broadband ultrasonic probe, and acts as a frequency filter without reducing the wave amplitude. These behaviors are contributed to electromechanical and mechanical properties at the PZT matching layer, and are investigated in this study by a series of experiments on PZT matching plates with different electromechanical properties and polarization and surface charge conditions.

Traditional passive matching layers, such as ceramic-polymer composites, are also studied. Three different ceramic-epoxy composite are developed and their impedance properties studied. Among the three, the zirconium oxide-epoxy composite exhibits a tolerable attenuation level and an optimum impedance value. It is then integrated on to a home-made HIFU transducer to test its effectiveness. The beam profile of the matched HIFU transducer is characterized by a hydrophone, and an in-vivo experiment is carried out to gauge its performance.

In this study, structure materials such as porous ceramics and porous ceramic-epoxy composites are also proposed as candidate materials for impedance matching for water and human tissues due to their low attenuations and impedances.

Key words : matching layer, filter, HIFU, composite, porous ceramic



Content

摘要	I
Abstract	III
Content	V
List of Figures	VII
List of Tables	IX
1. Introduction	1
2. Literature Review	4
2.1 Ferroelectric Materials	4
2.1.1 Fundamental Theories	5
2.1.2 Piezoelectricity	11
2.1.3 Resonant Method Characterization	12
2.2 Acoustical Matching Theory	17
2.2.1 Impedance Matching	18
2.2.2 Thickness Matching	20
2.3 Acoustical Matching Materials	23
2.3.1 Polymers	23
2.3.2 Ceramics	24
2.3.3 Ceramic-Polymer Composites	25
2.3.4 Metal-Polymer Composites	26
2.4 High-Intensity Focused Ultrasound	26
2.4.1 HIFU Applications	27
2.4.2 Development	28
3. Experiment Procedure	30
3.1 Manufacture of Ceramic-Epoxy Composites	30
3.2 Manufacture of Aluminum Oxide Matching Layers	31
3.3 Preparation of PZT Matching Layers	32
3.4 Measurement of Wave Velocity	33
3.5 Measurement of Frequency Distribution	33
3.6 Characterization by Scanning Electron Microscopy	34
4. Results and Discussion	38
4.1 Epoxy-Ceramic Composite System	38
4.2 Active PZT Matching Layers	39
4.2.1 Electroded Poled PZT (G)	39
4.2.2 Short-Circuited Poled PZT (EC)	53
4.2.3 Unpoled PZT (U)	53
4.2.4 Unpoled PZT without Electrodes (UN)	74
4.2.5 Electroded Poled PZT with Second Composite Matching Layer (GML)	

.....	74
4.2.6 Short-Circuited Poled PZT with Second Composite Matching Layer (ECML)	76
4.2.7 Conclusion	76
4.3 Structured Materials	96
4.3.1 Structured Porous Aluminum Oxides.....	96
4.3.2 Epoxy-Loaded Structured Porous Aluminum Oxides.....	97
4.4 Experimental Errors	98
5. Design of HIFU Transducer.....	102
5.1 Manufacture of a Home-Made HIFU Transducer	103
5.2 Characterization of HIFU Transducer Beam Profiles.....	103
5.3 Characterization with In-vivo Experiment.....	104
5.4 Beam Profiles of HIFU Transducer	104
5.5 In-vivo Experiment on HIFU Transducer	105
6. Conclusion	112
6.1 Future Research.....	114
Reference	115



List of Figures

Figure 2.1 Classification of 32 point groups.....	8
Figure 2.2 The direction of polarization switched by an applied electrical field.	9
Figure 2.3 The unit cell of BaTiO ₃	9
Figure 2.4 Composition-dependent crystal transition of PZT	10
Figure 2.5 Switching systems of tetragonal and rhombohedral ferroelectric crystals	10
Figure 2.6 (a) Polarization hysteresis curve of a ferroelectric material	14
Figure 2.6 (b) Strain hysteresis curve of a ferroelectric material.....	15
Figure 2.7 Constitutive relationships of the thermal, electric and mechanic properties.....	15
Figure 2.8 The resonant and anti-resonant frequencies of a BaTiO ₃ with thickness of 1.06 cm and diameter of 18.8 mm.....	16
Figure 2.9 Amplitude summations of the waves reverberated in matching layer and then transmitted to water.....	22
Figure 2.10 Waves traveling within matching layer have a 180° phase shift at PZT-matching layer interface, and leave a quarter-wavelength matching layer with the same phase and interfere constructively.	22
Figure 2.11 Schematics of Bowl-type HIFU transducers demonstration	29
Figure 3.1 Processing of ceramic-epoxy composite.....	36
Figure 3.2 Processing of porous Al ₂ O ₃ matching layer.....	36
Figure 3.3 Schematic of the wave velocity measurement system.....	37
Figure 3.4 Schematic of the frequency distribution measurement system.....	37
Figure 4.1 Wave reflections in epoxy and ceramic-epoxy composites.	45
Figure 4.2 Original frequency distributions of 1, 5 and 10 MHz transducers	46
Figure 4.3 Electroded poled PZT plates characterized by 10 MHz transducer.....	47
Figure 4.4 Electroded poled PZT plates characterized by 5 MHz transducer	47
Figure 4.5 Frequency distributions of the 10 MHz transducer based on the piezoelectric resonant frequencies of the matching PZT plates.	49
Figure 4.6 Frequency distributions of the 10 MHz transducer based on the piezoelectric resonant frequencies of the matching PZT plates.	51
Figure 4.7 Electroded-poled PZT plates characterized by 1 MHz transducer	52
Figure 4.11 Effect of elimination of induced inverse electric field by poled PZT with electrodes connected.....	64
Figure 4.12 Reflected wave forms inside 1 MHz unpoled PZT	64
Figure 4.16 (a) NF and frequency distribution of 2 MHz unpoled PZT on 1 MHz probe	72

Figure 4.16 (b) NF and frequency distribution of 3 MHz unpoled PZT on 1 MHz probe.....	72
Figure 4.16 (c) NF and frequency distribution of 5 MHz unpoled PZT on 1 MHz probe.....	73
Figure 4.23 Micro-bubbles resided inside Zirconium dioxide-epoxy matching layer	90
Figure 4.24 Shift of resonant frequency by integration of matching layer	91
Figure 4.28 SEM pictures of porous aluminum oxides	101
Figure 4.29 Frequency distribution of composites of porous aluminum oxides loaded with epoxy as 2 MHz unpoled PZT	101
Figure 5.1 The home-made HIFU transducer.....	106
Figure 5.2 Impedance spectrum of the home-made HIFU transducer	106
Figure 5.3 Manufacture of acoustic matching layer for the home-made HIFU transducer	107
Figure 5.4 Schematic of the beam profile measurement system for the home-made HIFU transducer	107
Figure 5.5 In-vivo experiment for the home-made HIFU transducer	108
Figure 5.6 (a) Axial and lateral beam profiles of the home-made HIFU transducer	109
Figure 5.6 (b) Determination	110
Figure 5.7 In-vivo experiment setup.....	111
Figure 5.8 The lesion inside the pork bulk.....	111

List of Tables

Table 3.1 The Al ₂ O ₃ green compacts composition of Al ₂ O ₃ powder and PVC powder (pore forming agent).	35
Table 3.2 Types of PZT plates.	35
Table 4.1 Parameters of ceramic-epoxy composites.....	42
Table 4.2 Symbols for six types of PZT matching layers	43
Table 4.3 (a) Natural frequency modes for PZT circular plates with E = 53 GPa..	57
Table 4.3 (b) Natural frequency modes for PZT circular plates with E = 61 GPa..	57
Table 4.4 Parameters of the structured porous aluminum oxides.....	99
Table 4.5 Parameters of the epoxy-loaded structured aluminum oxides.	99





1. Introduction

High intensity-focused ultrasound (HIFU) is a novel technology for noninvasive surgery and is designed to treat tumors. Some clinical experiments for prostate cancer, which is a common disease in older men, have been proceeded in the past few years. However, there are still many questions and challenges concerning the medical science, ultrasound theory and engineering technology for HIFU instruments. From the view point of materials science, the most important component of a HIFU transducer is the piezoelectric ceramic material. The acoustic impedance of piezoelectric ceramics is relatively high in comparison to the impedance of human tissues and water, which are about 1.5 MRayl. This large impedance mismatch makes the transmitted ultrasonic waves dissipated most of their energies at the device-human interface, reducing the overall output efficiency of a medical HIFU transducer.

Materials with optimum impedance values for acoustic impedance matching purposed have been developed for ultrasonic imaging applications. Medical ultrasonic imaging is applied to diagnose human body by the reflections of waves interfered with the organs and blood vessels. Many materials, such as ceramic-polymer composites, metal-polymer composites and polymers, are good matching candidates to reduce the impedance mismatch between the ultrasonic device and human body and are applied to commercial products. However, the required output power for ultrasonic imaging is

much lower than the requirement for HIFU.

The purpose of this study is to find a suitable matching material to integrate on to the HIFU device. The matching potentials of materials, such as ceramic-polymer composites and porous ceramics, are investigated. Furthermore, a new active matching method involving lead zirconate titanate (PZT) is proposed and examined both experimentally and theoretically.

In Chapter 2, ferroelectricity and acoustic matching theories are introduced, and conventional materials for matching layer application are listed. A brief introduction to the technology and development of HIFU is also given.

In Chapter 3, the preparation and manufacture of composite-based and porous matching layers are described. The establishments of measuring apparatus for beam profiles and frequency distributions are also presented.

In Chapter 4, the electromechanical properties and operating principles of PZT-based active matching layers are determined and explained. The impedance and attenuation properties of three different ceramic-epoxy composites, porous ceramics and porous ceramics-epoxy composite are compared. The feasibility and efficiency of the developed active and passive matching materials are discussed.

In Chapter 5, the aspects of in-vivo experiment for HIFU transducers are presented. The beam profile and transmitted efficiency of a home-made HIFU transducer are

discussed based on the measurements is generated from an in-vivo experiment. The home-made HIFU transducer is incorporated with a ceramic-epoxy composite matching layer developed in the present study.

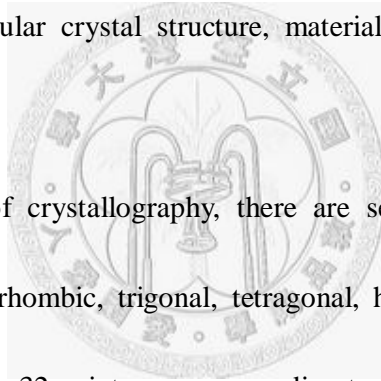
In Chapter 6, the developments of active and passive matching layers for HIFU applications are summarized.



2. Literature Review

2.1 Ferroelectric Materials

Ferroelectric phenomenon was first discovered in single-crystal Rochelle salt in 1921, and ferroelectric ceramics, barium titanate (BaTiO_3), was developed in the early 1940's. The most popular commercial ferroelectric material today, lead zirconate titanate (PZT), was developed in the mid-1950's, meanwhile lead lanthanum zirconate titanate (PLZT) and lead magnesium niobate (PMN) were developed later in the late 1960's and 1970's, respectively. Due to particular crystal structure, materials mentioned above possess ferroelectric property.



According to theories of crystallography, there are seven basic crystal systems, triclinic, monoclinic, orthorhombic, trigonal, tetragonal, hexagonal and cubic, which can be further classified into 32 point groups according to different symmetry elements^[1]. Of the 32 point groups, 11 are centrosymmetric and 21 are non-centrosymmetric (see Fig. 2.1^[2]). Of these 21 non-centrosymmetric classes, 20 are piezoelectrics and 10 are pyroelectrics which possess a spontaneous polarization in the absence of applied electric field. Furthermore, a limited number of materials within the 10 classes of pyroelectrics are ferroelectrics, which by definition possess the characteristic that the direction of polarization with them can be changed switch by an external applied electric or mechanical field. The basic theories of ferroelectricity are detailed in the next section.

2.1.1 Fundamental Theories

The most important characteristic of ferroelectric materials, distinguished from piezoelectric and pyroelectric materials, is that the direction of polarization within the materials can be switched by an applied electrical field to another direction (see Fig. 2.2).

BaTiO_3 , a classic ferroelectric material has a perovskite unit cell commonly known as a “ ABO_3 ” crystal structure. Within this structure, cation A occupies at the corner positions, oxygen locates at the face-center of the six lattice planes, and cation B occupies at the interstitial site within the AO octahedral structure (see Fig. 2.3 [3]).

Above the Curie temperature, about 130°C for BaTiO_3 , the unit cell is cubic. The unit cell transforms to a tetragonal crystal when temperature decreases below Curie temperature with Ti^{4+} ion (B-site cation) slightly displaced from the body center to one of the faces of unit cell by about 0.12 angstroms, yielding a noncentrosymmetric structure and a dipole moment along the direction of the motion of Ti^{4+} ion. The same phenomenon is observed in perovskite PZT which has a Curie temperature of about $200 - 350^\circ\text{C}$. Below the Curie temperature, cubic PZT transforms into a rhombohedral or tetragonal crystal, depending on the composition ratio of Zr^{2+} and Ti^{4+} . The possible directions of spontaneous polarization for the rhombohedral and tetragonal crystals are shown in Fig. 2.4 [4]. Additionally, the Morphotropic phase boundary (MPB)

composition of PZT lies on the Zr : Ti ratio of 52 : 48.

The difference between tetragonal and rhombohedral crystals in terms of ferroelectric properties involves the available switching systems (i.e., the possible directions that a dipole can adopt). As shown in Fig 2.5 ^[5], in a tetragonal crystal, there are six equivalent crystallographic directions along [100] axes for the central B-cation to adopt. In a rhombohedral crystal, there are eight equivalent crystallographic directions along [111] axes for the central B-cation to adopt. Thus, when exposing to a large electrical field, and below Curie temperature, the direction of spontaneous polarization would align itself closely to the external electrical field.

The macroscopic of relationships between electric field and polarization and electric field and strain for the ferroelectric materials can be best explained by their measured polarization and strain hysteresis curves, as shown in Fig. 2.6 (a) and (b) ^[6]. At point O, there is no applied electric field and dipoles randomly orient without net polarization and strain change. As the electric field increases, dipoles gradually lengthen generating net polarization and lattice elongation along the field applied axis. When the applied field is increased above the coercive field (E_c), the polarization and strain increases dramatically (most vertical part of OA line), due to the switchings of dipoles which align themselves to the field direction. Eventually, the increment of polarization and strain slow down when polarization saturation is reached (point A). When the electric

field is removed, the polarization decreases to point B with a retained remanent polarization. The material is now poled and its remanent polarization is in the direction of applied electric field. When a negative (inverse) electric field is applied, the polarization starts to decrease as the dipoles begin to switch to the opposite direction. Upon reaching negative E_c , the polarization increases sharply as majority of dipoles non switch to the opposite direction, and eventually reach saturation (point D). The material is polarized again in the opposite direction. For the strain hysteresis, a sharp change in strain also proceeds when most dipoles suddenly switch. The dipoles go through multiple $90^\circ C$ switches and complete $180^\circ C$ switches. This is shown by temporary decreases in size during $180^\circ C$ switching (points C and F).

Again, upon removing the negative electric field, the material is poled in the opposite direction with a negative remanent polarization. Both the polarization and strain hystereses curves repeat themselves during a cyclic electric field loading.

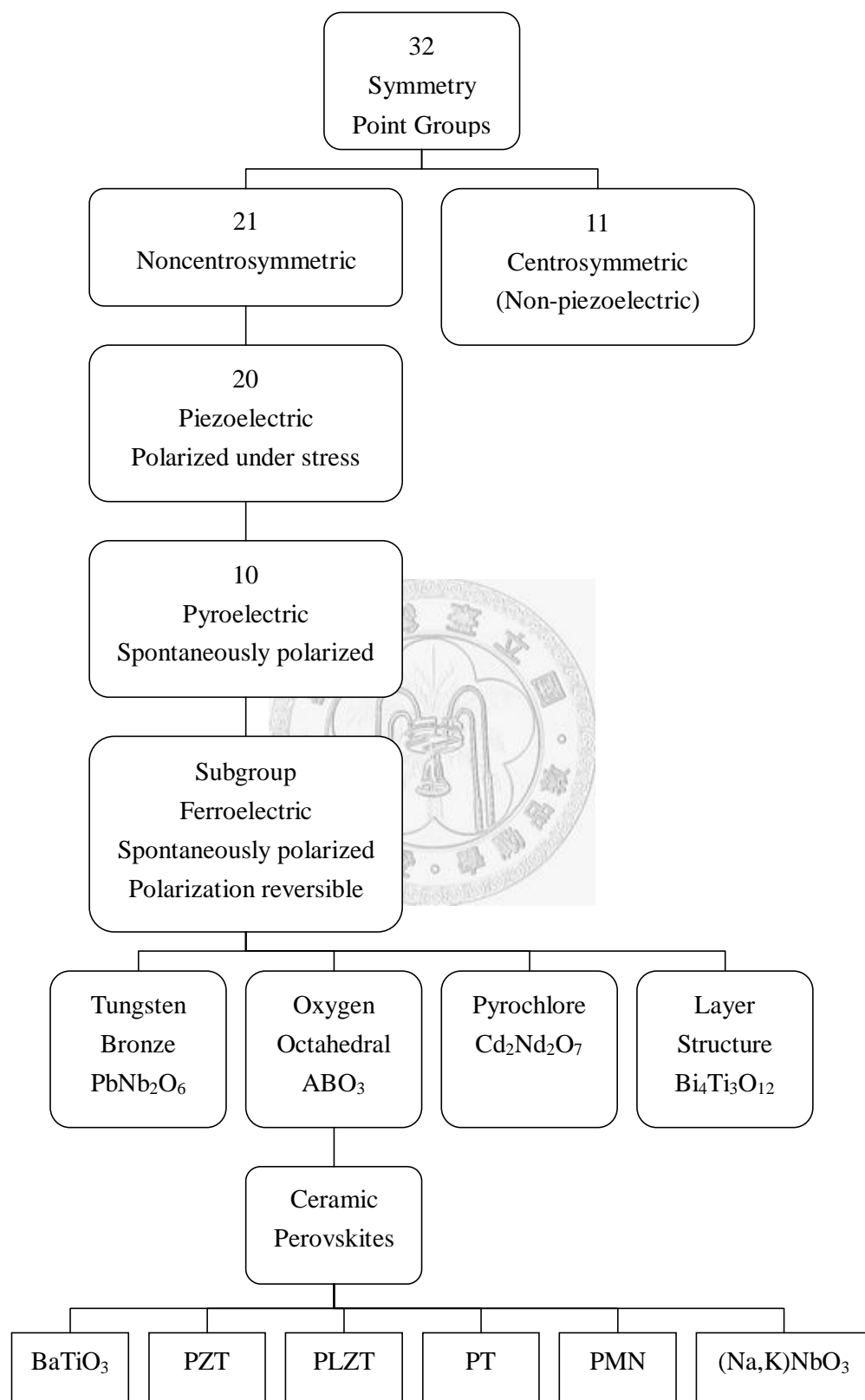


Figure 2.1 Classification of 32 point groups ^[2]

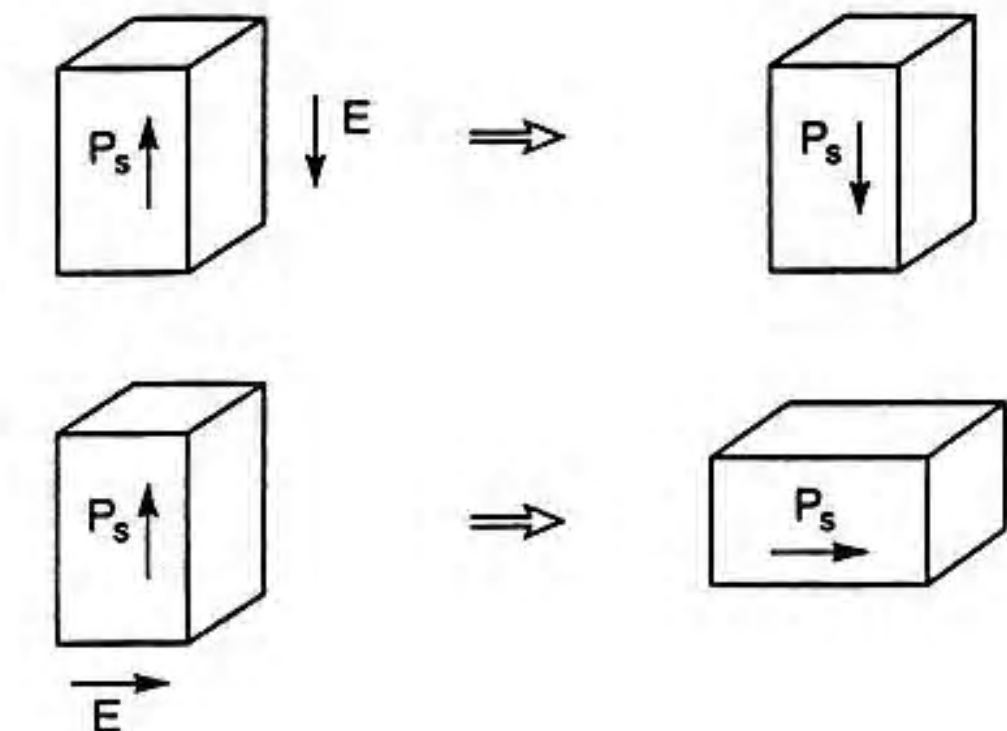


Figure 2.2 The direction of polarization switched by an applied electrical field.

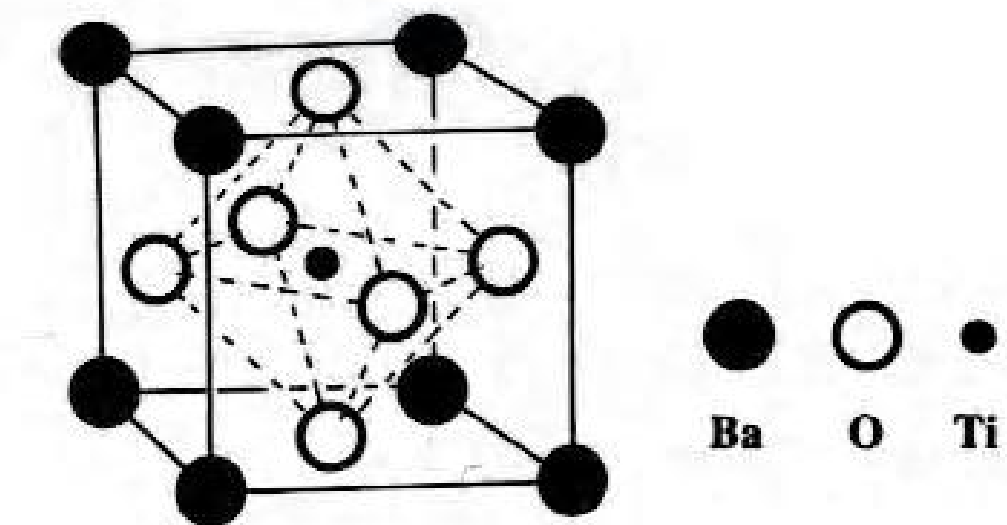
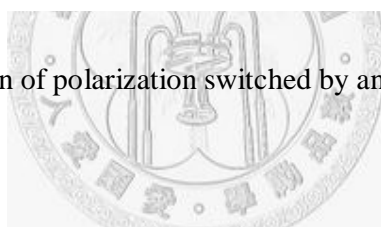


Figure 2.3 The unit cell of BaTiO_3 ^[3].

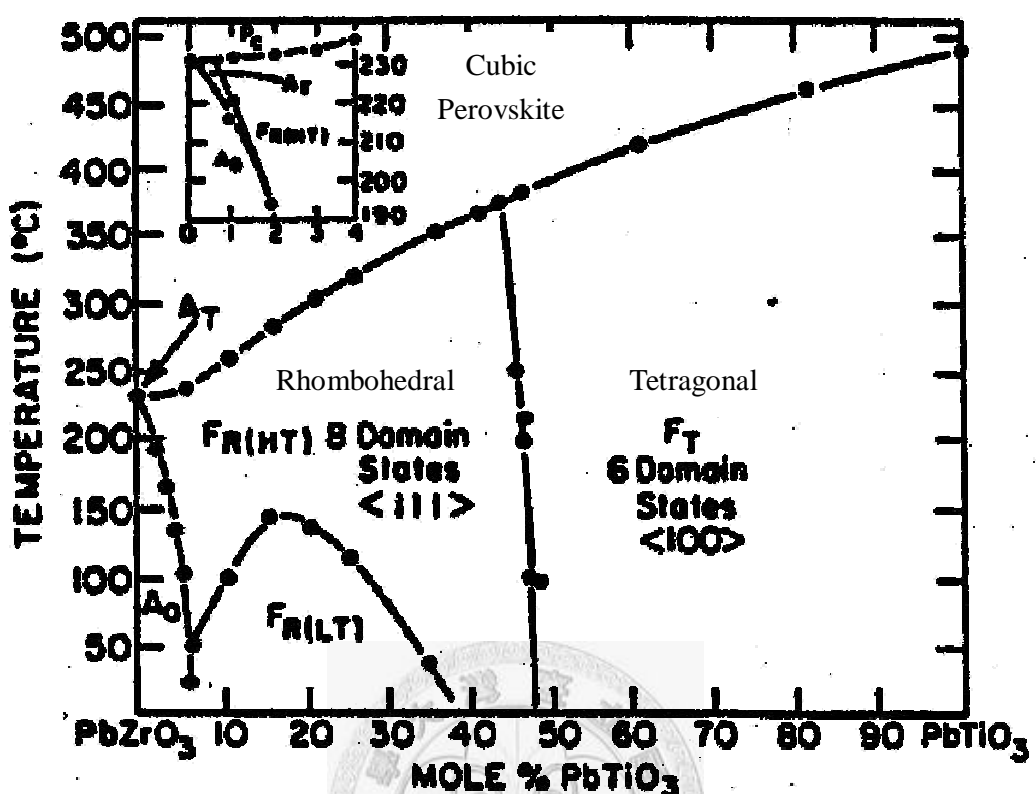


Figure 2.4 Composition-dependent crystal transition of PZT.

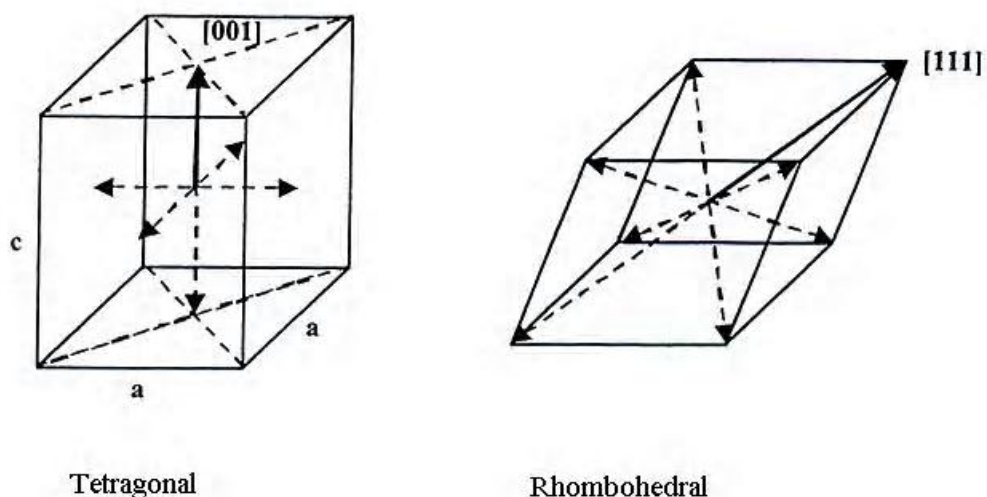


Figure 2.5 Switching systems of tetragonal and rhombohedral ferroelectric crystals ^[5].

2.1.2 Piezoelectricity

When a ferroelectric material is poled, it possesses piezoelectric properties, which generate electrical charges from mechanical stresses (direct piezo effect) and strain changes from applied electrical fields (converse piezo effect). The piezoelectric relationships can be described by mathematical equations ^[7] :

$$D = dE + \epsilon^T E \cdots (2.1)$$

$$S = s^E T + dE \cdots (2.2)$$

where D is the dielectric displacement, T the stress, E the electric field, S the strain, d the piezoelectric charge coefficient, s the material compliance, and ϵ the permittivity. The superscripts indicate quantities which are held constant. Piezoelectricity is a linear effect, which can be visualized from the linear region of the polarization and strain hysteresis curves (see 2.6 (a) and (b)).

The piezoelectric relationships are best shown in the Nye principle (see Fig. 2.7^[8]). The three corners represent the electrical, mechanical and thermal properties of materials with the outer corners representing the stimulus and inner corners representing the responses. Among the piezoelectric properties, the piezoelectric coupling factor (κ) determines the efficiency of conversion between electric energy and mechanical energy, or vice versa. κ can be expressed as below^[7] :

$$\kappa^2 = \frac{\text{Stored Mechanical Energy}}{\text{Electrical Energy Applied}} \cdots (2.3.1)$$

$$\kappa^2 = \frac{\text{Stored Electrical Energy}}{\text{Mechanical Energy Applied}} \dots (2.3.2)$$

Eqn. 2.3.1 is applied to an electrically loaded piezoelectric component, while Eqn. 2.3.2 is applied to a mechanically stressed component.

2.1.3 Resonant Method Characterization

When a small alternating electric field applied, piezoelectric materials start to vibrate with lattices extending and contracting along applied axis. Materials have their own characteristic frequencies, varying with composition, thickness, shape, and boundary condition, and at these resonant frequencies, materials will resonate freely at greater amplitude than at other frequencies, with lower impedance. And an anti-resonant frequency immediately comes after with higher impedance and minimum oscillatory amplitude. A typical resonance plot of impedance versus frequency for a piezoelectric ceramic near a resonant frequency is shown as Fig. 2.8.

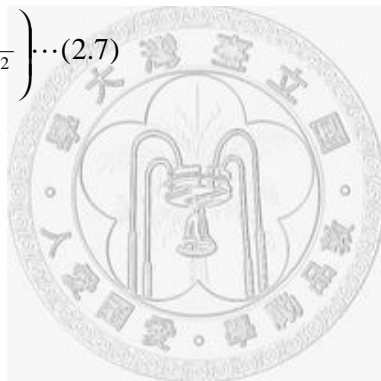
With the measurement of resonant and anti-resonant frequencies, the coupling coefficients, κ_p , κ_{31} , and κ_{33} , are described by as equations^[9] :

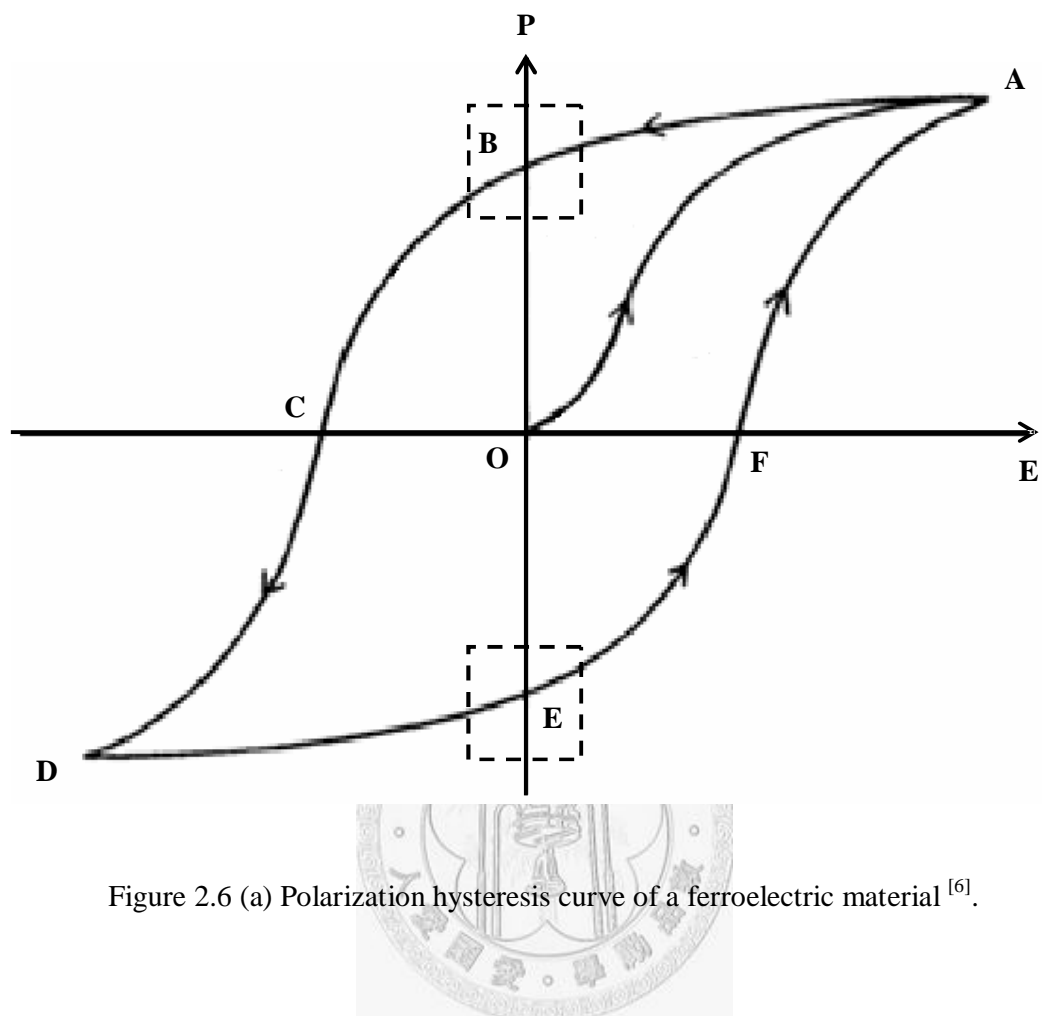
$$\kappa_p = \frac{f_a^2 - f_r^2}{f_r^2} \dots (2.4)$$

$$\kappa_{33}^2 = \frac{\pi/2}{1 + (f_a - f_r)/f_r} \tan \left[\frac{\pi(f_a - f_r)/2f_r}{1 + (f_a - f_r)/f_r} \right] \dots (2.5)$$

$$\kappa_{31}^2 = \frac{\Phi}{1 + \varphi} \dots (2.6), \text{ where } \varphi = \frac{\pi}{2} \left[1 + \frac{f_a - f_r}{f_r} \right] \tan \left[\frac{\pi(f_a - f_r)}{2f_r} \right]$$

where κ_p , κ_{31} , and κ_{33} are defined for planar, length extensional, and thickness extensional modes, respectively. Furthermore, the resonant property is also defined by mechanical quality (Q_M), which is related to the sharpness of the resonant frequency and is the ratio of the mechanical energy stored to the mechanical energy dissipated. For ultrasonic transducers, broadband probes are distinguished from narrowband probes with lower Q_M values, due to the bluntness of the resonant frequency. Q_M can also be defined by mathematical equation with f_a and f_r [9] :

$$Q_M = \frac{1}{2\pi f_r Z_m C_0} \left(\frac{f_a^2}{f_a^2 - f_r^2} \right) \dots (2.7)$$




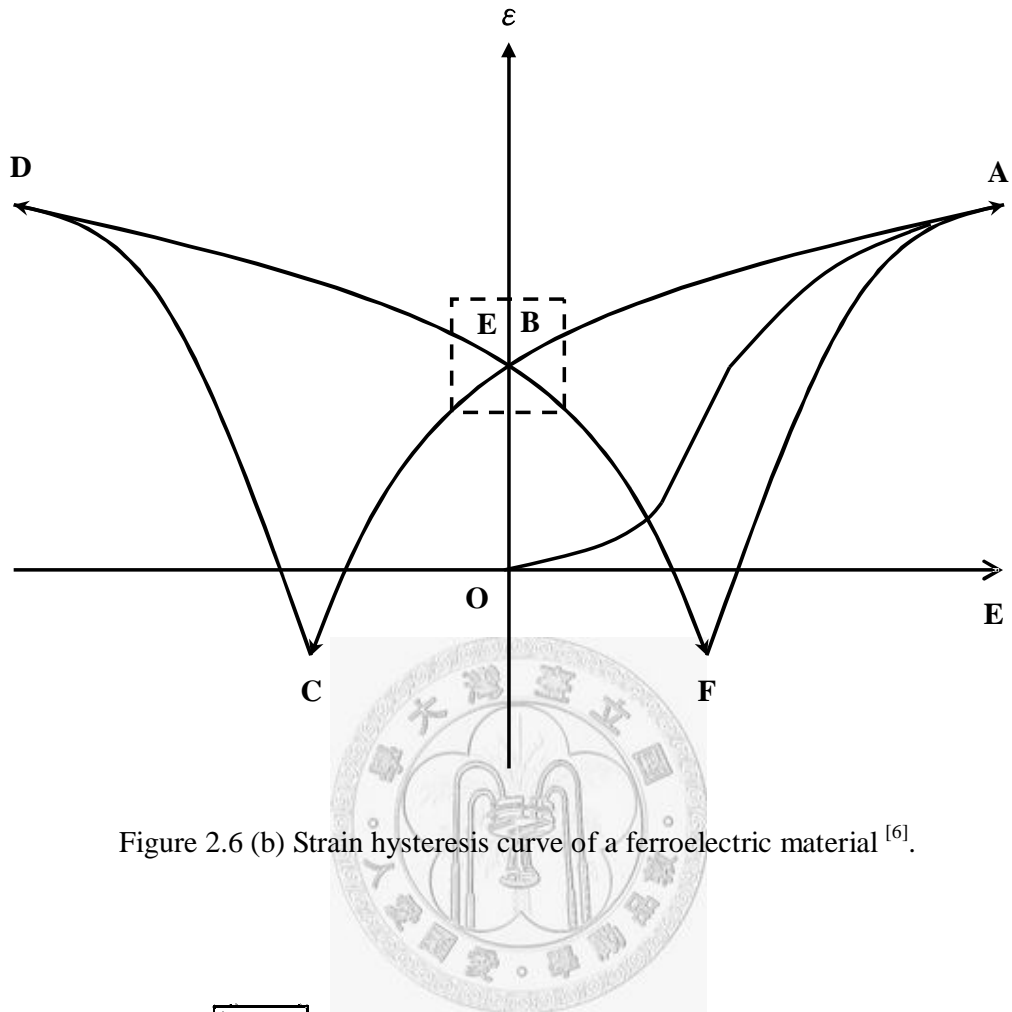


Figure 2.6 (b) Strain hysteresis curve of a ferroelectric material [6].

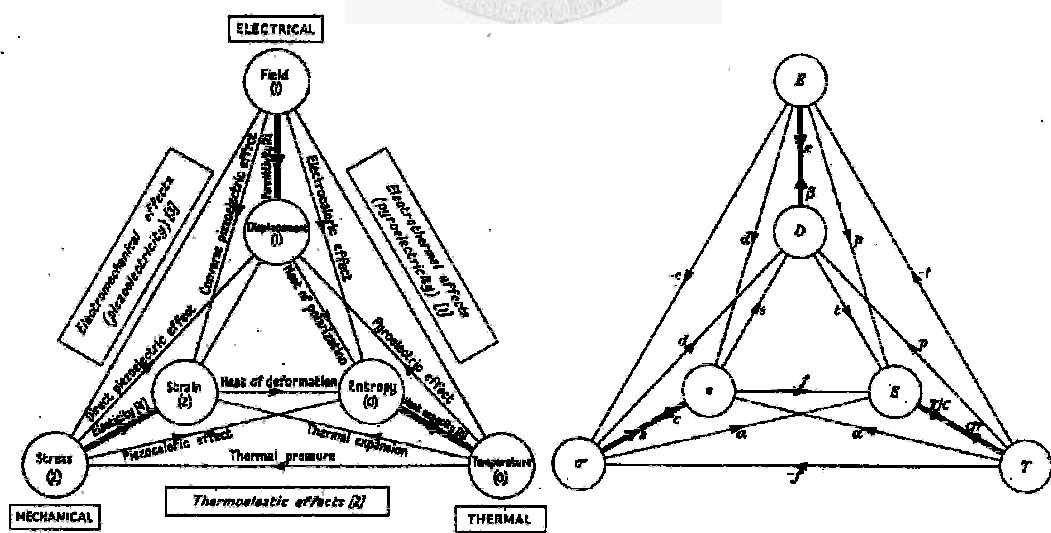


Figure 2.7 Constitutive relationships of the thermal, electric and mechanic properties^[8].

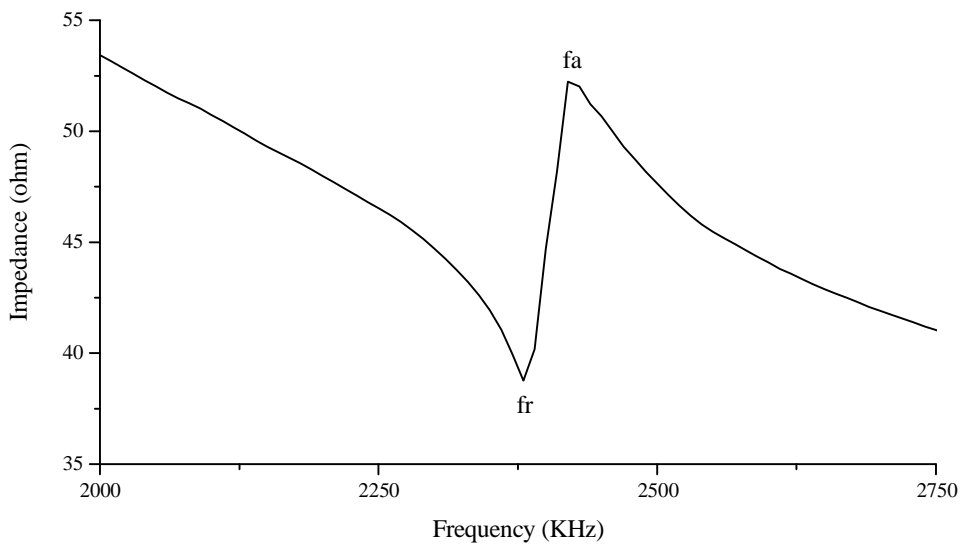
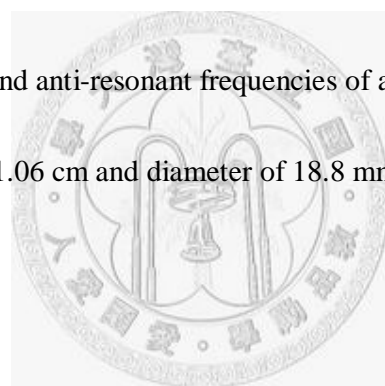


Figure 2.8 The resonant and anti-resonant frequencies of a BaTiO₃ with thickness of 1.06 cm and diameter of 18.8 mm.

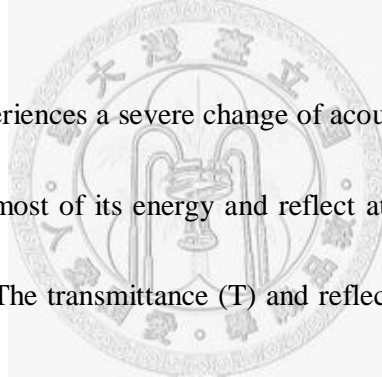


2.2 Acoustical Matching Theory

Acoustic impedance (Z) is the primary parameter to describe behaviors of acoustic waves traveling through the interface between different materials ; In other words, it defines the quantities of transmittance and reflectance, and the ability of an acoustic wave to pass through the interface. The acoustic impedance of a material is defined as the product of density and acoustic velocity in material ^[10], or the ratio of sound pressure to particle velocity in open field, and its dimension is denoted as MRayl, which

is equal to $\frac{Kg}{m^2 \cdot s}$.

If the acoustic wave experiences a severe change of acoustic impedance between two materials, it will dissipate most of its energy and reflect at the interface, and therefore less energy is transmitted. The transmittance (T) and reflectance (R), can be calculated by Fresnel's equations ^[11] :



$$T = \frac{4Z_1 Z_2}{(Z_1 + Z_2)^2} \dots (2.8)$$

$$R = \left(\frac{Z_1 - Z_2}{Z_1 + Z_2} \right)^2 \dots (2.9)$$

For HIFU ultrasonic transducers, the acoustic impedance of the embedded active piezoelectric ceramic material is around 33 to 35 MRaly, which is much larger than that of human tissues and water (1.5 MRayl). Due to this large impedance mismatch, the ultrasound wave dissipates most of its energy at the interface before transmitting to water. An acoustic matching layer is therefore needed to apply to reduce the large

impedance difference between the two media in order to increase the quantity of wave transmitted. However, the transmitting efficiency of an acoustic matching layer depends on its impedance value and thickness. A critical impedance value and thickness are required for achieving maximum transmitting efficiency.

2.2.1 Impedance Matching

For single matching layer, the optimum acoustic impedance is defined as ^[12] :

$$Z_{ML} = \sqrt{Z_P Z_W} \cdots (2.10)$$

where Z_{ML} , Z_P and Z_W represent the acoustic impedances of matching layer, active piezoelectric material and water, respectively. The equation is proved by Alvarez-Arenas ^[13] and based on the optimization of energy transfer through the interface. Here, we use a PZT-matching layer-water (P-ML-W) system as an example.

To calculate the critical value of matching layer impedance, two interfaces, PZT ceramic-matching layer and matching layer-water, are involved. At a plane interface between media A and B, having acoustic impedance Z_A and Z_B , respectively, solution of reflection and transmission for normal incidence are given by ^[14] :

$$u_t = \frac{2Z_A}{Z_A + Z_B} u_i \cdots (2.11.1)$$

$$u_r = \frac{Z_B - Z_A}{Z_B + Z_A} u_i \cdots (2.11.2)$$

where u is the velocity of atomic vibration, and subscripts i, r, and t denotes incident, reflected and transmitted waves, respectively.

The transmitted wave through a matching layer, from PZT ceramics to water, is the sum of the contribution of each of the multiple reverberations within the matching layer, demonstrated as Fig. 2.9. At the resonant frequency of a critical thickness matching layer, all wave components in this summation are in the same phase when they leave the matching layer; a geometrical series is therefore obtained. The amplitude of the overall transmitted wave, which is calculated from the summation of the series is given by :

$$t_1 t_2 \sum_{n=0}^{\infty} (r_1 r_2)^n = \frac{t_1 t_2}{1 - r_1 r_2} \dots (2.12), \quad r_1 r_2 < 1$$

where t represents the ratio of transmitted to incident wave amplitude, and r represents the ratio of reflected to incident wave amplitude. From Eqn. 2.11, they are given as :

$$t_{1,2} = \frac{2Z_{P,ML}}{Z_{P,ML} + Z_{ML,W}} \quad \text{and} \quad r_{1,2} = \frac{Z_{ML,W} - Z_{P,ML}}{Z_{ML,W} + Z_{P,ML}}. \quad \text{Subscripts 1 and 2 denote the two}$$

interfaces involved : PZT ceramic-matching layer and matching layer-water, respectively.

Considering plane waves, the ratio of energy flux transmitted to the water to the energy flux incident on the matching layer (γ_t) is given as :

$$\gamma_t = \left(\frac{t_1 t_2}{1 - r_1 r_2} \right)^2 \frac{Z_w}{Z_p} \dots (2.13)$$

For maximum transmitted energy without considering traveling attenuation in matching layer, the ratio γ_t is closely equal to 1, and with the given values of Z_p , Z_w , the value of Z_{ML} is given the same as Eqn. 2.10.

For medical imaging application, an ultrasonic probe is required for broad frequency

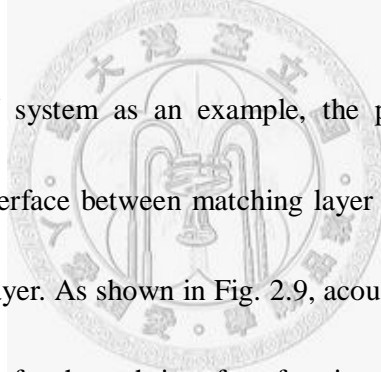
distribution to receive as much as the waves reflected. Thus the broadband probes are designed with multi matching layers ^[15], or single matching layer with a novel impedance value ^[16], these approaches are expressed as below :

$$Z_{ML}^{(j)} = \sqrt[n+1]{Z_p^{n-j+1} Z_w^j} \dots (2.14)$$

$$Z_{ML} = \sqrt[3]{Z_p Z_w^2} \dots (2.15)$$

where superscript j denotes the level of the matching layer and n denotes the number of matching layers integrated on.

2.2.2 Thickness Matching



Again using a P-ML-W system as an example, the phase of an acoustic wave, propagating through the interface between matching layer and water, is defined by the thickness of the matching layer. As shown in Fig. 2.9, acoustic waves reverberate inside the matching layer and transfer through interface forming an overall constructed wave with each component wave in the same phase. If the waves are not in the same phase, they are partially destructed by each other, resulting in a decrease in the sum of amplitude smaller, or for the worst case, with a 180° phase difference, there would be no combined wave due to the full destructive interface between wave components. Therefore, to achieve the maximum transmitting efficiency for a matching layer, the optimum thickness of the matching layer is $\frac{\lambda}{4}$ ^[17, 18, 19], where λ is the wavelength of a wave traveling in the matching medium.

When an acoustic wave is generated from the transducer and propagates through the matching medium entering the interface between matching layer and water, a part of it is transmitted to the water and the remaining is reflected, as shown in Fig. 2.10. According to Fresnel's equation [11], the reflection and transmission coefficients of a normal incident wave are the root of reflectance and transmittance, respectively, and are expressed as below :

$$r = \frac{Z_1 - Z_2}{Z_1 + Z_2} \dots (2.16)$$

$$t = \frac{2Z_1}{Z_1 + Z_2} \dots (2.17)$$

where r and t represent the reflection and transmission coefficients, respectively. If an acoustic wave travels from a low acoustic impedance medium to a higher one, the reflection coefficient is negative, and based on Fresnel's rule, the wave will reflect with a 180° phase shift. Therefore, the reflected wave from the water-matching layer interface will reflect again at the PZT-matching layer interface with a 180° phase shift. Besides, the double reflected wave also travels half wavelength with a 180° phase shift, and when transmitting to water again, the phase is the same as the wave transmitted before, forming a constructive interface with maximum transmitting efficiency.

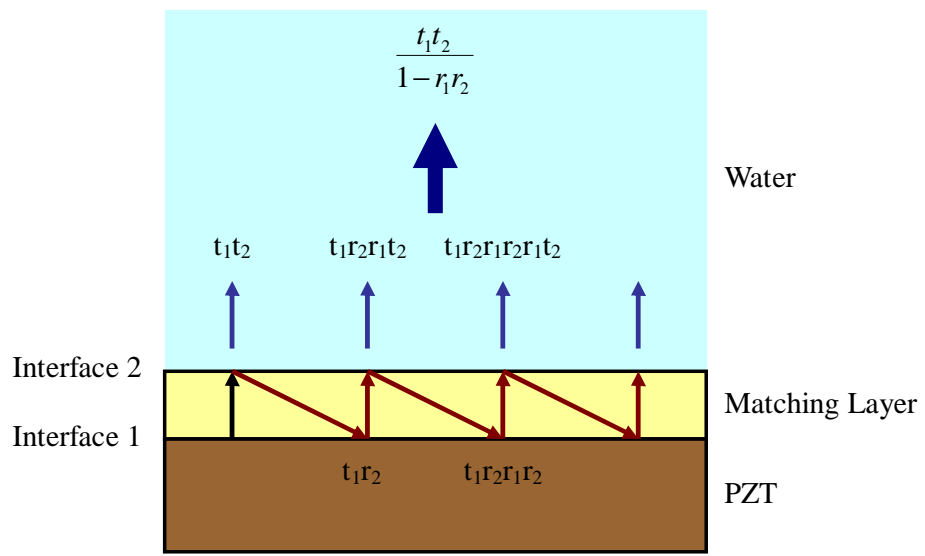


Figure 2.9 Amplitude summations of the waves reverberated in matching layer and then

transmitted to water.

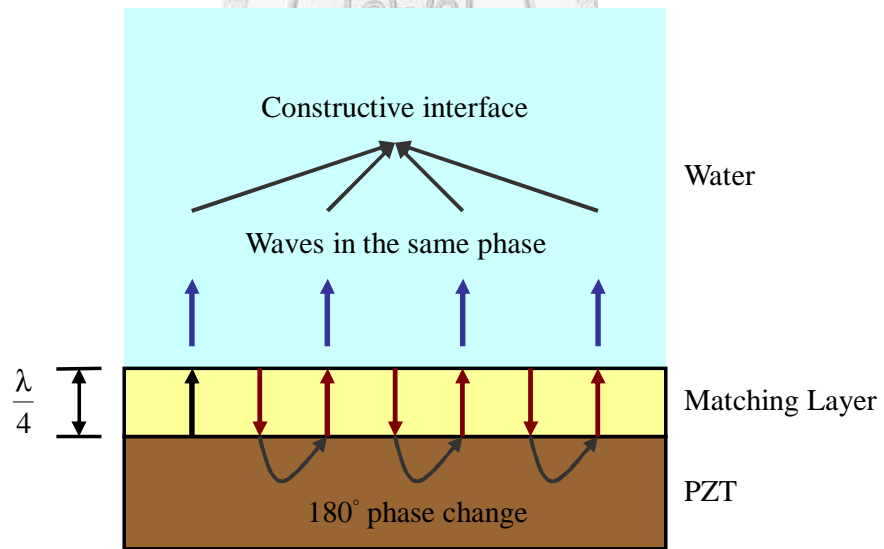


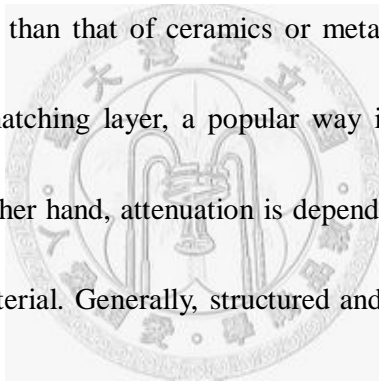
Figure 2.10 Waves traveling within matching layer have a 180° phase shift at

PZT-matching layer interface, and leave a quarter-wavelength matching layer with the

same phase and interfere constructively.

2.3 Acoustical Matching Materials

The selection of matching material bases on two principles, suitable acoustic impedance and low attenuation. As mentioned before, the acoustic impedance of a material is defined as the product of material density and acoustic velocity in the material. For most materials, the distribution of acoustic velocity ranges from 2000 ms^{-1} to 4000 ms^{-1} , and the variation is quite limited when compared to the variation in density. Take polymers and ceramics or metals as examples, the density of polymers are conventionally much lower than that of ceramics or metals. Therefore, to control the impedances value of the matching layer, a popular way is to combine high and low density materials. On the other hand, attenuation is dependent on the structures and the elastic properties of the material. Generally, structured and less viscous materials have lower attenuation coefficient.



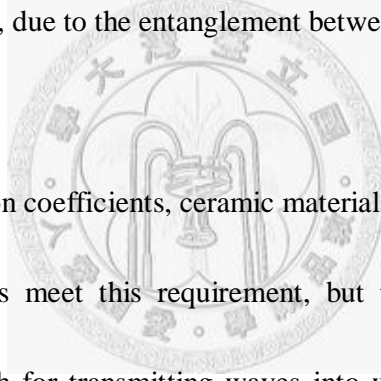
2.3.1 Polymers

For low density and highly shapeable properties, polymer matching layers are widely used in medical imaging application with Spin-coating methods are usually adopted for the integration of the layers ^[20]. Polymer materials commonly used for matching applications are parylene ^[21], polyurethane ^[22], and epoxy ^[23] with acoustic impedances of 2.83, 1.38-2.36, 2.7 MRayl, respectively. The low density of polymers gives rise to their low impedances, which in turn make them unsuitable for acoustic matching in

single-matching layer water-immersion ultrasonic transducers. The required impedance value for a single-matching layer design is about 7 MRayl according to Egn. 2.10. However, in medical imaging, the contrast-to-noise ratio is primarily concerned, and does not strongly affected by the quantity of total transmitting energy.

Porous polymers are also utilized in many different applications, such as the outer layer in the multi-matching layer design, for obtaining a much lower impedance. The main disadvantage of the polymer matching layer is its high attenuation coefficient compared to other materials, due to the entanglement between polymer chains.

2.3.2 Ceramics



To achieve low attenuation coefficients, ceramic materials with high young's modulus and good elastic properties meet this requirement, but the acoustic impedances of ceramics are much too high for transmitting waves into water and human tissues. To reduce the impedance, both the density and wave velocity within the ceramic need to be lower. The control of wave velocity in the material is much complicated than controlling the density. Therefore, porous ceramics materials are produced, such as microporous membranes ^[24] and filtration ceramic materials ^[25,26], to quantitatively lower the density. The porous design can be considered as a air-ceramic composite with air having the acoustic impedance of 0.0004 MRayl.

The porous ceramics are manufactured with homogeneous pore distribution and the

pore diameter shorter than the wavelength of the wave traveling in the material. If the pore size is larger than the wavelength, the wave will be scattered at the ceramics-air interface, and the attenuation would increase accordingly. The density can be controlled by the volume percentage of air. Thus, if the pores in the ceramic are not distributed homogeneously, a lower uniformity in impedance is produced.

2.3.3 Ceramic-Polymer Composites

Ceramic-polymer composites are one of the most popular matching layers applied to commercial products due to their modifiable impedances achieved by adjusting the volume percentages of components. The traditional method to produce ceramic-polymer composites are by mixing epoxy and hardener with ceramic powders^[27, 28] (e.g. silicon oxide) and then cured at room temperature. The only limitation is that the particle size is restricted to below the acoustic wavelength, or else the propagating wave will be strongly scattered by the ceramic particles, resulting in the increase of attenuation.

Because of the development of ultrasonic transducers of higher resonant frequencies for medical imaging applications, the required matching layer thickness becomes thinner, ranging from hundred nanometers to few micrometers. Therefore, for the homogeneity of the matching layer, the average ceramic particle size is limited to few nanometers. Generally speaking, the impedances of ceramic-loaded epoxies range from 2.8 to 11.3 MRayl, depending on the material type and mixing ratio. Some researches

have mentioned that the aging process of cured ceramic-epoxy composites can increase their impedances^[29].

2.3.4 Metal-Polymer Composites

For the purpose of acoustic matching, metal-polymer composites operate on the same principle as the ceramic-polymer composites. Metal-loaded epoxies such as silver epoxy [30, 31] and copper epoxy^[32] and silicon rubber mixed with metal powders^[33] are wildly commercialized as matching layers.

Because of the high density of metals, the volume percentage of metal powders in the composite is decreased to lower the impedance. Decreasing the volume percentage of metal powders reduces the number of interfaces between loaded powers and the polymer matrix, resulting in a lower attenuation. The acoustic wave now travels through the matching layers with less interference from impedance mismatch.

2.4 High-Intensity Focused Ultrasound

High intensity-focused ultrasound (HIFU) is a method to generate a large amount of heat at the focal point of a transducer, with operating frequency typically ranging from 1 MHz to 3 MHz. The energy transmitted depends on the area of the transducer and its focal length. The heat generated is higher with a larger transducer area and a shorter focal length. Besides, material parameters such as the piezoelectric coupling coefficient and the efficiencies of the acoustic matching layer and electrical matching are important

factors to determine the performance of a HIFU transducer.

2.4.1 HIFU Applications

The HIFU technology is recently applied as a noninvasive surgery for ablation of

tumors [34-39]. Compared to traditional surgical resections with high surgical risks, HIFU

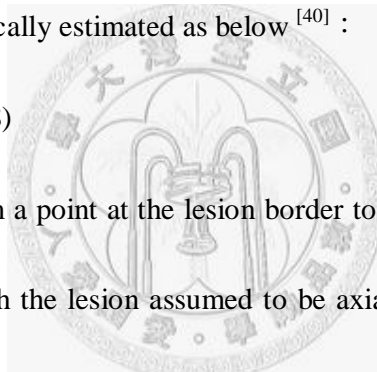
allows the ultrasonic energy to enter tissues generating heats which “kill” the tumors.

The ultrasonic focus of the HIFU transducer causes a lesion, which grows with

increasing treating time and cells near the lesion are destroyed by heat. The thermal

lesion volume is mathematically estimated as below [40] :

$$V = \sum_{n=1}^N \pi \cdot (r_n)^2 \cdot D \dots (2.18)$$



where r is the distance from a point at the lesion border to its central axis, and D is the

thickness of each slice, with the lesion assumed to be axially symmetrical and splitted

into n slices. Notice that HIFU can also be used to cut off nutrition sources and blood for

tumor.

The HIFU treatment is known to be accelerated due to “cavitation” [40], a

phenomenon which generates a great quantity of bubbles from abrasions between

molecules, resulting in a local increase in attenuation which transforms more acoustic

energies into heats. However, the generation of bubbles along the transmitting path

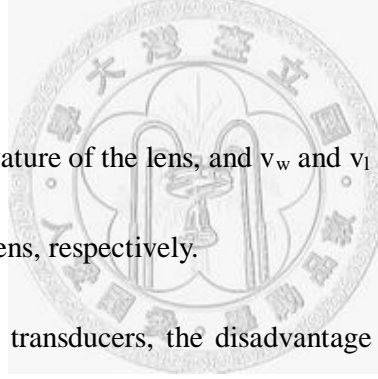
causes the thermal lesion growing backward (i.e. toward HIFU source), causing

unwanted damages to the surrounding healthy cells.

2.4.2 Development

Traditional HIFU probes are designed as bowl-type transducers to focus the acoustic beams at geometrically focal point as demonstrated in Fig. 2.11(a). It is a simple method to treat cancers with placing tumors at the focal point of transducers. Another design of bowl-type transducers involves a flat piezoelectric material with a concave lens acting as an acoustic matching layer (see Fig. 2.11(b)). The focal length can be calculated as [41] :

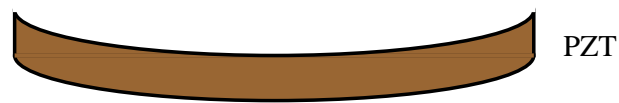
$$f = \frac{r}{1 - \frac{v_w}{v_l}} \dots (2.19)$$



where r is the radius of curvature of the lens, and v_w and v_l are the wave velocities in the water (human tissues) and lens, respectively.

For the traditional HIFU transducers, the disadvantage lies in the inconvenience to repeatedly move the transducer to cure different parts of a same tumor. A phase array HIFU transducer capable of changing its focal length by the combination of phases of different acoustic waves from different elements has been designed^[42]. The position of the highest level of constructive interface would be the focal point. The phase array approach for the design of HIFU is the dominant trend due to the capability of varying focal length.

(a)



(b)

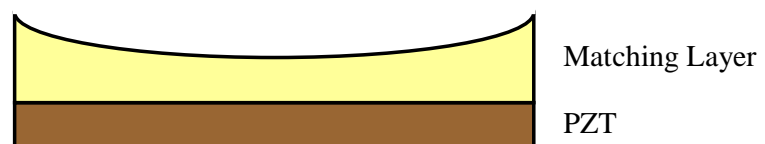


Figure 2.11 Schematics of Bowl-type HIFU transducers demonstration.



3. Experiment Procedure

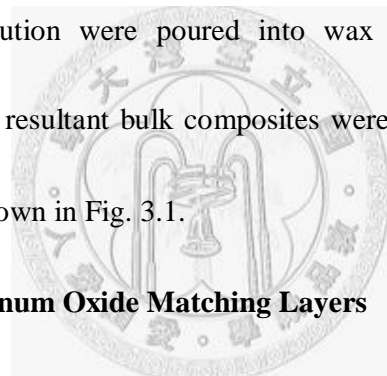
The methods of manufacturing composites of high and low acoustic impedance are described in this chapter. The processes of non-structured and structured composites are also described, and their impedances compared. The internal wave velocity, frequency behavior, and microstructure of each prepared matching layer material sample are measured, characterized, and described from Section 3.4 onwards.

3.1 Manufacture of Ceramic-Epoxy Composites

Ceramic-epoxy composites are popularly adopted as acoustic matching layers for commercial ultrasonic transducers as mentioned in Chapter 2. In order to produce highly dense ceramic-epoxy composites, a new method involving the control of viscosity and bubble formation was utilized in this study. The raw polymer and ceramic materials were two-part epoxy (Cheng-E Co., Taiwan), aluminum oxide powder (Al_2O_3 , Taimax Materials Co., Taiwan), zirconium dioxide powder (ZrO_2 , Yageo Co., Japan) and barium titanate powder (BaTiO_3 , Yageo Co., Japan). The mean particle sizes were 223.5 nm for ZrO_2 , and 1.619 and 1.669 μm for Al_2O_3 and BaTiO_3 , respectively, characterized by Zetapotential (Zetasizer, Malvern Co., Taiwan).

The epoxy was pre-heated to 120°C in the oven (Channel Co., Taiwan) and held for 10 minutes to lower its viscosity and release the residual bubbles. Three different ceramic particles were mixed separately with the pre-heated epoxy. 20.22, 30.00 and

30.66 grams of Al_2O_3 , ZrO_2 , and BaTiO_3 powders were put in, respectively, to form colloidal solutions of volume 10 ml. The colloidal solutions were again thoroughly mixed at 120°C, and then placed in vacuum for 5 minutes at a time for multiple times to ensure that the bubbles trapped between the ceramic particles escaped the solutions completely. The degree of compaction of the ceramic particles gradually increased during this procedure, and the epoxy eventually became excessive. The excess epoxy liquid was removed, and the epoxy hardener (Chen-E Co., Taiwan) was added into the solutions. Finally, the solution were poured into wax molds and cured at room temperature for 24 hr. The resultant bulk composites were aged at 80°C for 5 hr. The entire processing flow is shown in Fig. 3.1.



3.2 Manufacture of Aluminum Oxide Matching Layers

To produce low impedance materials, another approach is the use of porosity, e.g. porous ceramics with continued “skeletons”. The continuous structure within the porous material would give a superior acoustic transmission efficiency. The process of porous Al_2O_3 matching layer was therefore carried out in this study (see Fig 3.2.).

The Al_2O_3 powder was first mixed with the pore forming agent, polyvinyl chloride (PVC, Acros Organic Co., Taiwan), in an ethanol solution. The mixture was then ball-milled in planetary ball mill with zirconium dioxide mill balls (TS Technology Co., Japan) for 24 hr. Five mixtures of Al_2O_3 ceramics with different pore forming agent

volumes were prepared (see Table 3.1). The mixtures were dried in the oven at 80°C for 24 hr. and then sieved with a 100-mesh sieve. This drying-sieving procedure was repeated again to totally remove the ethanol. The mixed powders were compacted into circular green compacts with diameter 25 mm. These green compacts were debinded at a slow heating rate of 5°C/min, in order to prevent the generation of microcracks. This procedure was maintained at 400°C for 2 hr and then the compacts were furnace cooled. The Al₂O₃ compacts were then sintered at 1600°C for 1 hr with a heating rate of 10°C/min. After sintering, the structured porous Al₂O₃ ceramics are formed

Additionally, five porous Al₂O₃ ceramics of porosities were immersed in the epoxy solution and then cured for 24 hr. Due to the capillary action, the air pores within the porous Al₂O₃ would be filled with epoxies. After aging at 80°C for 24 hr, the structured Al₂O₃ ceramics with epoxy pores were now formed. They were manufactured to compare with the structured Al₂O₃ ceramics with air pores and the non-structured ceramic-epoxy composites.

3.3 Preparation of PZT Matching Layers

A novel active matching layer based on ferroelectric materials, was tested in this research. Widely available ferroelectric lead zirconate titanate (PZT) plates were purchased from Eleceram Technology Co., Taiwan. Due to PZT's wide range of electromechanical and acoustical properties, six different conditions of PZT plates were

chosen for the study (see Table 3.2). Each of the PZT plates would be either poled or unpoled, with or without electrodes, short-circuited or not short-circuited, and with or without a passive matching layer (ZrO_2 -epoxy composite). Additionally, four different resonant frequencies, 1, 2, 3 and 5 MHz, were ordered for each PZT plate type.

3.4 Measurement of Wave Velocity

To determine the acoustic impedance of a material, the wave traveling velocity in the material was a necessary parameter. Each of the prepared matching layer materials was ground to a flat-disc sample and adhered with ultrasonic gel on to ultrasonic probe (GE Panametrics Co., USA). The ultrasonic probe was used to transmit and receive ultrasound waves under a pulser-receiver (GE Panametrics Co., USA) setup. The pulser-receiver transferred the reflected wave signals to an oscilloscope (Lecroy Co., USA). Recording the time interval between each reflecting wave and knowing the sample thickness led to the value of wave velocity. The measurement system for wave velocity is shown in Fig. 3.3.

3.5 Measurement of Frequency Distribution

In order to prevent frequency coupling effect between the transmitting and receiving waves within an ultrasonic probe, an external hydrophone (ONDA Co., Taiwan) was utilized to receive the acoustic waves. The hydrophone measurement was set up under water to minimize attenuation and maximize the hydrophone efficiency. Each matching

layer material sample was set up similarly as mentioned in Section 3.5 on a ultrasonic probe triggered by a pulser-receiver setup. After traveling through the sample, the ultrasonic waves were received by the hydrophone and then transformed into electrical signals to the oscilloscope. The measured wave forms were converted to frequency spectrum using Fast Fourier Transform (FFT). The measurement system for frequency distribution is demonstrated in Fig. 3.4.

3.6 Characterization by Scanning Electron Microscopy

Microstructures of the prepared matching layer materials were characterized by scanning electron microscope (SEM, Philips Co., Netherlands) to determine the ceramic distribution within the epoxy matrix and the structures of the porous ceramics. The matching layer samples were first polished with sandpapers of number 800 to 2000 and then cleaned in a methanol solution by an ultrasonic cleaner. The porous ceramic samples were thermally aged at 1400°C for 30 min. The observing surfaces of the samples were sputtered with platinum thin films for 45 seconds before observed under SEM.

Table 3.1 The Al₂O₃ green compacts composition of Al₂O₃ powder and PVC powder
(pore forming agent).

Type	Al ₂ O ₃ volume %	PVC volume %
Pure Al ₂ O ₃	98.3 volume %	1.7 volume %
10 vol% porous Al ₂ O ₃	90 volume %	10 volume %
20 vol% porous Al ₂ O ₃	80 volume %	20 volume %
30 vol% porous Al ₂ O ₃	70 volume %	30 volume %
40 vol% porous Al ₂ O ₃	60 volume %	40 volume %

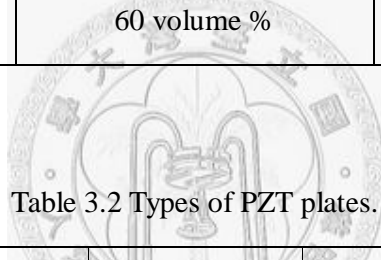


Table 3.2 Types of PZT plates.

Type	Poling	Electrode	Connecting Electrodes	Matching Layer
1	Yes	Yes	No	No
2	Yes	Yes	Yes	No
3	No	Yes	No	No
4	No	No	No	No
5	Yes	Yes	No	Yes
6	Yes	Yes	Yes	Yes

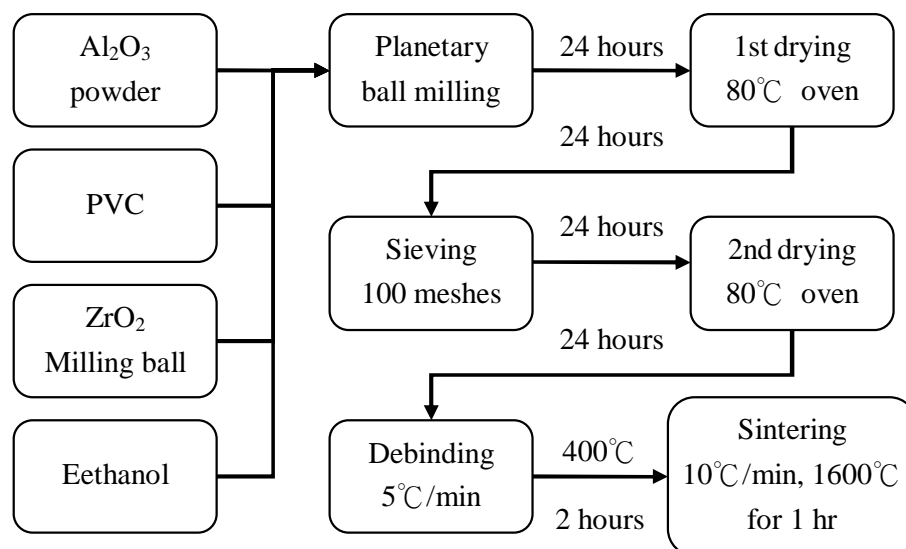
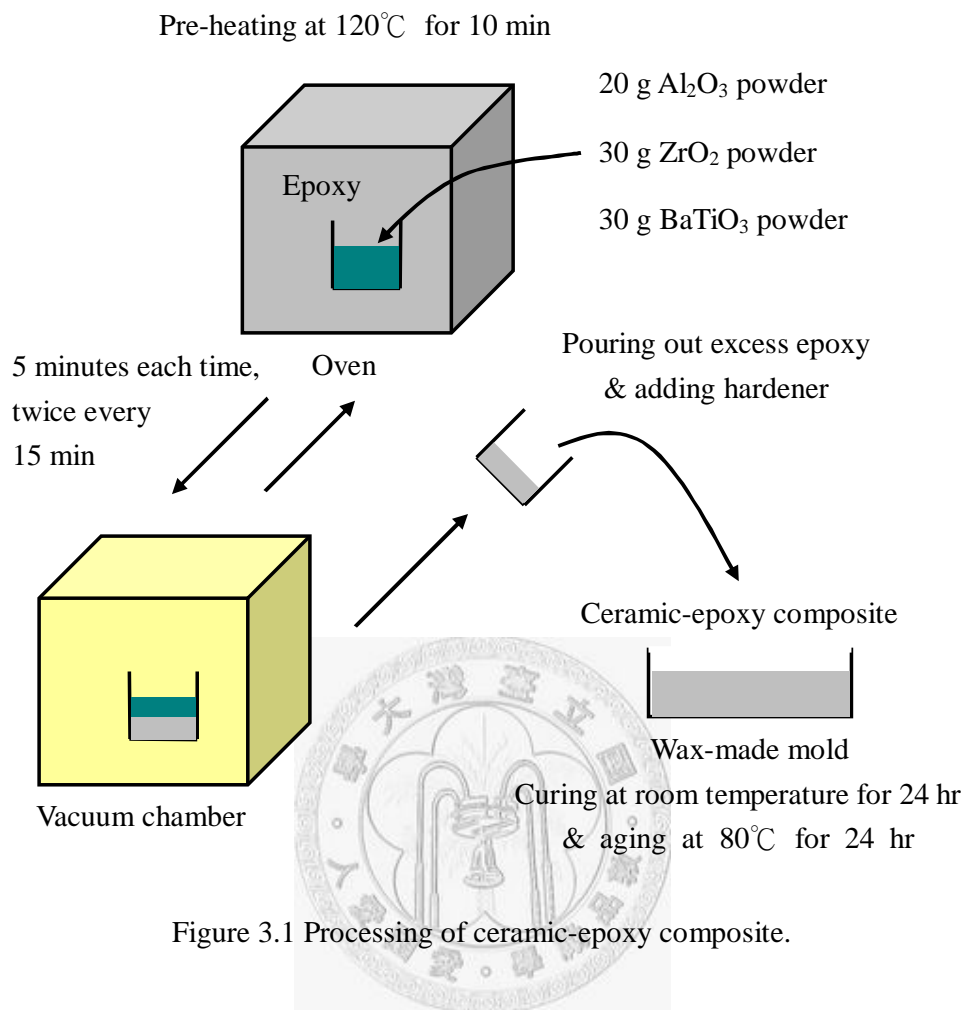


Figure 3.2 Processing of porous Al₂O₃ matching layer.

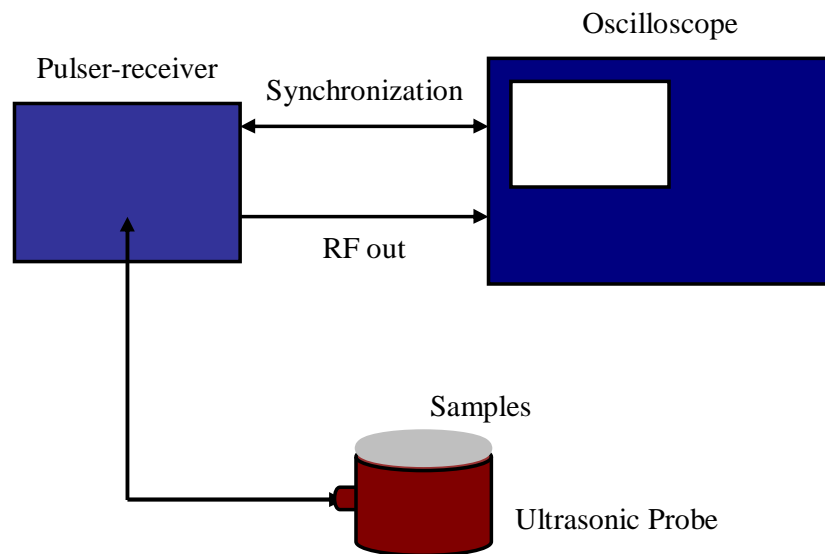


Figure 3.3 Schematic of the wave velocity measurement system.

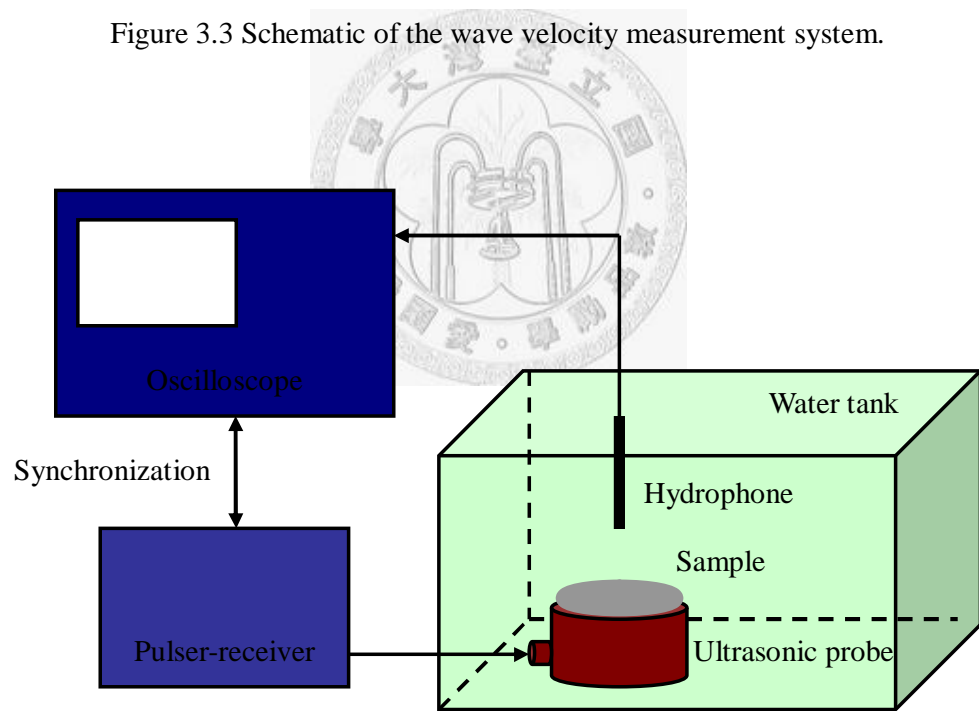


Figure 3.4 Schematic of the frequency distribution measurement system.

4. Results and Discussion

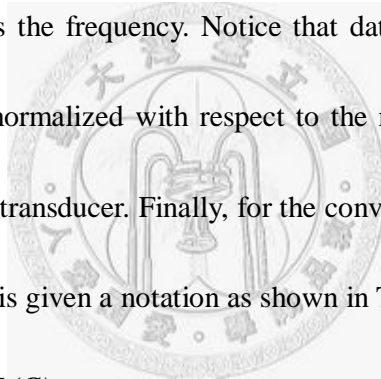
4.1 Epoxy-Ceramic Composite System

Three ceramic powders, ZrO_2 , Al_2O_3 and BaTiO_3 , are mixed separately with the epoxy to compare their impedance and attenuation values. Values of density, wave velocity inside, impedance and attenuation are listed at Table 4.1. The internal wave velocity is calculated by the reflection time of 1 MHz wave traveling through double thickness, and because of a 180° phase shift occurred at the composite-probe interface, a wave crest becomes a wave trough, as shown in Fig 4.1, and the selected points for calculation of reflection times and attenuation are marked.

The attenuation is increased after epoxy loaded with ceramic powders, due to the great quantities of ceramic-polymer interfaces to dissipate acoustic energy. However, the impedance of epoxy is too low for single matching layer application. A matching layer material with low attenuation and impedance close to 7 MRayl is desired for transmitting waves in the water/human tissues. The impedance for single matching layer is calculated by Eqn. 2.10. Al_2O_3 -epoxy composite has the lowest attenuation with the lowest impedance, and BaTiO_3 -epoxy composite has the highest attenuation with medium impedance. Therefore, ZrO_2 -epoxy composite is the most suitable material due to its impedance of close to 7 MRayl.

4.2 Active PZT Matching Layers

The behaviors of six types of PZT matching layers with four resonant frequencies (1, 2, 3 and 5 MHz) for each type, as listed in Table 3.2, are discussed here. Ultrasonic transducers with three resonant frequencies, 1 and 5 and 10 MHz, were utilized to determine the electromechanical and mechanical properties of the six active matching layers. The original frequency spectrums of the transducers without the active matching layer are shown in Fig. 4.2 with the vertical coordinate as the normalized amplitude and the horizontal coordinate as the frequency. Notice that data of frequency distributions shown in this chapter are normalized with respect to the maximum amplitudes of the original distributions of the transducer. Finally, for the convenience of comparison, each of the PZT matching layers is given a notation as shown in Table 4.2.



4.2.1 Electroded Poled PZT (G)

This section discussed the behaviors of poled electroded PZT matching layer. For a ultrasonic transducer of resonant frequency higher than that of the PZT matching layer, the original broad frequency distribution of the transducers is “filtered” into several frequency peaks separated by the same distance depending on the resonant frequency of the PZT matching layer. As shown in Fig. 4.3 Fig. 4.4, the frequency peaks are separated by 1, 2, 3 and 5 MHz when the PZT matching layers of resonant frequencies 1, 2, 3 and 5 MHz are integrated on to the transducers, respectively. In other words, the

filtered frequency peaks lie on the integer multiple numbers of the resonant frequency of the PZT matching layer applied.

It is believed that this filtration effect is dominant by the electromechanical properties of the matching layer. The higher harmonic modes of the PZT matching layer are excited, and energies are supplied by the broadband ultrasonic transducer. The positions of the peaks and how far they separated are determined by the resonant frequency of the thickness mode of the PZT layer. This idea can be seen in Fig. 4.5 and Fig. 4.6 where the PZT plates of different resonant frequencies are integrated onto the 10 MHz and 5 MHz transducers, respectively. The frequencies of the first peaks shown in these figures are the thickness mode resonant frequencies of the PZT matching layers, and all peaks are separated by these thickness mode frequencies. Take the 5 MHz PZT matching layer coupled with the 10 MHz transducer for example, the thickness resonant frequency of the 5 MHz PZT layer is about 5.5 MHz (processing fluctuation), and thus the second peaks lies on 11 MHz.

When the 1 MHz transducer is coupled with the 1 MHz PZT layer, similar behaviors are observed. In contrast, when coupled with the 2, 3 and 5 MHz PZT matching layers, only some low frequency components are transmitted through the PZT matching layers, as shown in Fig. 4.7. This is because that (1) the 1 MHz transducer does not have enough energy output in the high frequency range, and (2) the lower natural frequency

modes of the PZT plates are “channels” for releasing the acoustic waves (explained more in section 4.2.3). As the thickness of the PZT layer decreases, the amplitude of the transmitted low frequency component increases. Fig. 4.7 shows that the amplitude of the transmitted wave surpasses the original profile of the 1MHz transducer when it is attached with the 5 MHz PZT layer. This effect is caused by the mechanical properties of the PZT layer and is further discussed in Section 4.2.3 using unpoled PZT matching layers, which exhibit the same behaviors.



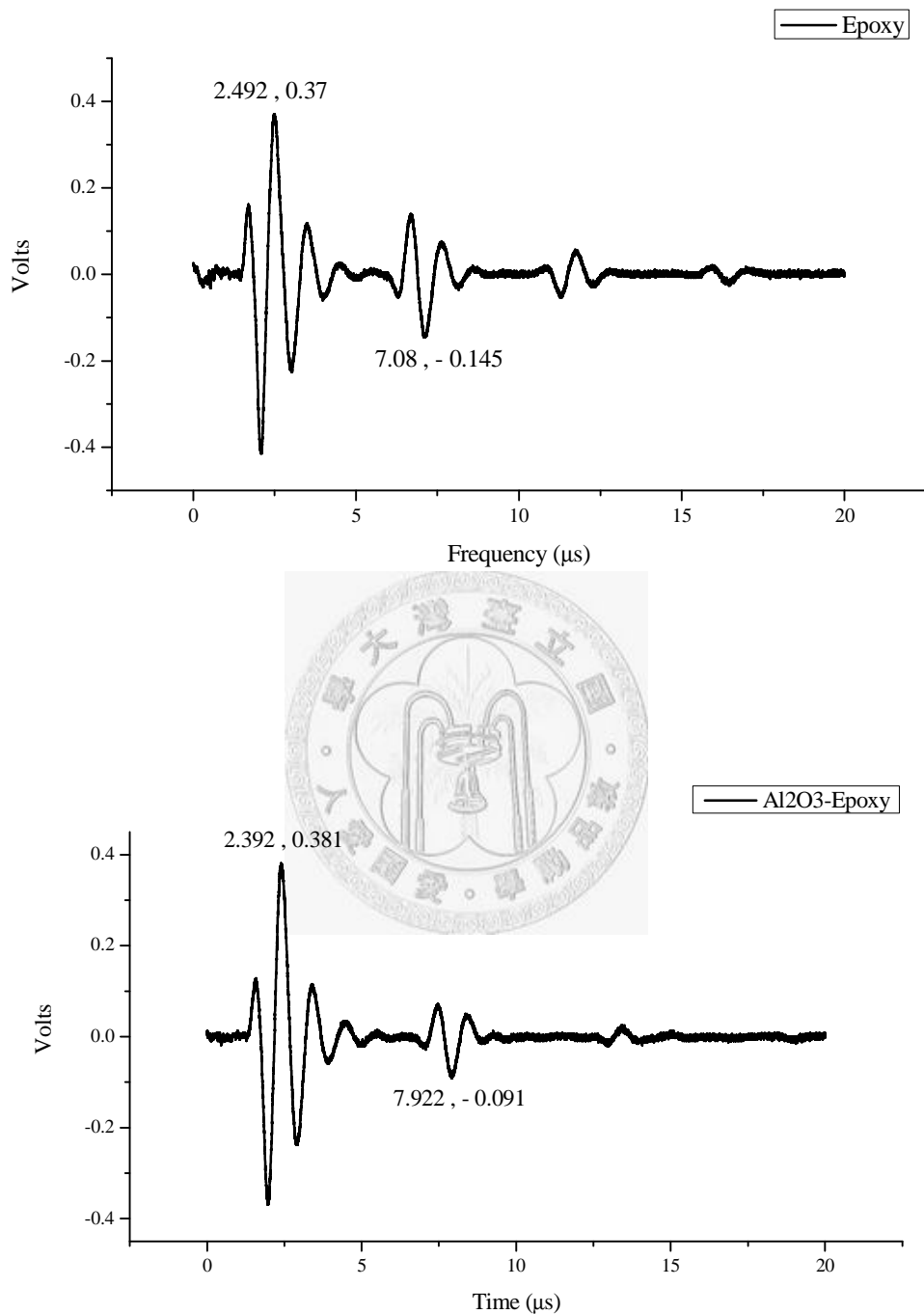
Table 4.1 Parameters of ceramic-epoxy composites

Composite	Density (g/cm ³)	Velocity (m/s)	Impedance (MRayl)	Attenuation (Np/cm)
Epoxy	1.162	2566.260	2.982	0.797
Al ₂ O ₃ -Epoxy	1.748	2835.081	4.956	0.916
ZrO ₂ -Epoxy	2.517	2503.831	6.302	0.973
BaTiO ₃ -Epoxy	2.633	2322.122	6.114	1.095



Table 4.2 Symbols for six types of PZT matching layers

Type	Name	Symbol	Poling	Electrode	Connecting Electrodes	Matching Layer (ZrO_2 composite)
1	Electroded poled	G	Yes	Yes	No	No
2	Short-circuited poled	EC	Yes	Yes	Yes	No
3	Unpoled	U	No	Yes	No	No
4	Unpoled, without Electrodes	UN	No	No	No	No
5	Electroded poled with second composite matching layer	GML	Yes	Yes	No	Yes
6	Short-circuited poled with second composite matching layer	ECML	Yes	Yes	Yes	Yes



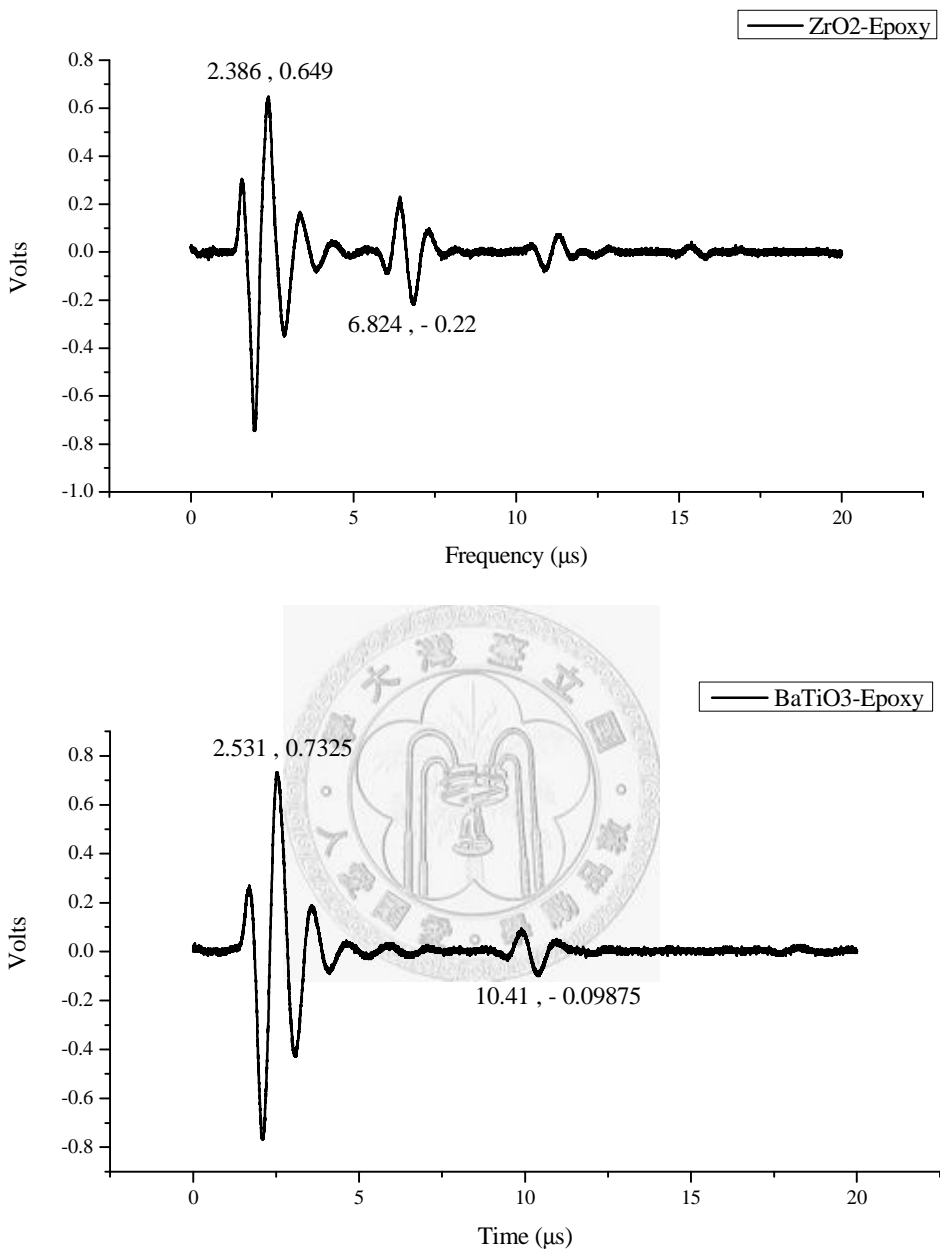


Figure 4.1 Wave reflections in epoxy and ceramic-epoxy composites.

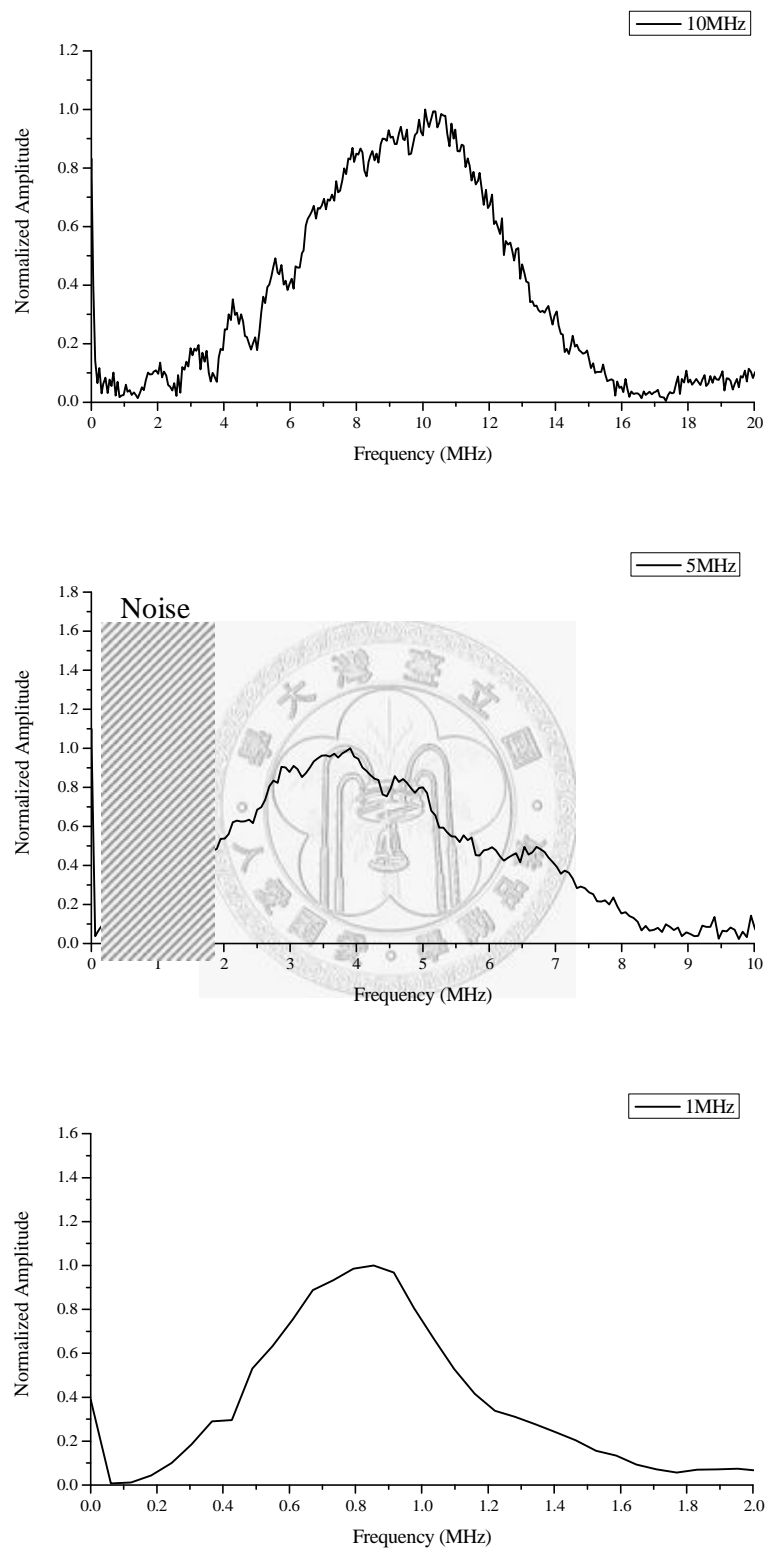


Figure 4.2 Original frequency distributions of 1, 5 and 10 MHz transducers.

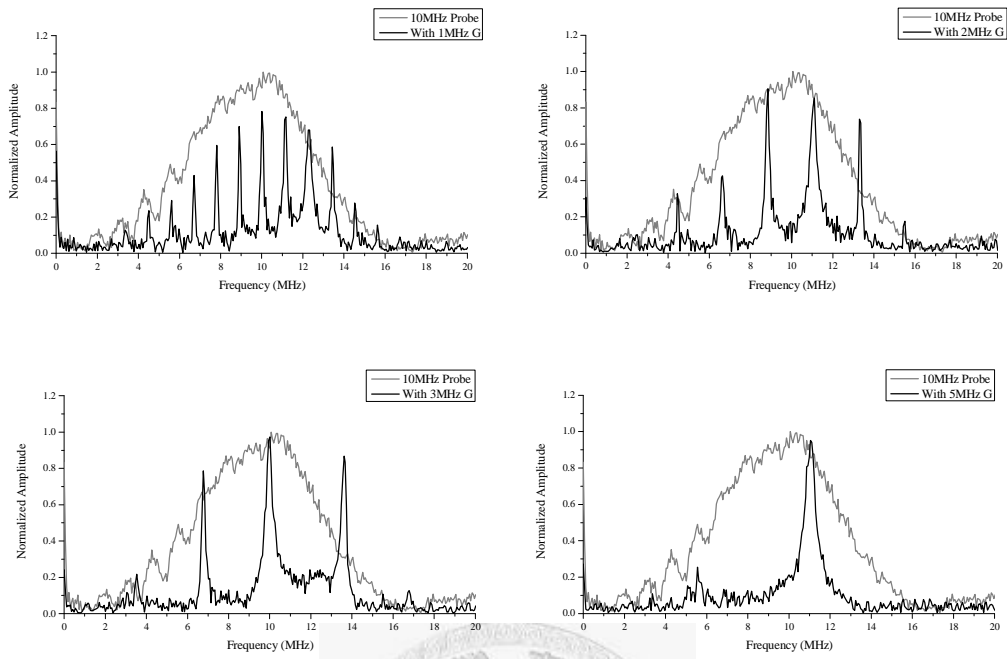


Figure 4.3 Electroded poled PZT plates characterized by 10 MHz transducer.

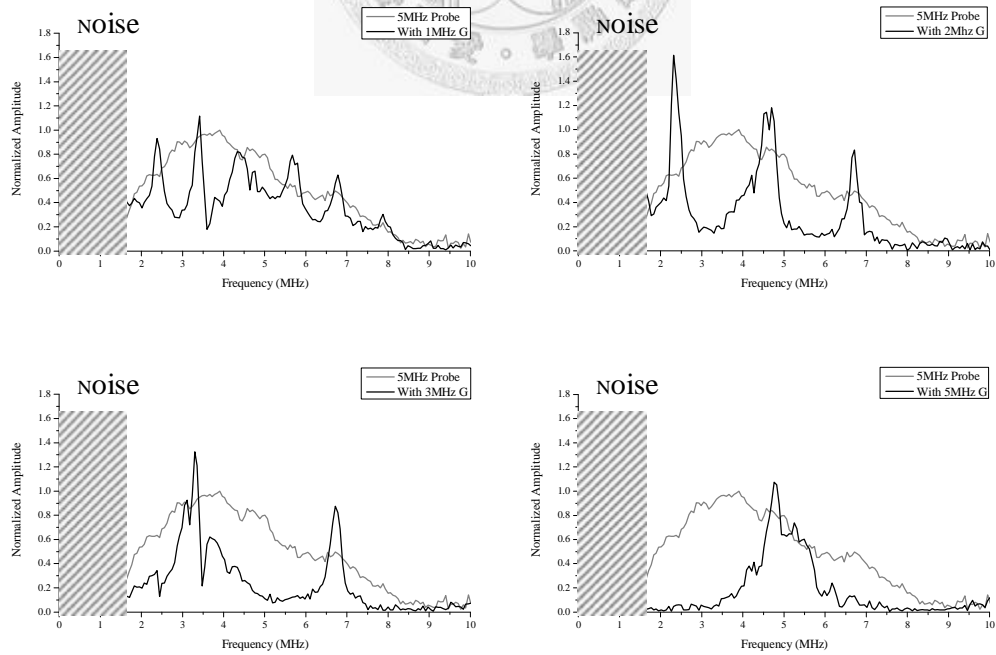
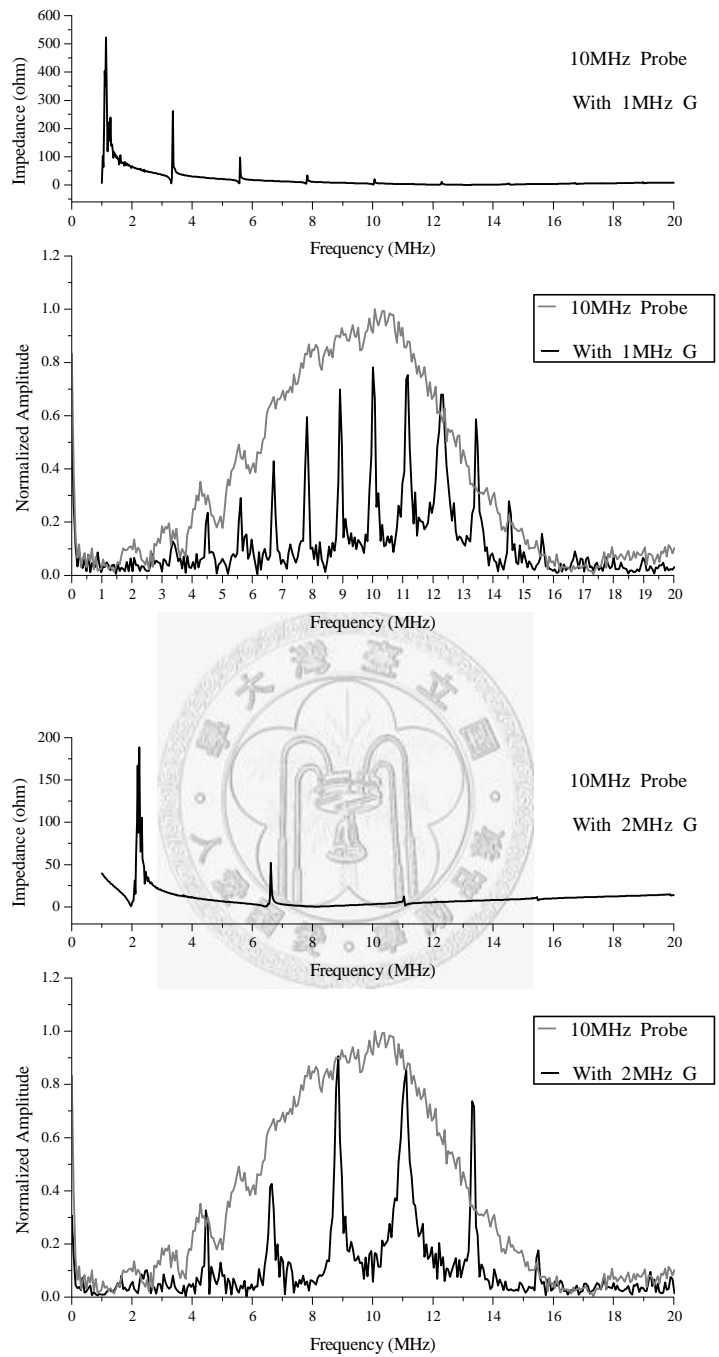


Figure 4.4 Electroded poled PZT plates characterized by 5 MHz transducer.



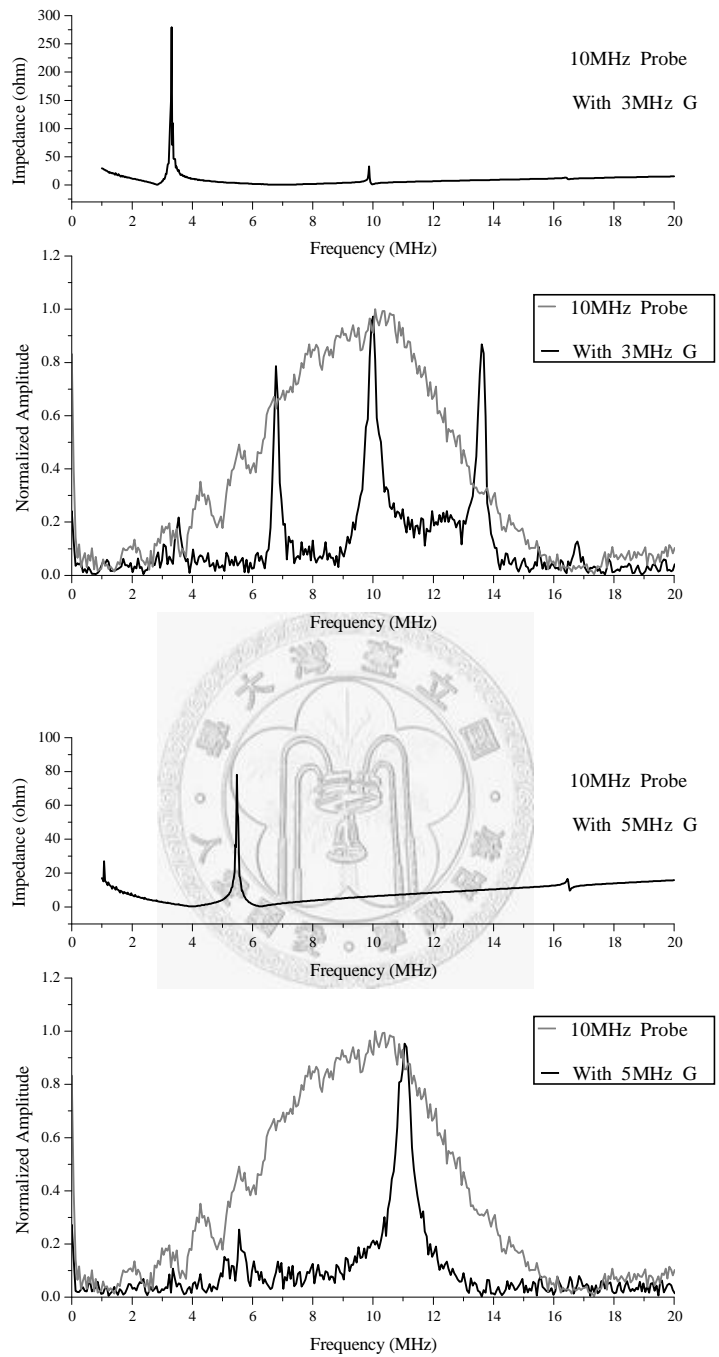
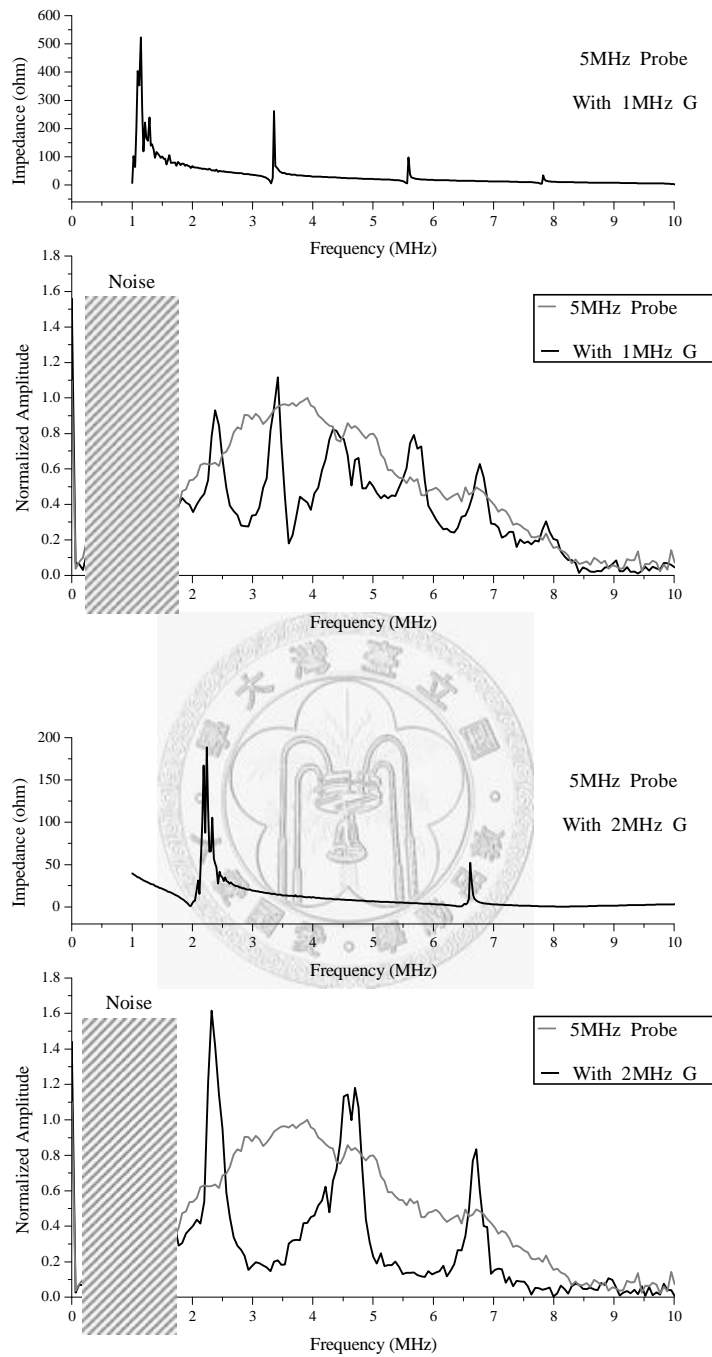


Figure 4.5 Frequency distributions of the 10 MHz transducer based on the piezoelectric resonant frequencies of the matching PZT plates.



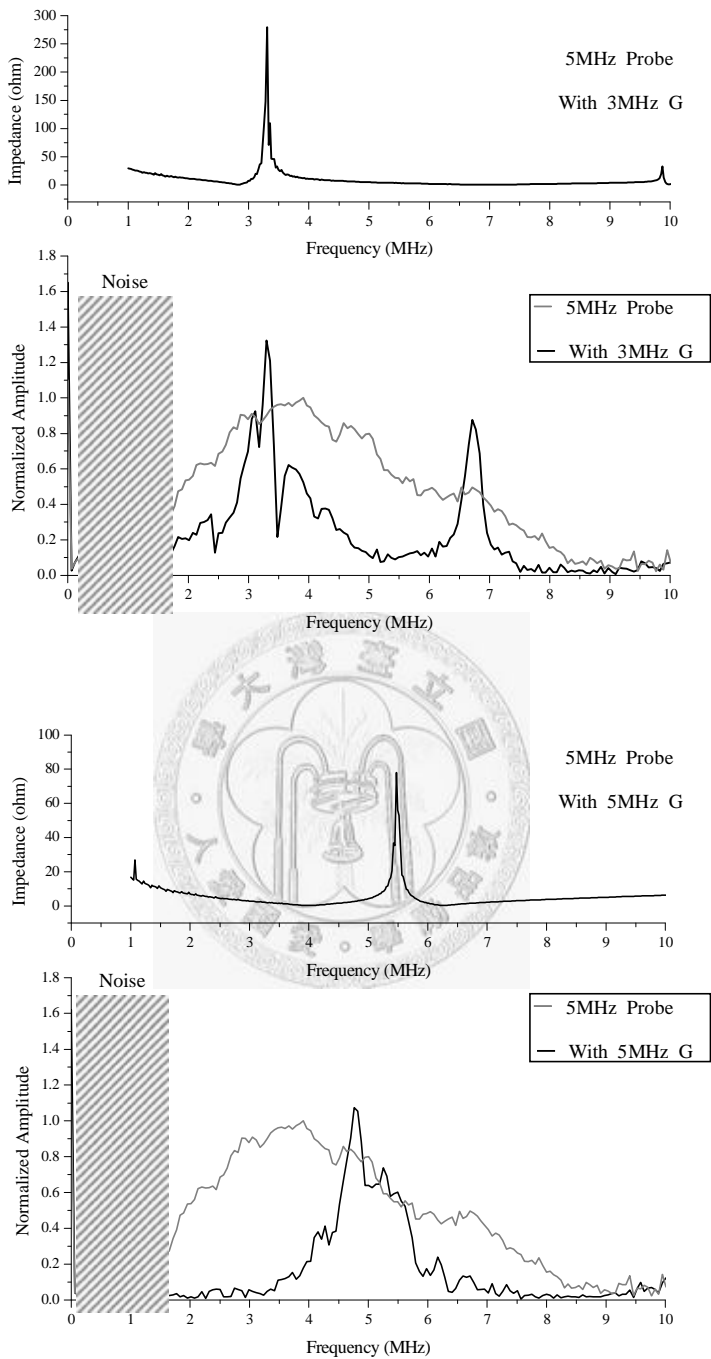


Figure 4.6 Frequency distributions of the 10 MHz transducer based on the piezoelectric resonant frequencies of the matching PZT plates.

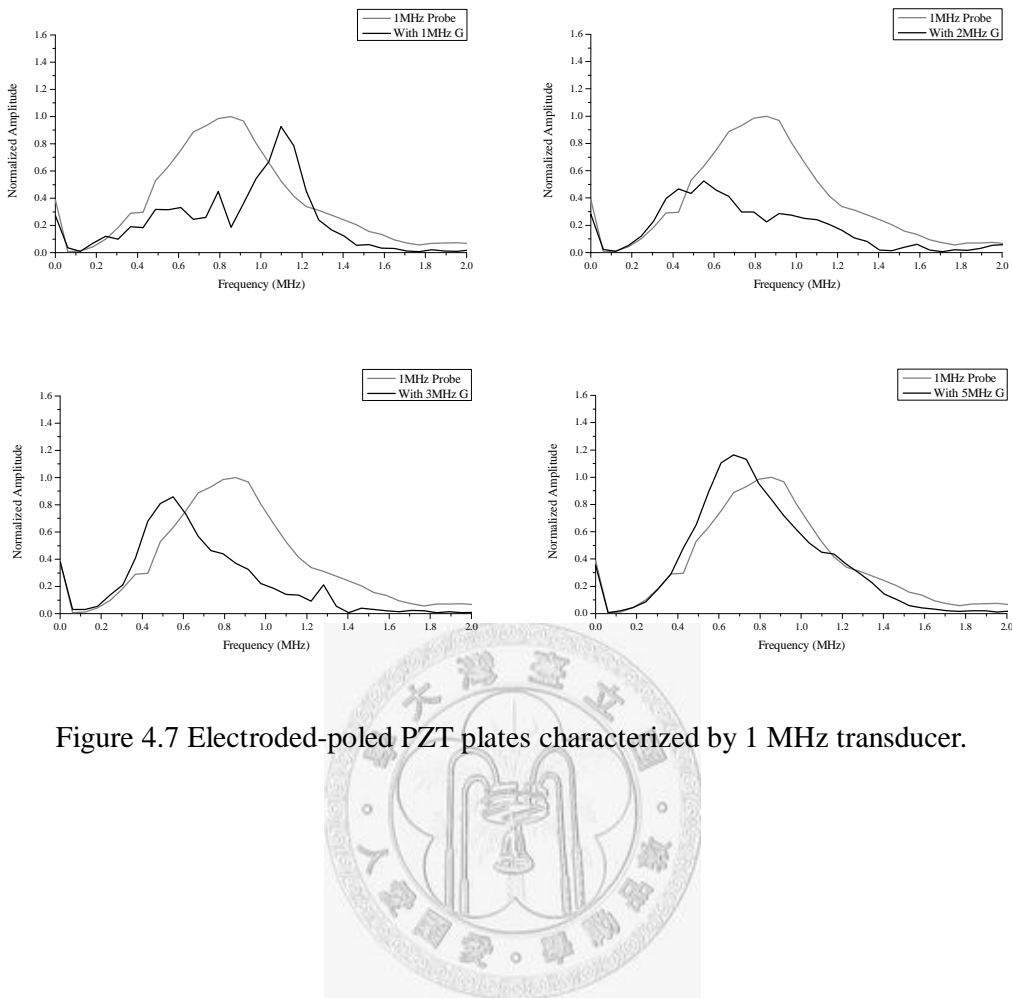


Figure 4.7 Electroded-poled PZT plates characterized by 1 MHz transducer.

4.2.2 Short-Circuited Poled PZT (EC)

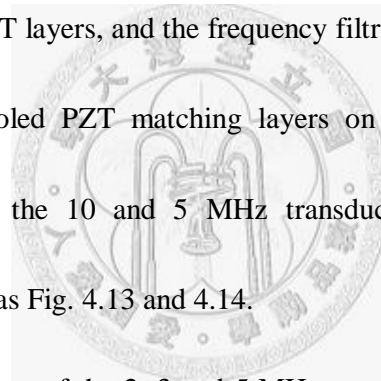
The two electrodes of the poled PZT matching layers are connected to form a short-circuited condition. The same behaviors on the frequency distribution as the open-circuited layers are observed for the short-circuited PZT matching layers. These short-circuited PZT matching layers not only filter the original broad frequency distributions of the transducers, but also make every peak frequency sharper and cleaner as shown in Fig. 4.8, 4.9 and 4.10 for the 10, 5, and 1 MHz transducers, respectively.

When encountering a mechanical strain, the piezoelectric characteristics of PZT induce an electric field which causes a mechanical movement to counter the external strain (see Fig. 4.11). Short-circuiting the PZT matching layers eliminates the piezoelectric effects and makes the layers vibrate more freely. Hence, the frequency peaks are sharper and cleaner.

4.2.3 Unpoled PZT (U)

Unpoled PZT matching layers do not have the electromechanical vibration modes induced by piezoelectricity. However, for the unpoled PZT matching layers coupled with the 10 and 5 MHz transducers, the frequency filtration behaviors are similar to the electroded poled PZT matching layers. The positions and separated distance of the peaks depend on the thickness of the coupled layer. This is a mechanical dominant effect governed by the traveling length and interference of reflected waves. Fig. 4.12

shows the wave forms of the reflected waves come to multiple times within a 1 MHz unpoled PZT matching layer. It is evident that all reflected waves are in phase without shift when leaving the PZT layer. The thickness of a commercial PZT plate is designed as the half wavelength of its resonant frequency ^[10]. With this half wavelength thickness and the behavior of reflection without phase shift, the travel length of a wave within the PZT plate under even number reflections is the integer multiple of its wavelength. Hence, the reflected waves interfere constructively at frequencies close to the resonant frequencies of the poled PZT layers, and the frequency filtration behaviors are similar to those of the electroded poled PZT matching layers on ultrasonic transducers. The frequency distributions at the 10 and 5 MHz transducers with the unpoled PZT matching layers are shown as Fig. 4.13 and 4.14.



The frequency distributions of the 2, 3 and 5 MHz unpoled PZT matching layers on the 1 MHz transducer, are similar whether the layers are poled or unpoled (see Fig. 4.15). This is believed to be a mechanical vibration (i.e. natural frequency) dominant effect. The nature frequencies of a circular plate are obtained by the Roark's formulation ^[43], determined as below :

$$f = \frac{K_n}{2p} \sqrt{\frac{Et^3 g}{12(1-\nu^2)}} \dots (4.1)$$

where E is the Young's modulus, v is the Poisson's ratio, t is the thickness, w is the weight, r is the radius, and g is the gravitational acceleration. K_n is an empirical value

and is listed for four modes as ^[43] : $K_1 = 5.25$, $K_2 = 9.08$, $K_3 = 12.2$, and $K_4 = 20.5$

And the Young's modulus of the PZT plates applied in this study is ranged from 53 to 61 GPa, and the Poisson's ratio is about 0.31. Notice that Equ. 4.1 is only suitable for circular plates.

Based on the calculations of the Roark's formulation, the natural frequency compared with the frequencies of a circular PZT plate are distributions of the 2, 3 and 5 MHz PZT matching layers on the 1 MHz transducer, shown in Fig. 4.16 (a), (b), and (c), respectively. The upper plot in the figure is the natural frequencies calculated using a Young's modulus of 57 GPa. The lower plot in the figure is the frequency distribution of the transducer. The gray line, dark line, and gray-dash line represent the frequency distributions of the transducer alone, transducer with unpoled PZT plate, and transducer with electroded poled PZT plate matching layers, respectively. The natural frequencies calculated for the circular PZT plate are listed in Table 4.3 (a) and (b).

Fig. 4.16 shows an increase in frequency amplitude when the 1 MHz transducer adds on an unpoled 5 MHz PZT matching layer. The 5 MHz unpoled PZT plate has three natural frequency modes below 1 MHz, while 2 MHz unpoled PZT plate has just one. The reason why the frequency amplitude of the 1MHz transducer with the 5 MHz unpoled PZT matching layer is higher than the original amplitude of the 1 MHz transducer alone is because that more acoustic waves can be transmitted via the low

natural frequency modes. Fig. 4.16 also shows that the frequency the amplitudes of the transducer with the 2, 3 and 5 MHz unpoled PZT matching layers are slightly higher than those with the electroded poled PZT matching layers. This is likely due the lost of Piezoelectricity as explained in Section 4.2.2.

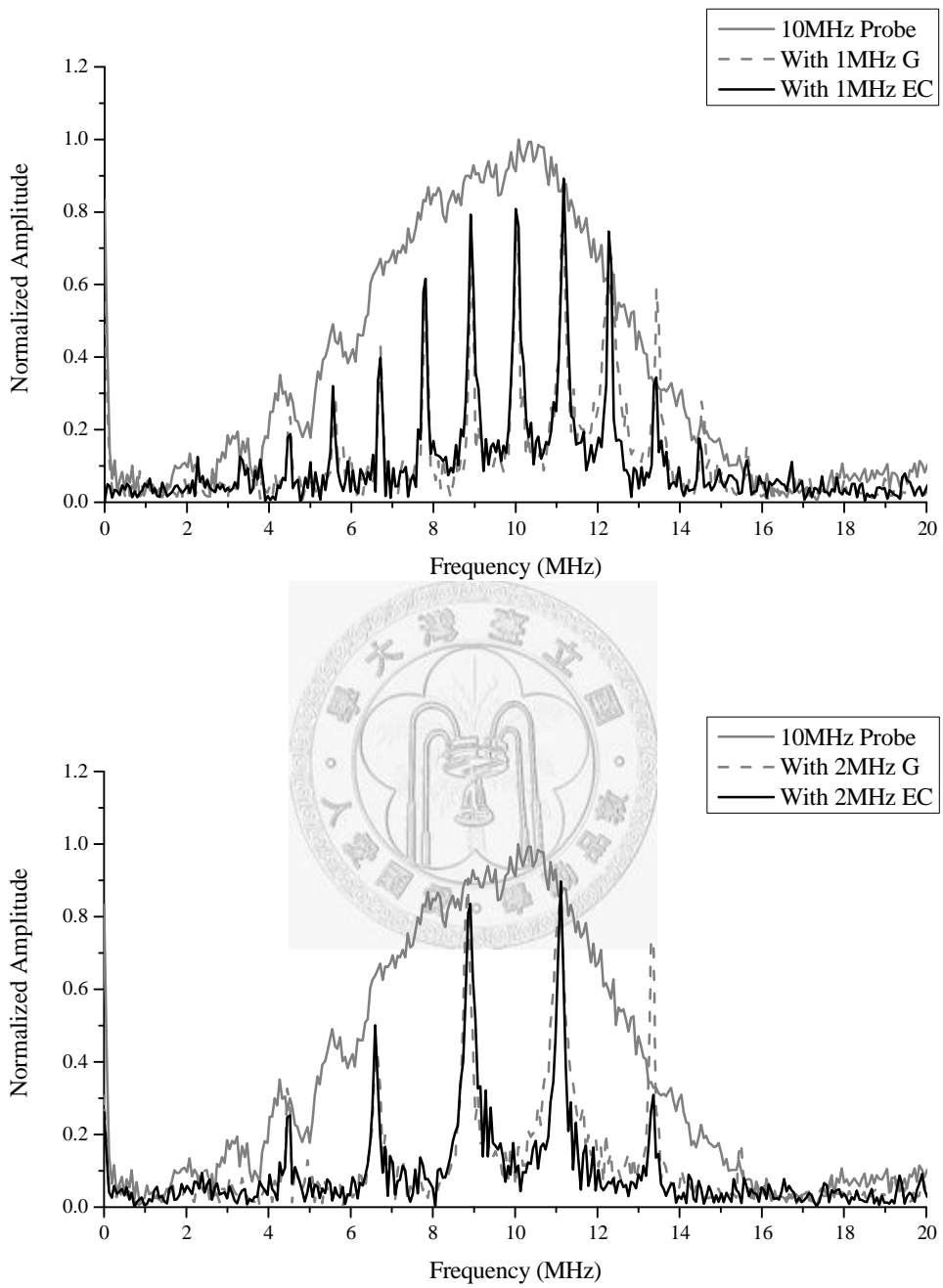


Table 4.3 (a) Natural frequency modes for PZT circular plates with E = 53 GPa.

PZT	Mode 1 (MHz)	Mode 2 (MHz)	Mode3 (MHz)	Mode 4 (MHz)
1 MHz	1.228	2.124	2.854	4.796
2MHz	0.644	1.114	1.496	2.515
3MHz	0.411	0.710	0.954	1.603
5MHz	0.252	0.436	0.586	0.985

Table 4.3 (b) Natural frequency modes for PZT circular plates with E = 61 GPa.

PZT	Mode 1 (MHz)	Mode 2 (MHz)	Mode3 (MHz)	Mode 4 (MHz)
1 MHz	1.317	2.279	3.062	5.070
2MHz	0.691	1.195	1.606	2.659
3MHz	0.440	0.762	1.024	1.695
5MHz	0.271	0.468	0.629	1.041



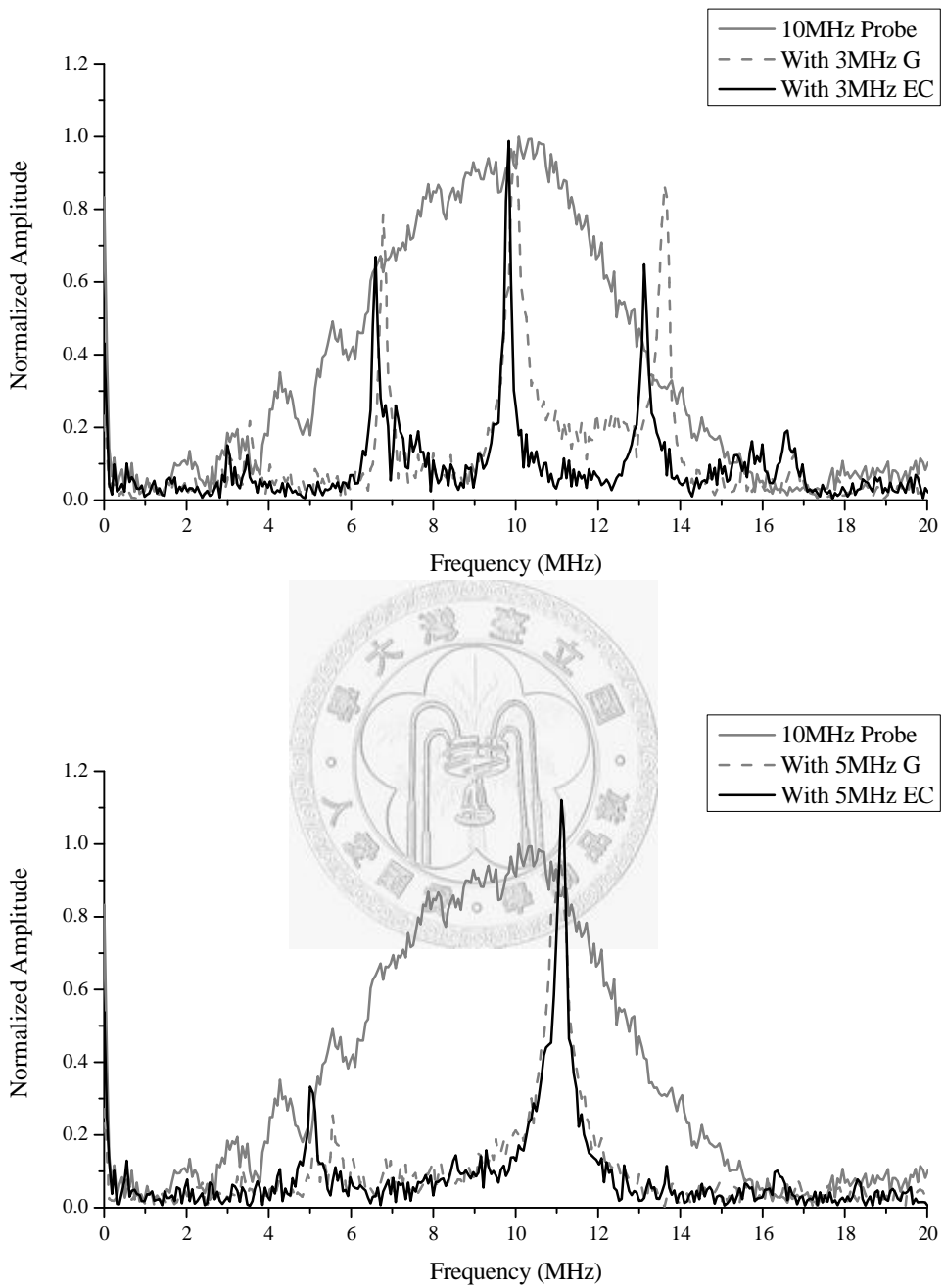
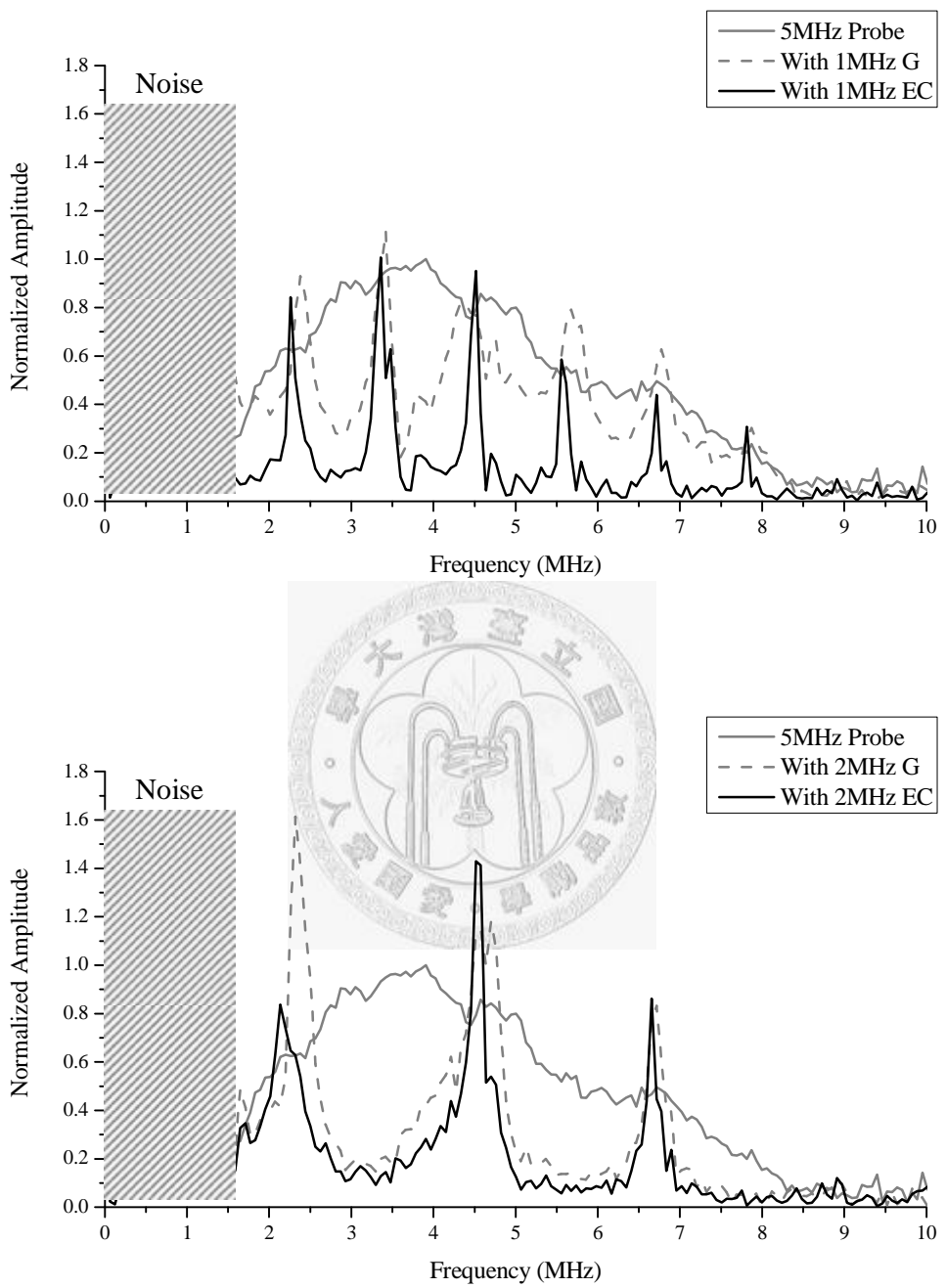


Figure 4.8 Short-circuited PZT plates (EC) characterized by the 10 MHz transducer, compared with electroded poled PZT plates (G).



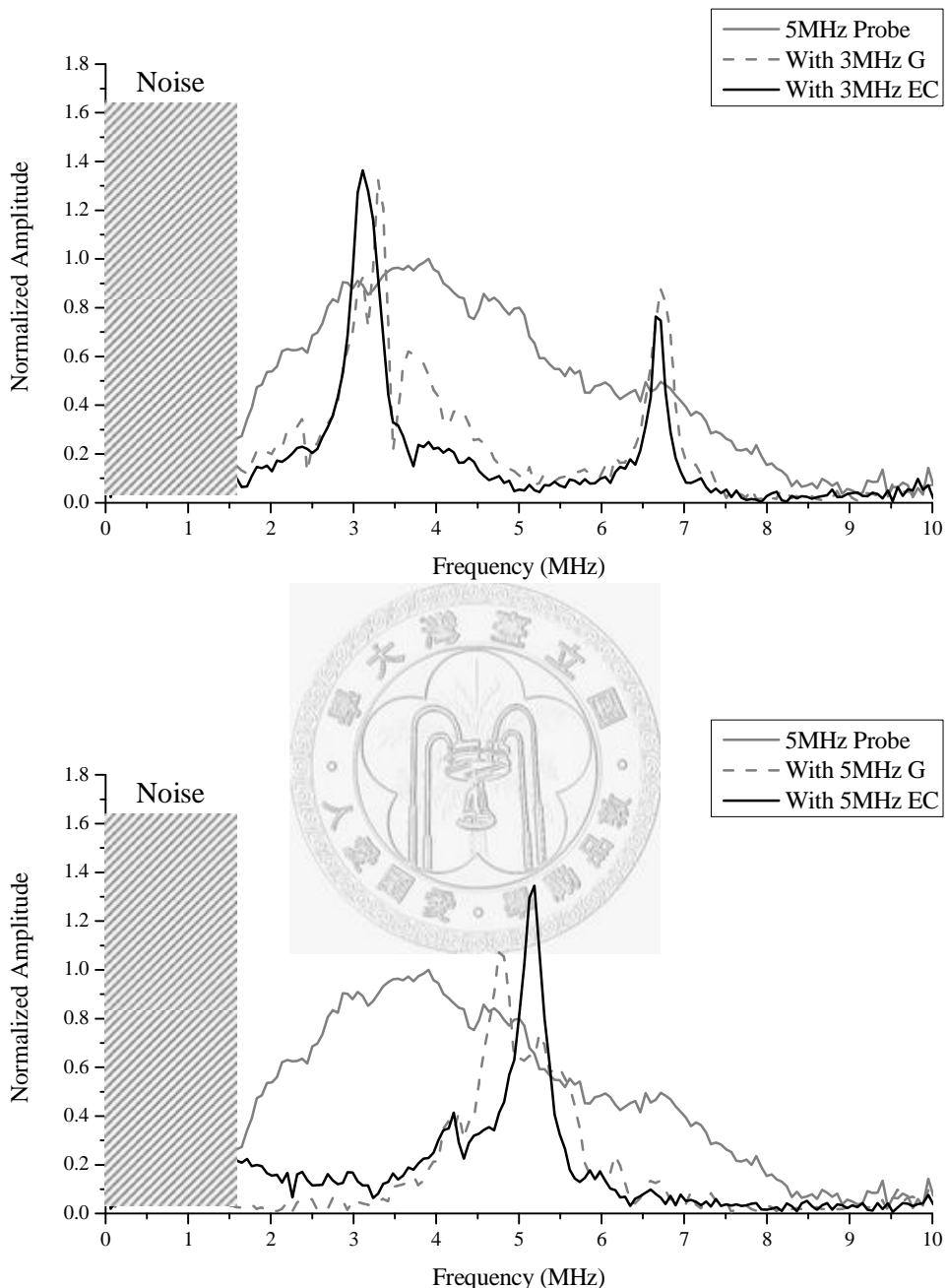
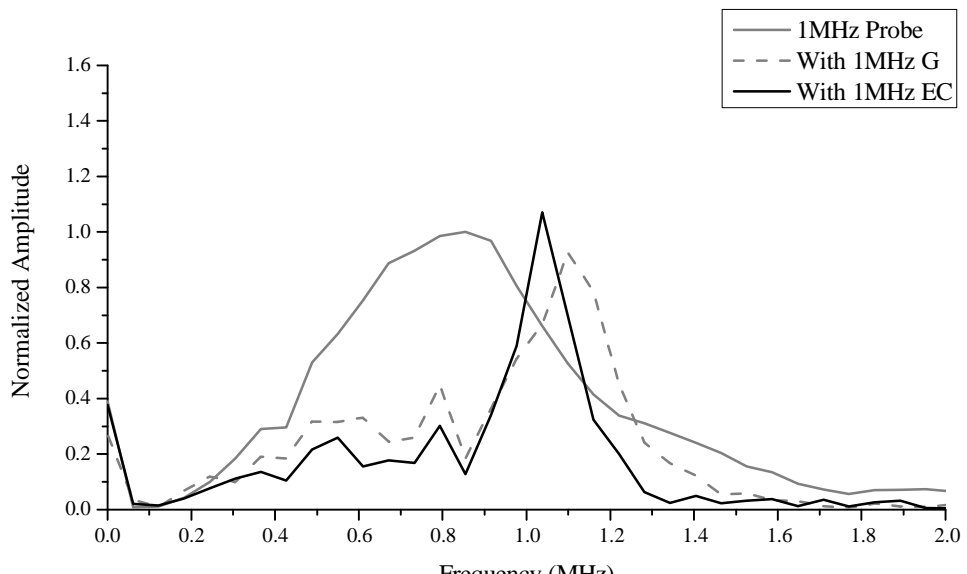
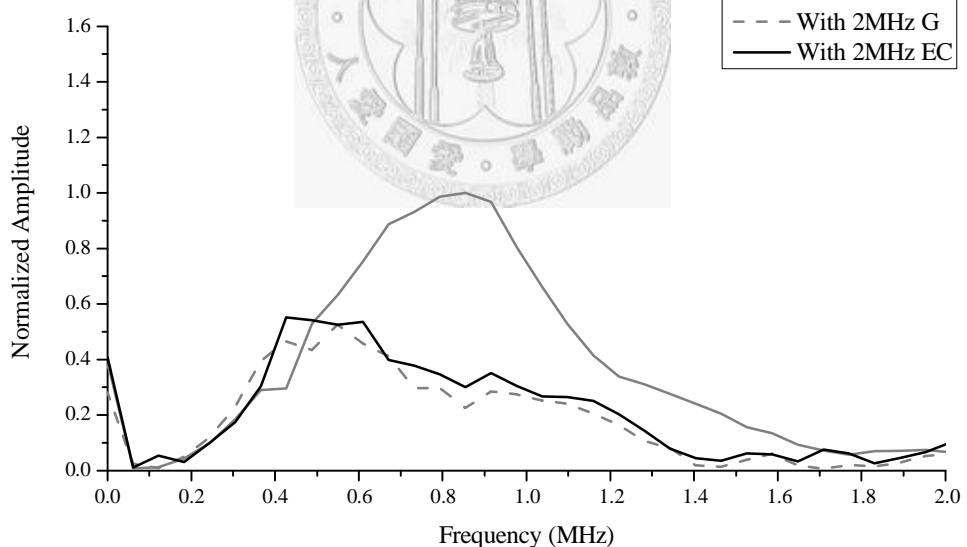


Figure 4.9 Short-circuited PZT plates (EC) characterized by the 5 MHz transducer, compared with electroded poled PZT plates (G).



Legend:

- 1MHz Probe (Solid Line)
- With 2MHz G (Dashed Line)
- With 2MHz EC (Solid Line)



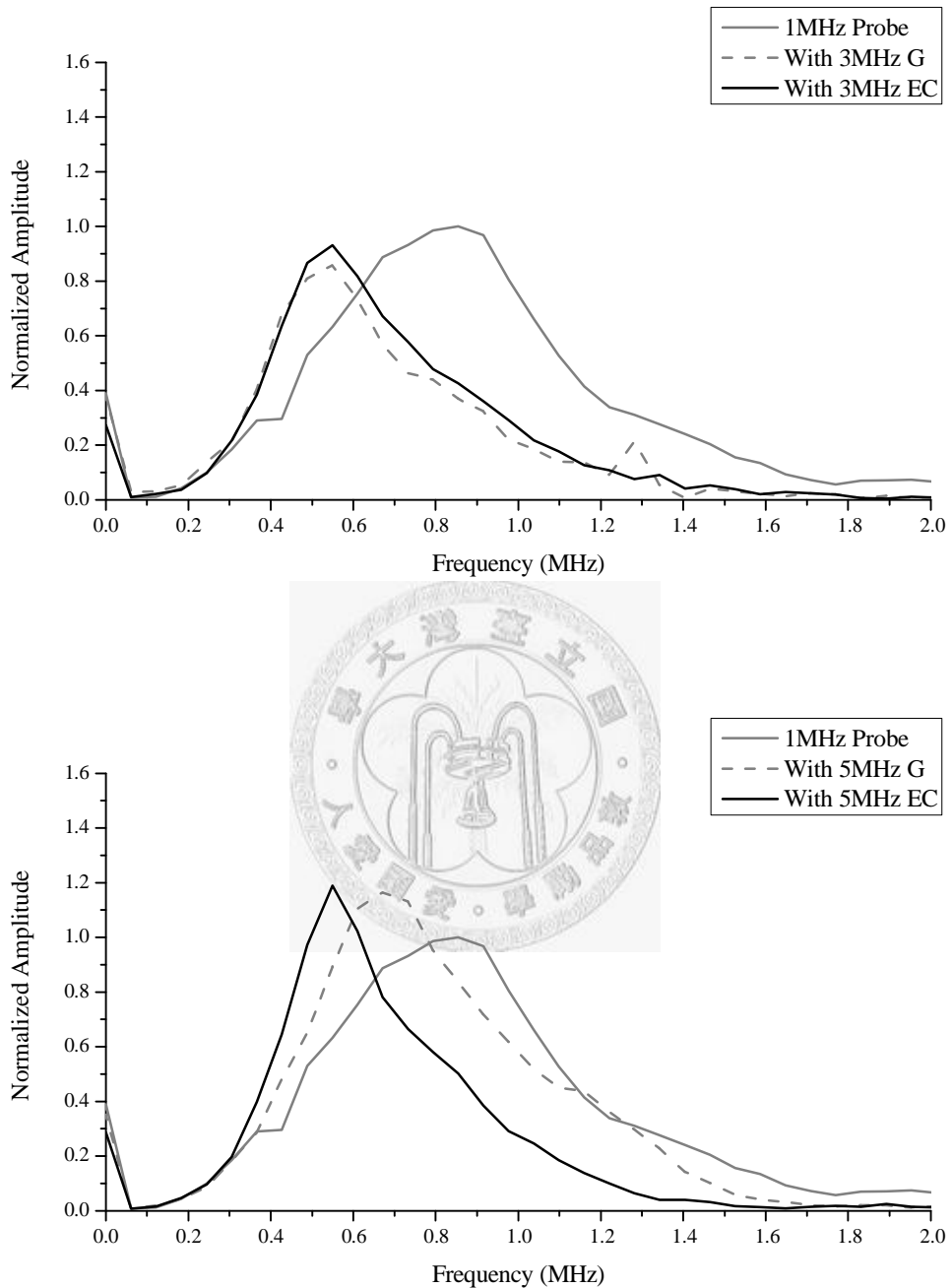


Figure 4.10 Short-circuited PZT plates (EC) characterized by the 1 MHz transducer, compared with electroded poled PZT plates (G).

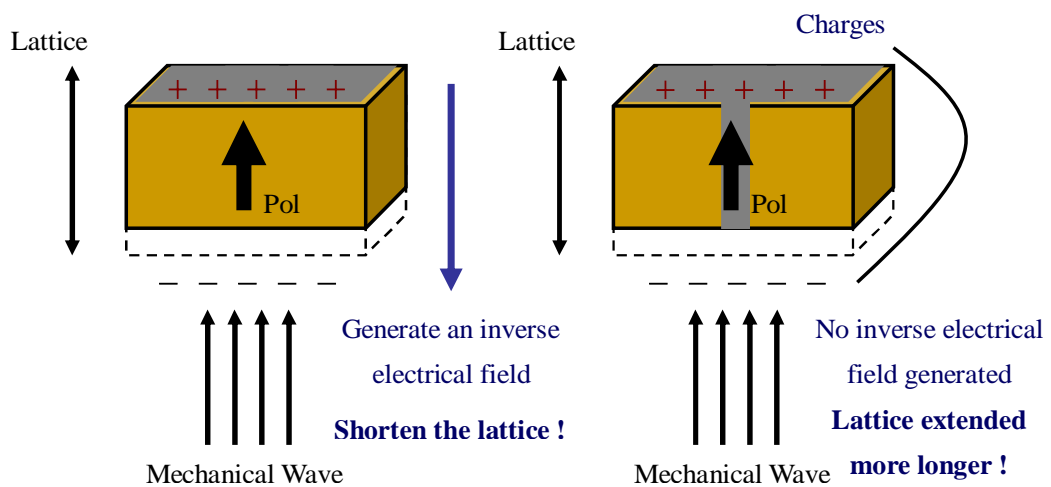


Figure 4.11 Effect of elimination of induced inverse electric field by poled PZT with

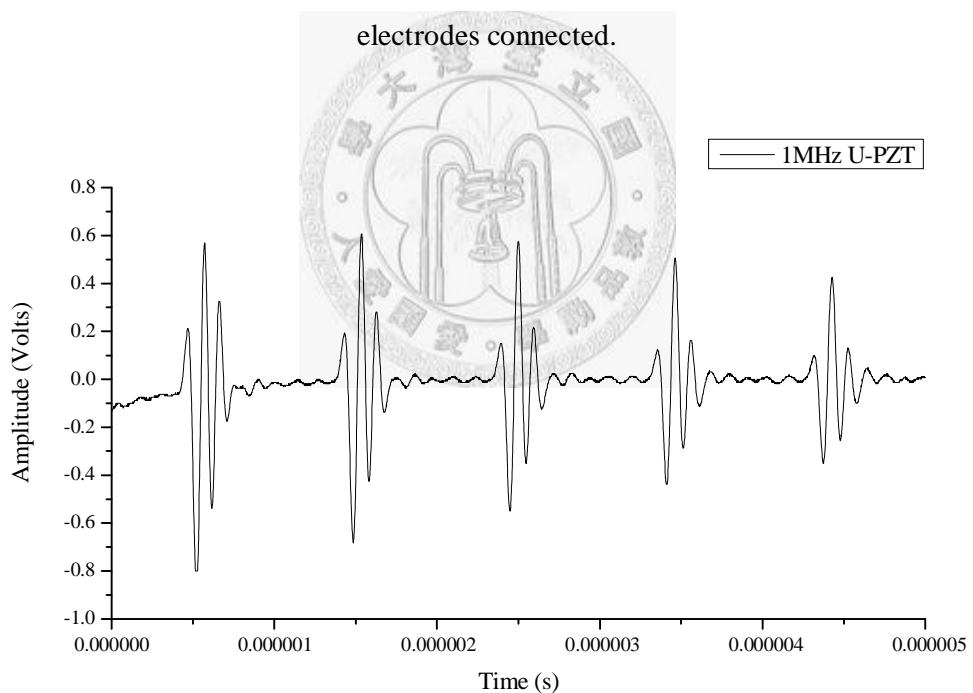
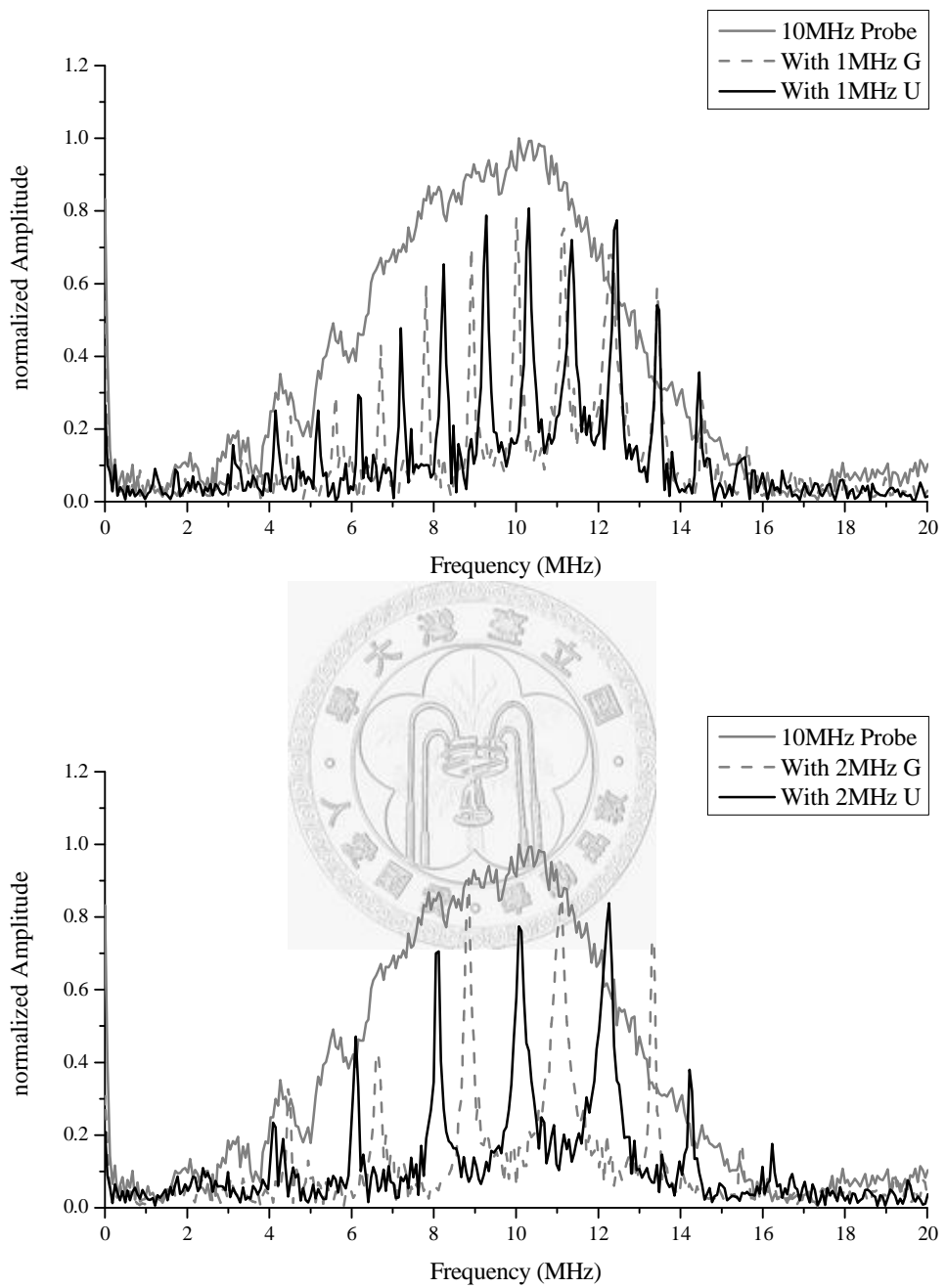


Figure 4.12 Reflected wave forms inside 1 MHz unpoled PZT.





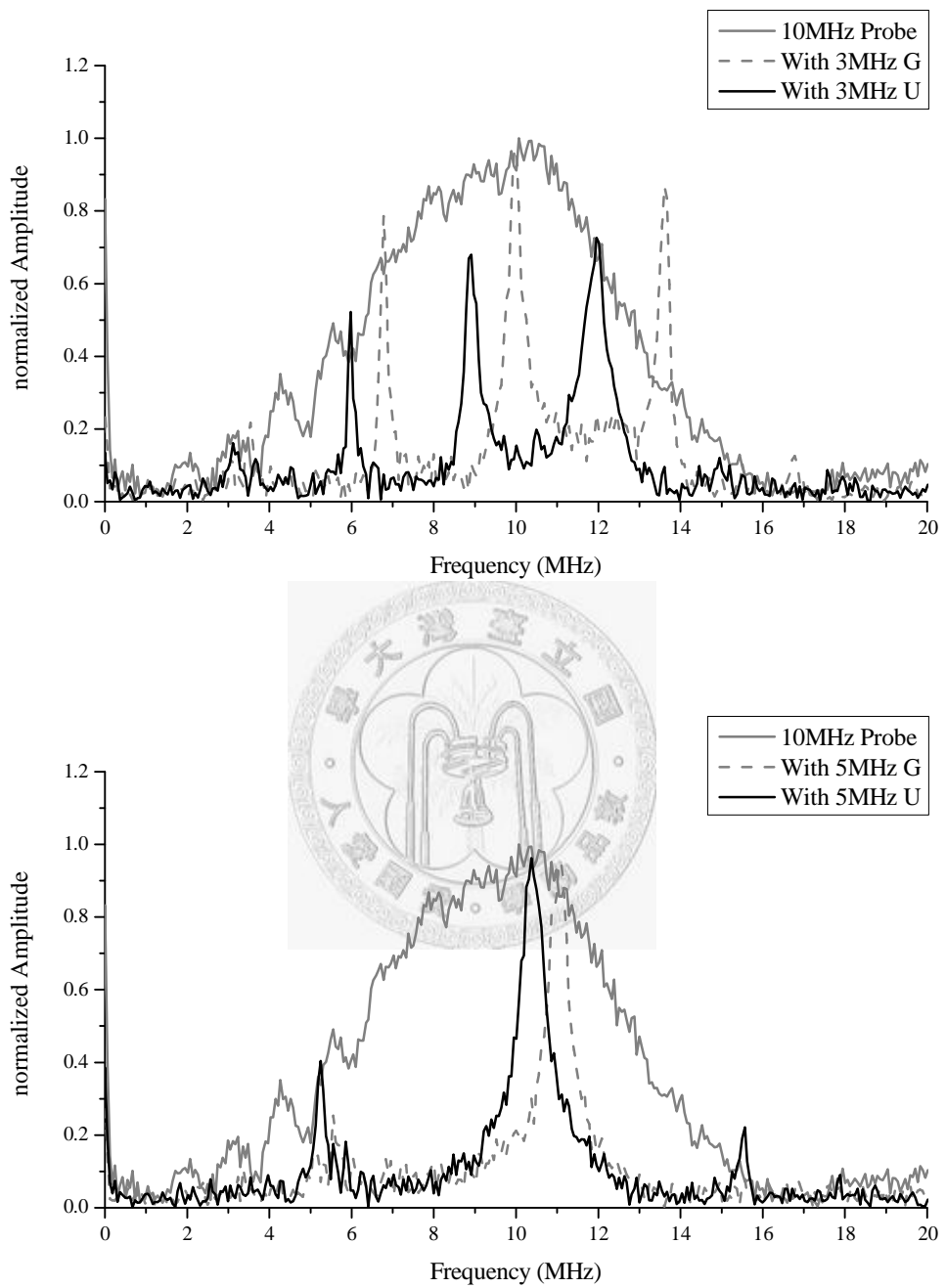
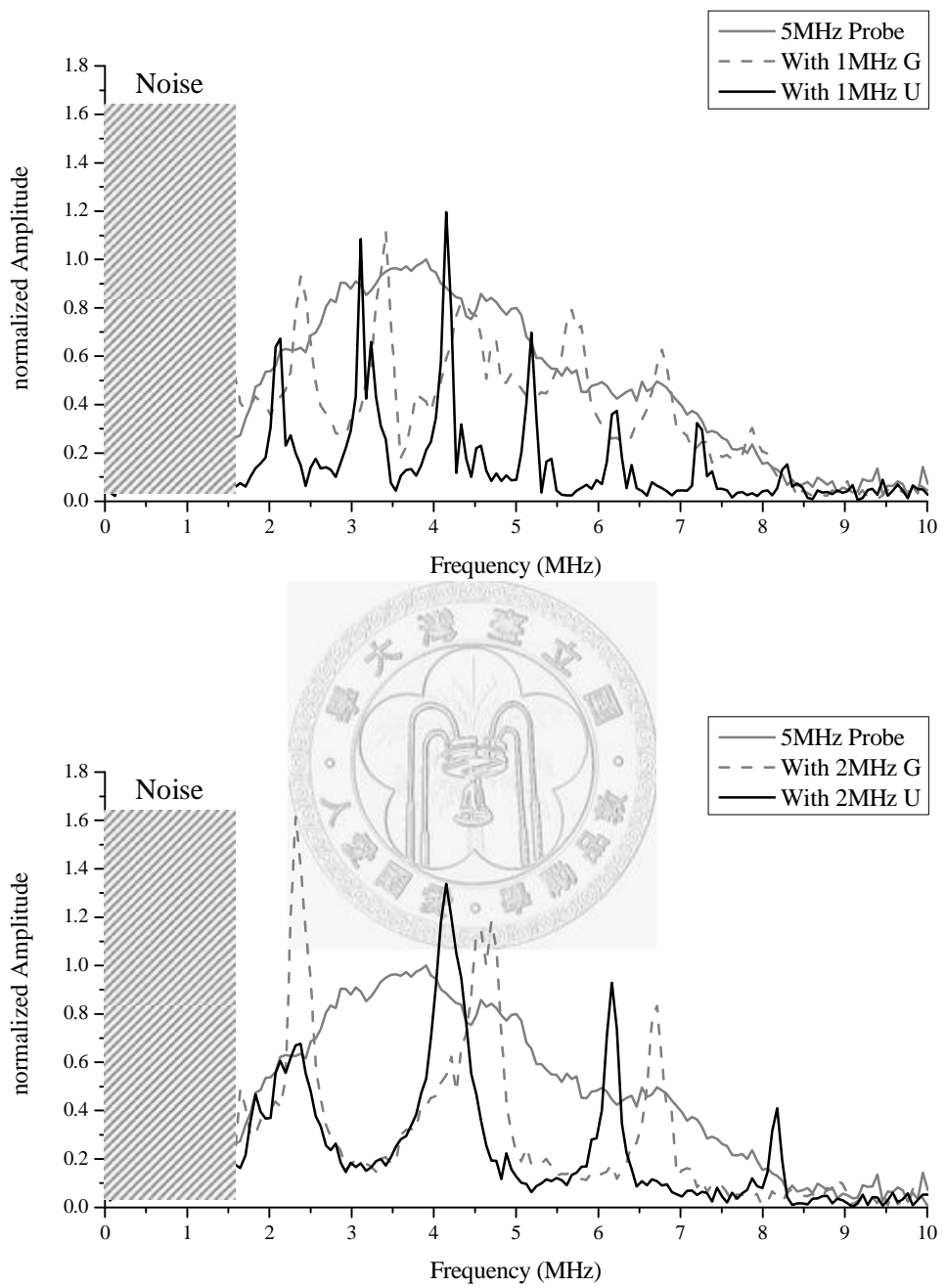


Figure 4.13 Unpoled PZT plates (U) characterized by the 10 MHz transducer, compared with electroded poled PZT plates (G).



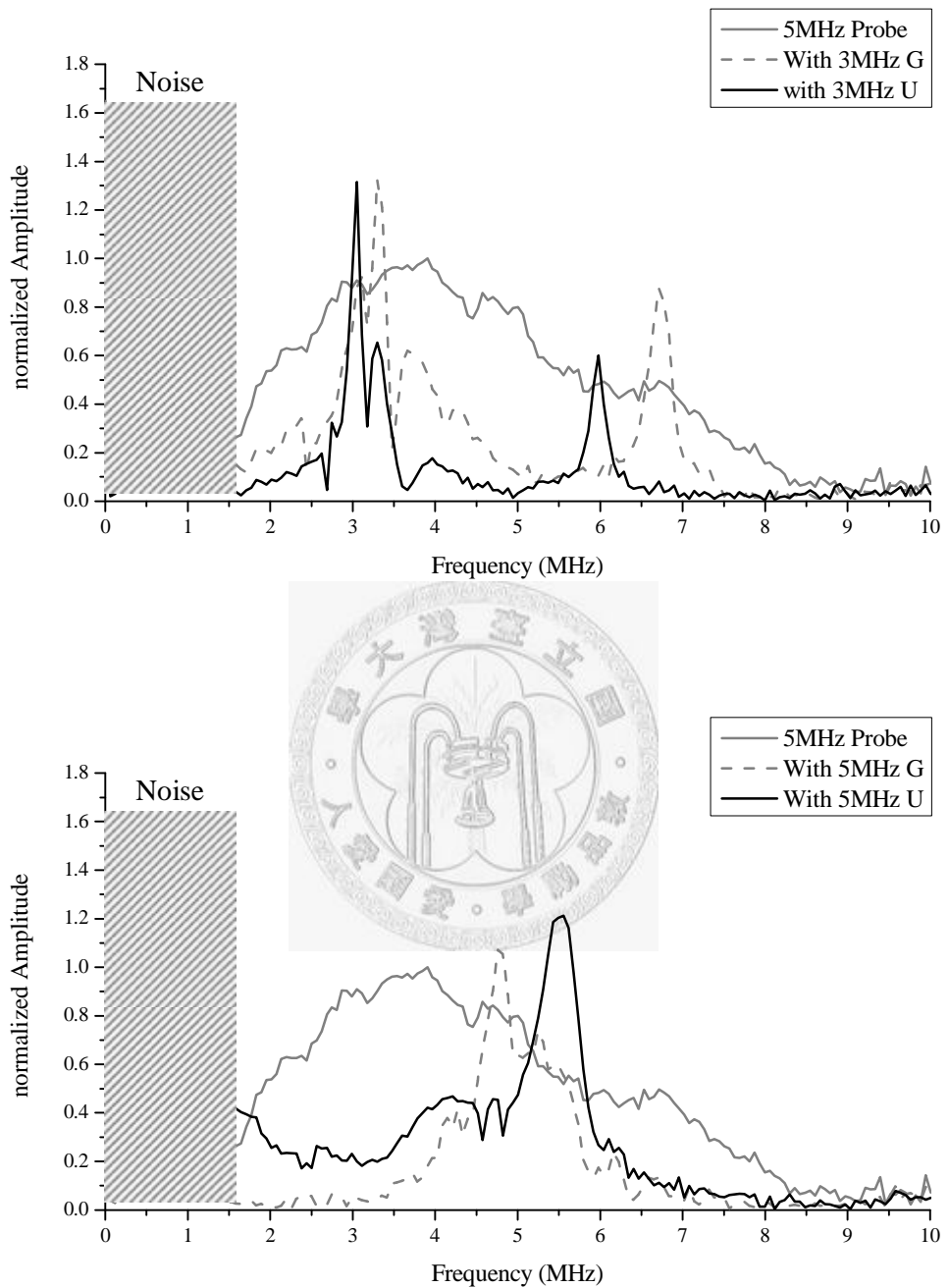
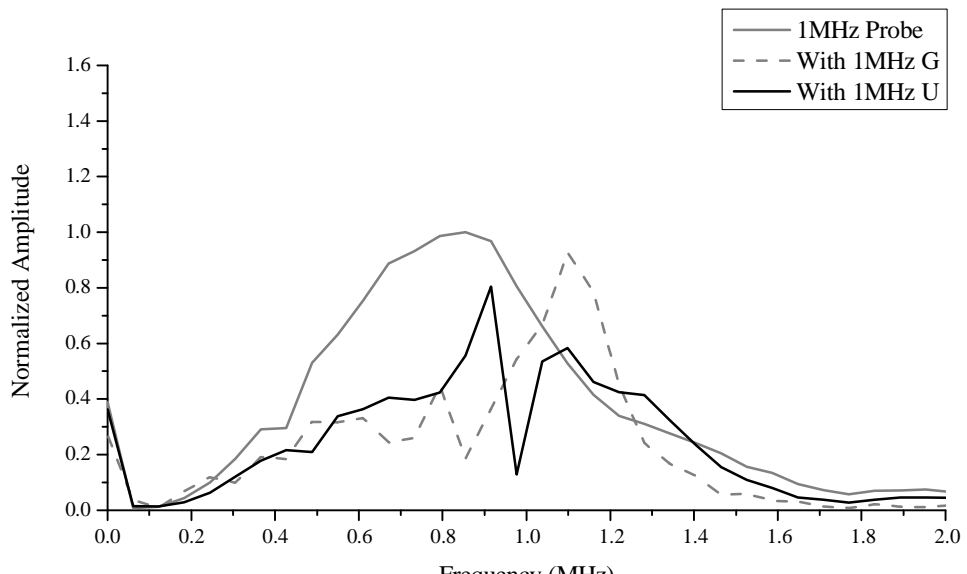
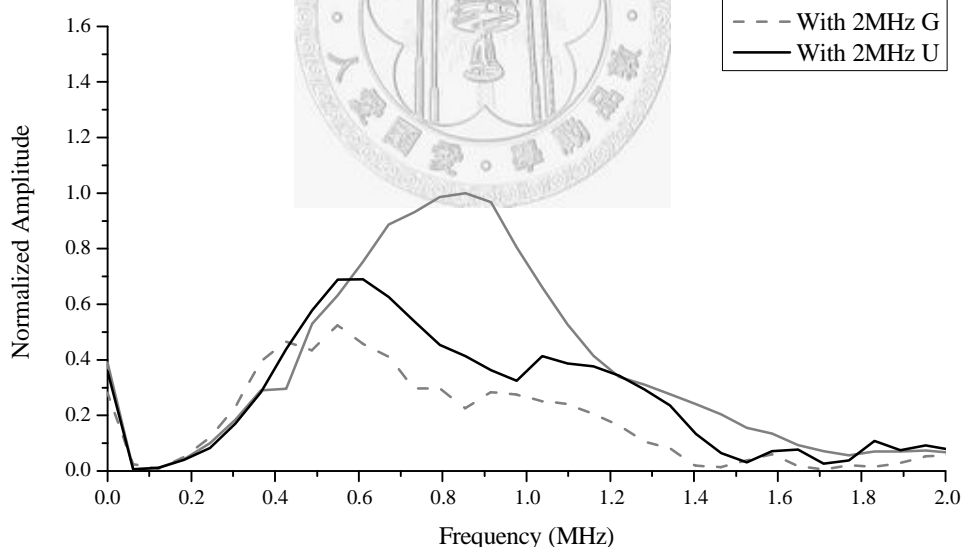


Figure 4.14 Unpoled PZT plates (U) characterized by the 5 MHz transducer, compared with electroded poled PZT plates (G).



Legend:

- 1MHz Probe (Solid Line)
- With 2MHz G (Dashed Line)
- With 2MHz U (Solid Line)



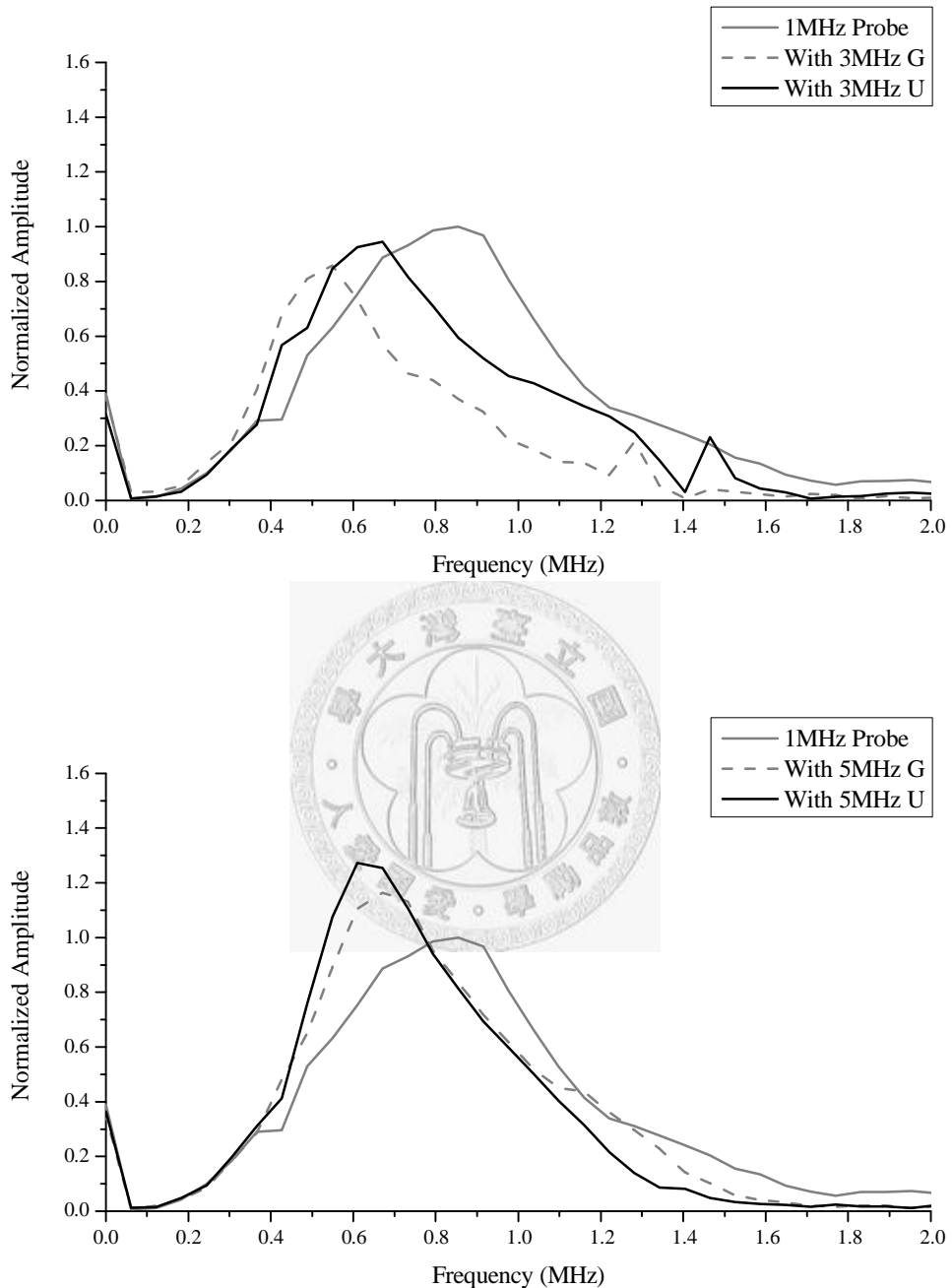


Figure 4.15 Unpoled PZT plates (U) characterized by the 1 MHz transducer, compared with electroded poled PZT plates (G).

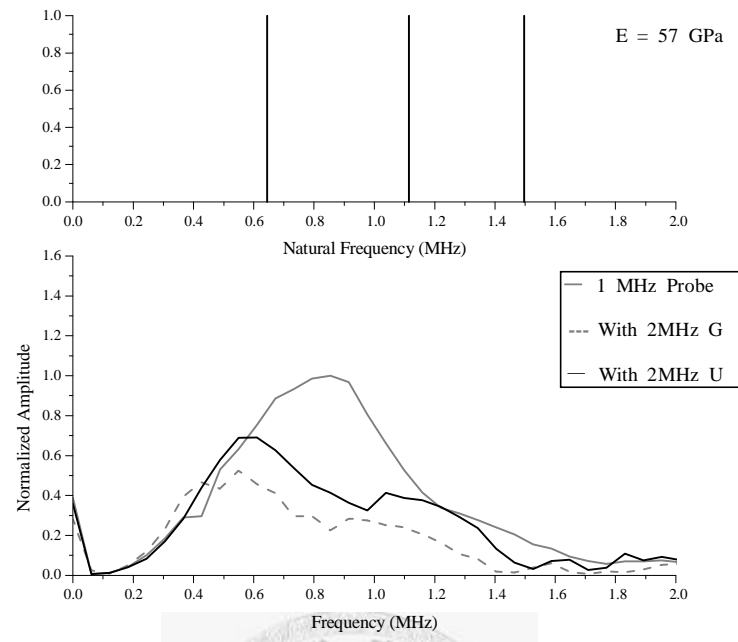


Figure 4.16 (a) NF and frequency distribution of 2 MHz unpoled PZT on 1 MHz probe.

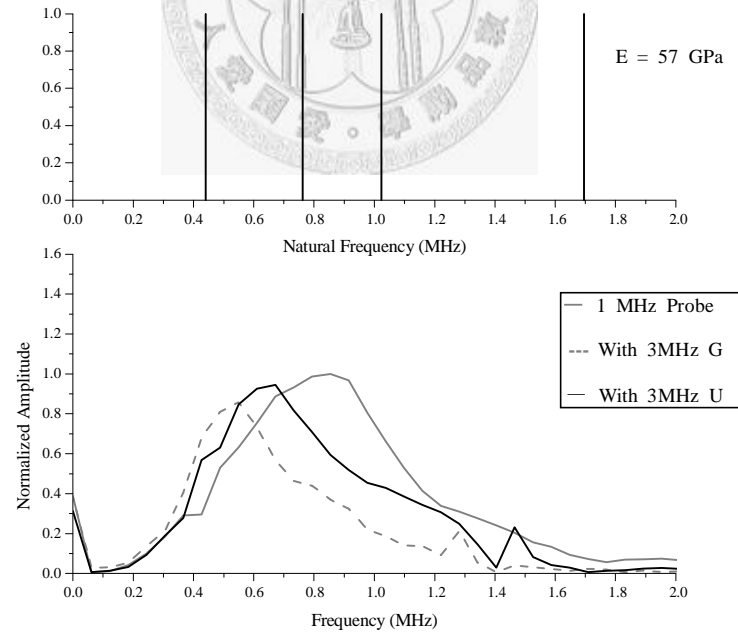


Figure 4.16 (b) NF and frequency distribution of 3 MHz unpoled PZT on 1 MHz probe.

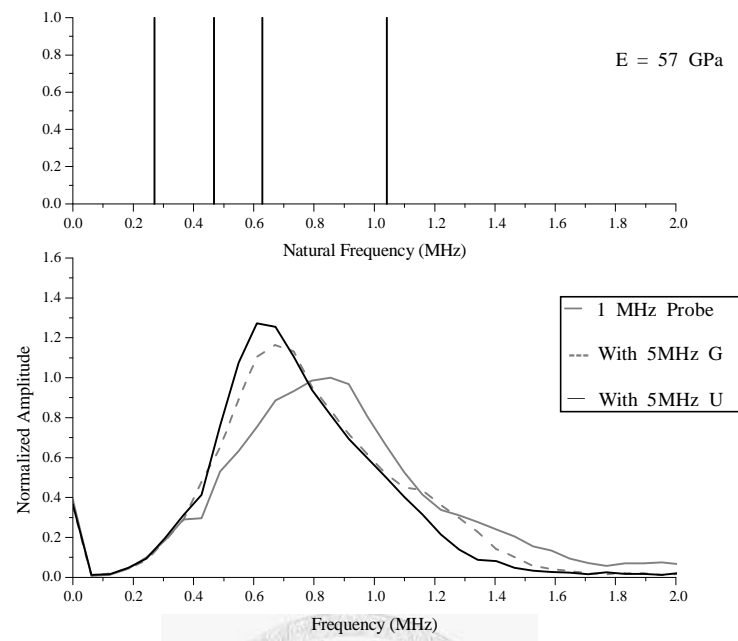
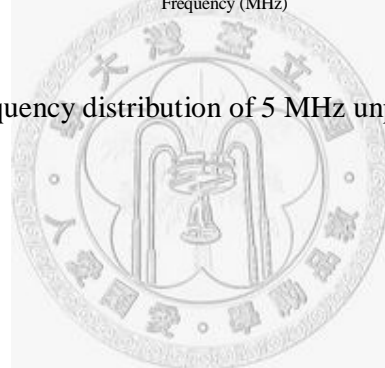


Figure 4.16 (c) NF and frequency distribution of 5 MHz unpoled PZT on 1 MHz probe.



4.2.4 Unpoled PZT without Electrodes (UN)

In order to identify if the surface electrodes have an effect in the frequency distribution, the surface electrodes of the unpoled PZT layer are removed. The frequency distributions of the 10, 5 and 1 MHz transducers with the unpoled-electroded PZT layers and with the unpoled-unelectrode PZT layers are compared and shown in Fig. 4.17, 4.18 and 4.19.

As shown in the figures that the effects of surface electrodes on the frequency distributions are minor. The position of the frequency peaks are slightly moved when the electrodes of the PZT layers are removed. This is due to the decrease in layer thickness, which is the most important factor in the mechanical dominant effect. Besides, the frequency distributions of the 1MHz transducer with the 3 MHz and 5 MHz PZT plates with no electrodes are determined by the natural frequencies. They are not governed by the traveling length of the reflected waves, and less sensitive to the PZT layer thickness.

4.2.5 Electroded Poled PZT with Second Composite Matching Layer (GML)

An intermediate low-impedance matching layer is necessary to reduce the large impedance mismatch between the active PZT layer and the water/human tissues. ZrO₂-epoxy composite with thickness equals to the quarter wavelength of the ultrasonic waves traveling inside is applied on to the active PZT plate as a second matching layer.

The frequency distributions of the electroded poled PZT plates with composite matching layers, compared to that of the electroded poled PZT plates, are characterized by the 10, 5, and 1 MHz transducers and the results are shown in Fig. 4.20, 4.21, and 4.22, respectively.

When coupled with the 5MHz and 1 MHz transducers, the efficiency of wave transmission is increased by adding the composite matching layer. Furthermore, the active-passive two-layer design for the 5 MHz and 1 MHz transducers gives rise to higher transmitted frequency amplitudes than the original frequency distributions. However for the 10 MHz transducer, the two-layer design reduces the frequency amplitude. This is because that the micro-bubbles within the composite layer (see Fig. 4.23) could potentially scatter the 10 MHz wave due to its shorter wavelength.

Besides, the resonant frequency of the active PZT layer appears to be shift by integration of the second composite matching layers ; The degree of this shift is dependant on the thickness of matching layers. Fig. 4.23 (a) shows the resonant modes of the 1 MHz electrode poled PZT plate, and its effect on the frequency distribution of the transducer ; Fig. 4.23 (b) shows the resonant modes of the 1 MHz electrode poled PZT plate with the second composite matching layer, and its effect on the frequency distribution of the transducer. It is evident that the integration of the second composite layer causes a shift in the frequency distribution. Nevertheless, with or without the

second composite layer, the frequency peaks align closely with the piezoelectric resonant modes - the electromechanical dominant effect behavior is demonstrated.

4.2.6 Short-Circuited Poled PZT with Second Composite Matching Layer (ECML)

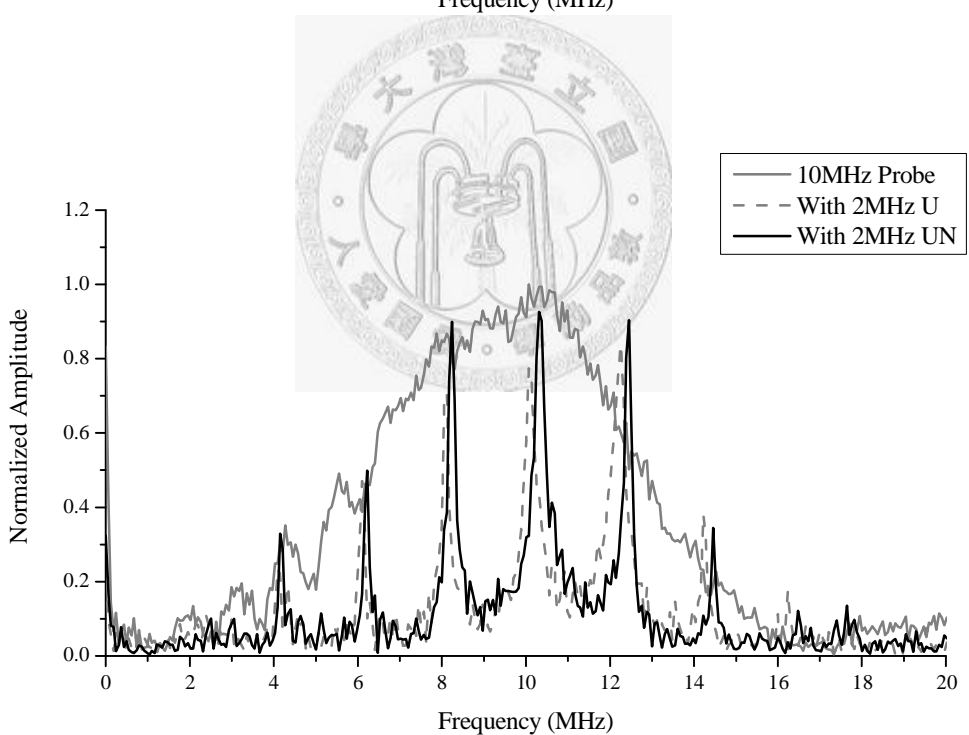
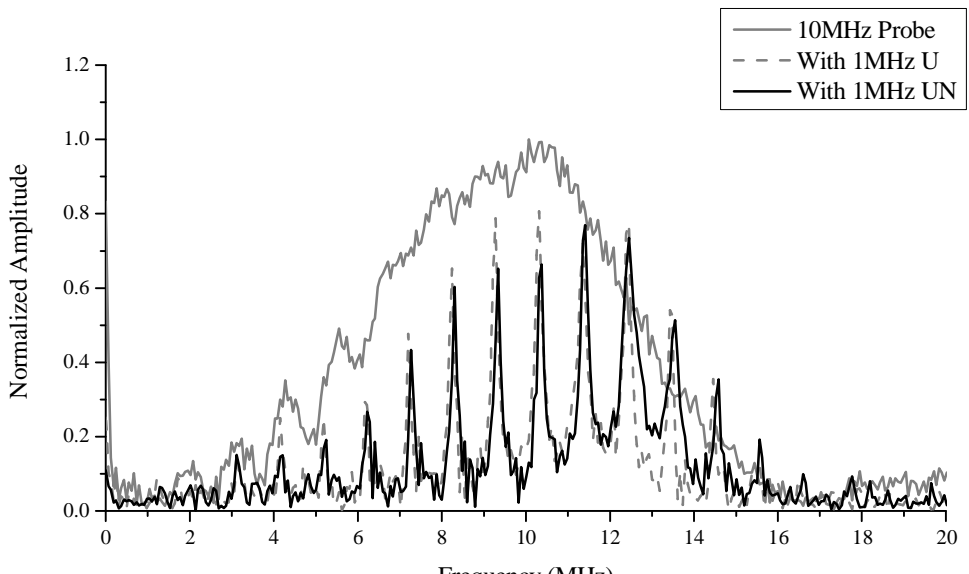
The poled short-circuited PZT plates with and without the second composite matching layer both give rise to sharper and cleaner frequency peaks (see Fig. 4.25, 4.26, and 4.27). Similar explanations based on the electromechanical characteristics and piezoelectrics, as mentioned in Section 4.2.2, are applied for this type of matching layer design.

4.2.7 Conclusion

The behavior of a particular matching layer design is either an electromechanical effect or a mechanical effect. Piezoelectric resonant modes and mechanical quality (Q) govern the electromechanical effect, while dimensions and natural frequencies govern the mechanical effect. Three conclusions are proposed :

1. For the short-circuited poled PZT plates, the electromechanical effect is dominant.
2. If the thickness mode resonant frequencies of the PZT plates are lower than that of the transducers, the electromechanical effect is dominant.
3. If the thickness mode resonant frequencies of the PZT plates are higher than that of the transducers or if the PZT plates are unpoled, the mechanical effect is dominant.





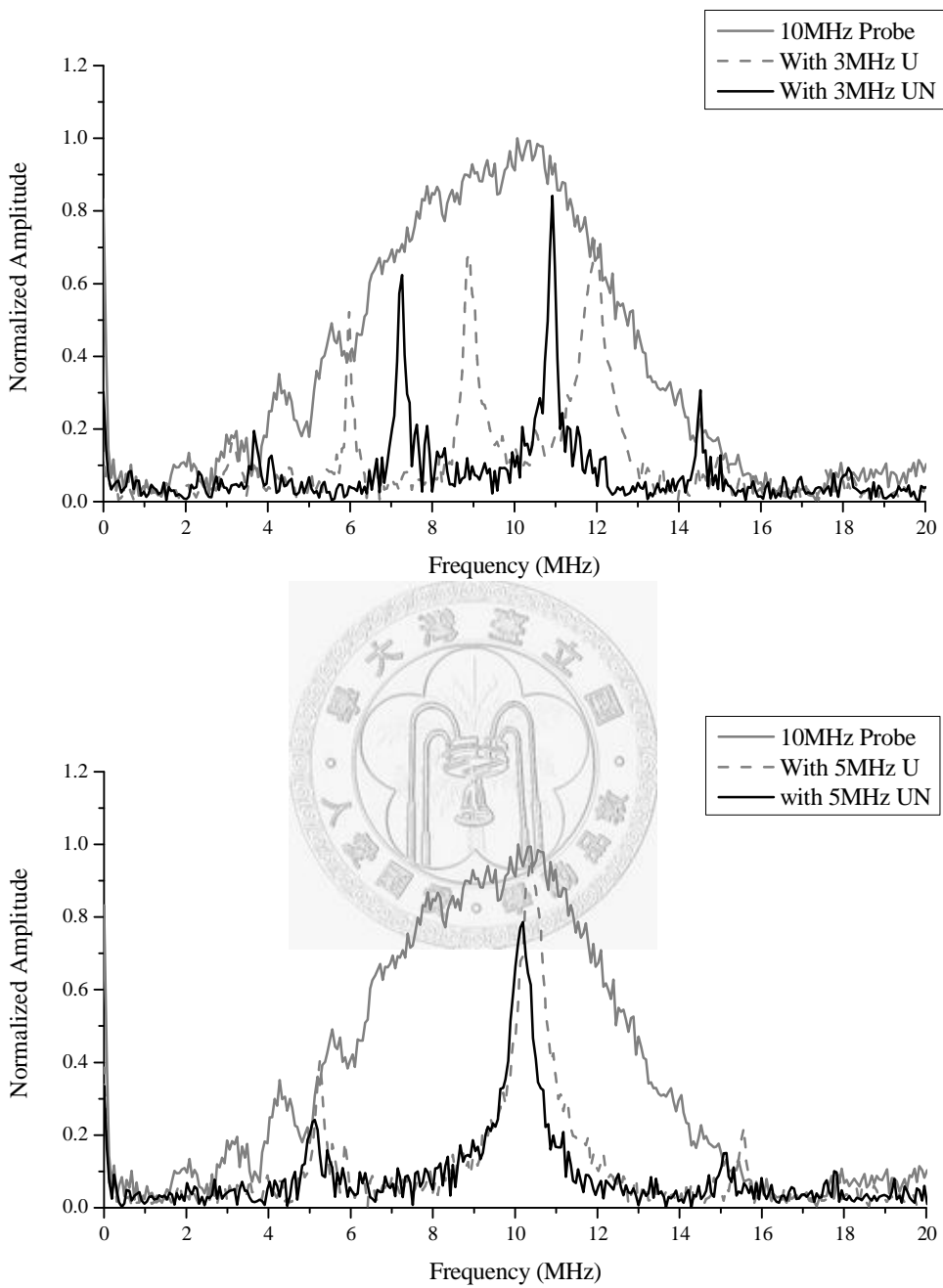
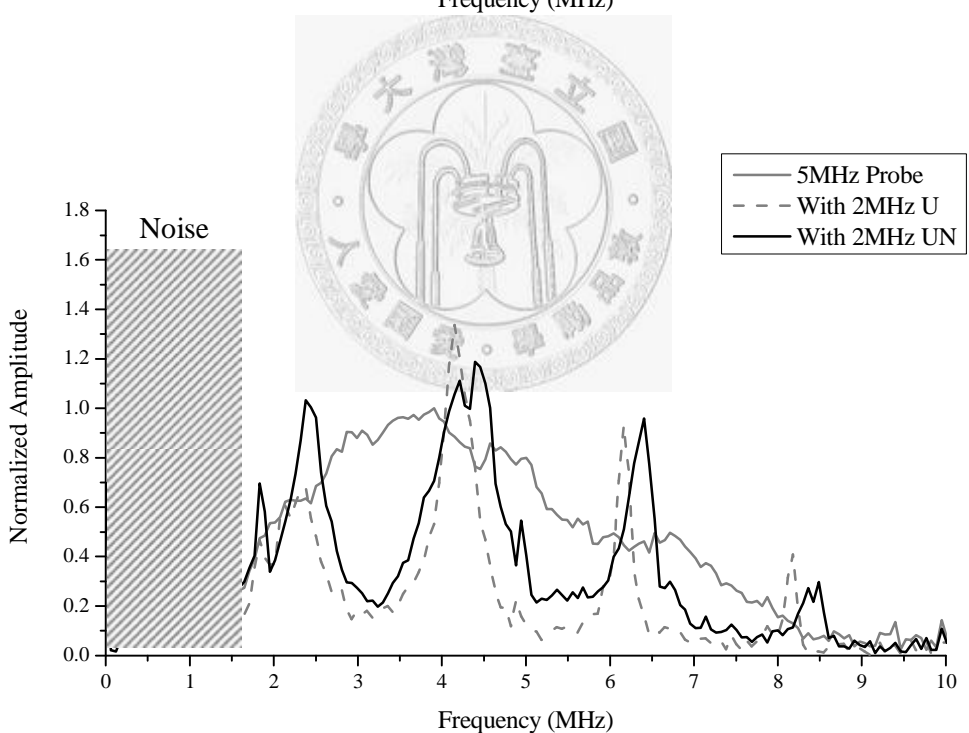
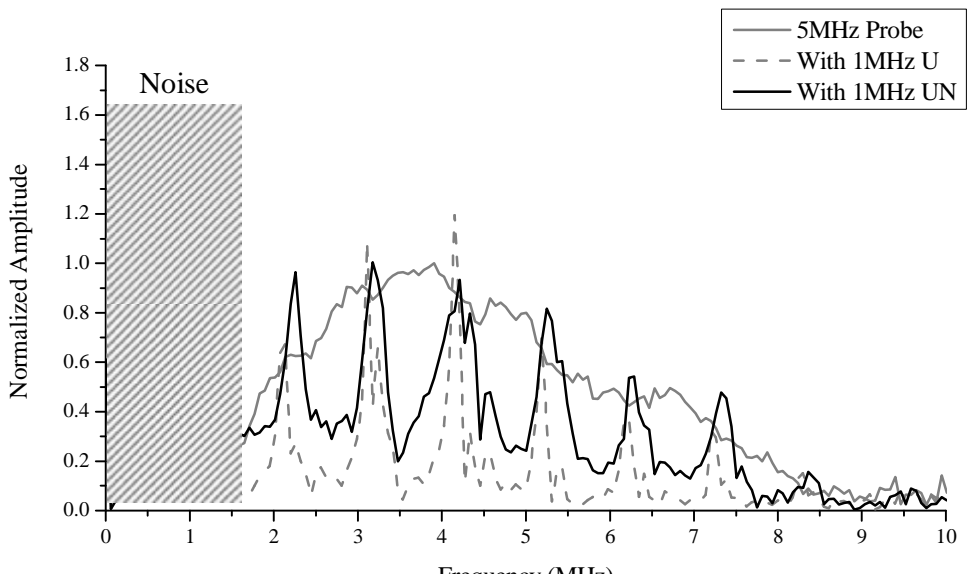


Figure 4.17 Unpoled PZT plates without electrodes (UN) characterized by the 10 MHz transducer, compared with unpoled PZT plates (U).



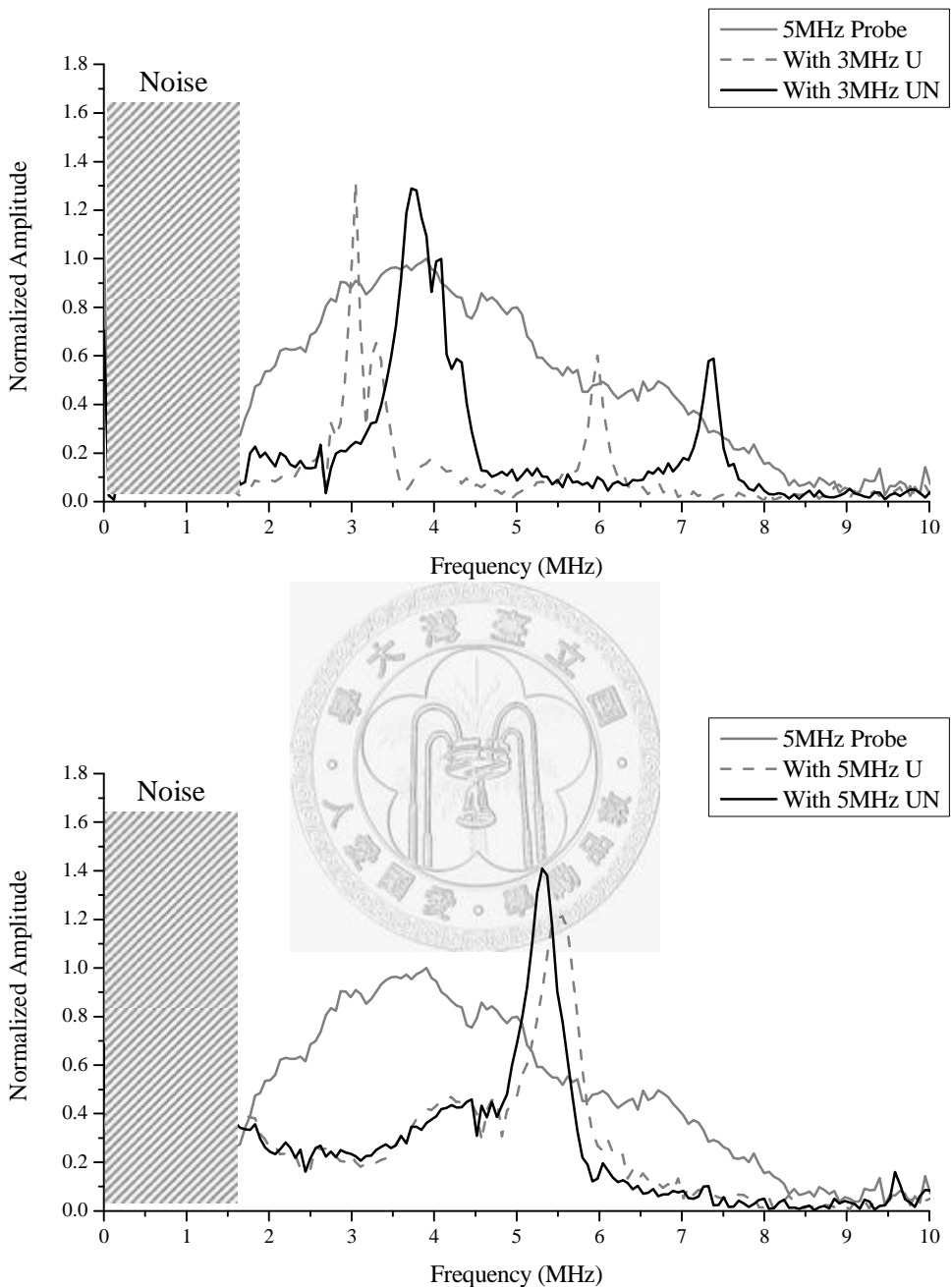
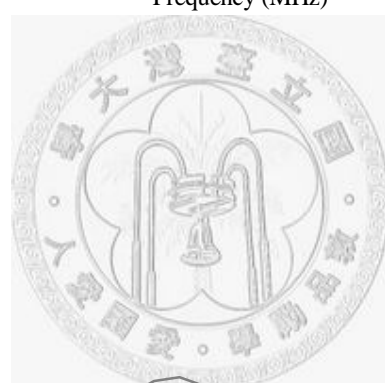
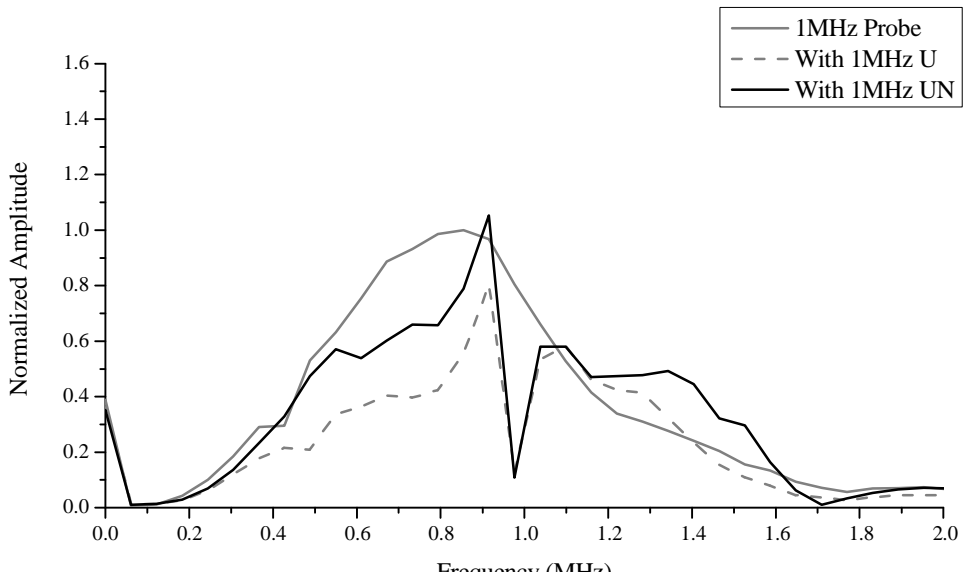
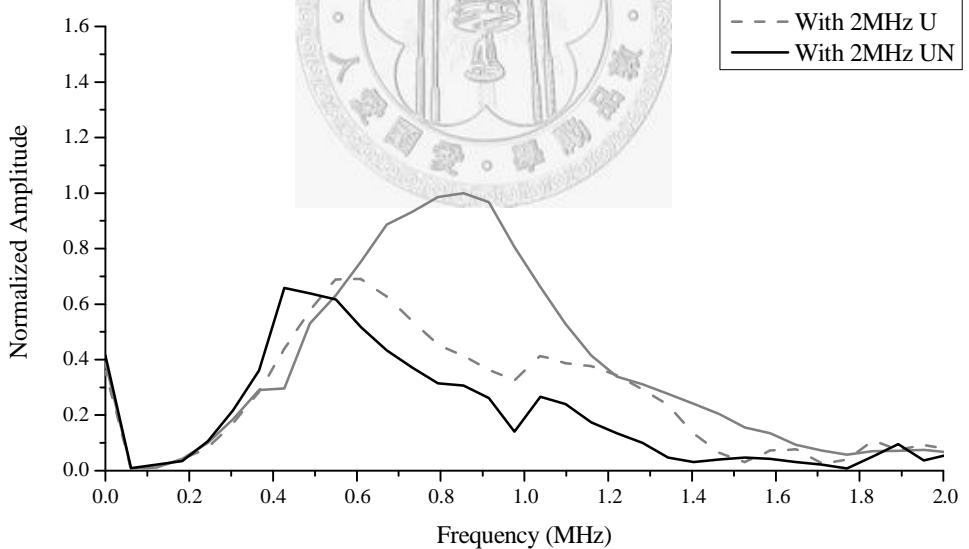


Figure 4.18 Unpoled PZT plates without electrodes (UN) characterized by the 5 MHz transducer, compared with unpoled PZT plates (U).



Legend:

- 1MHz Probe (Solid Line)
- With 2MHz U (Dashed Line)
- With 2MHz UN (Solid Line)



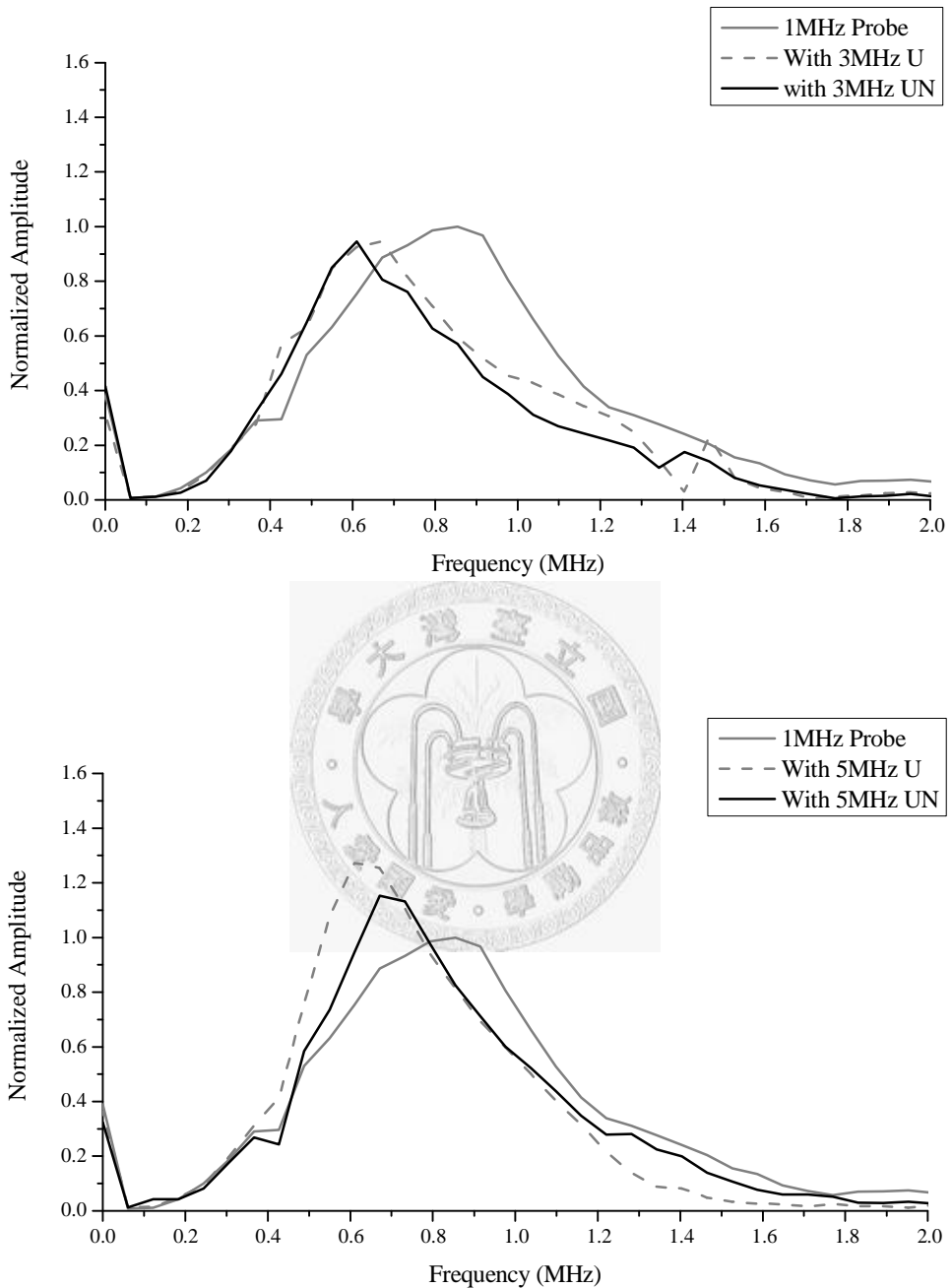
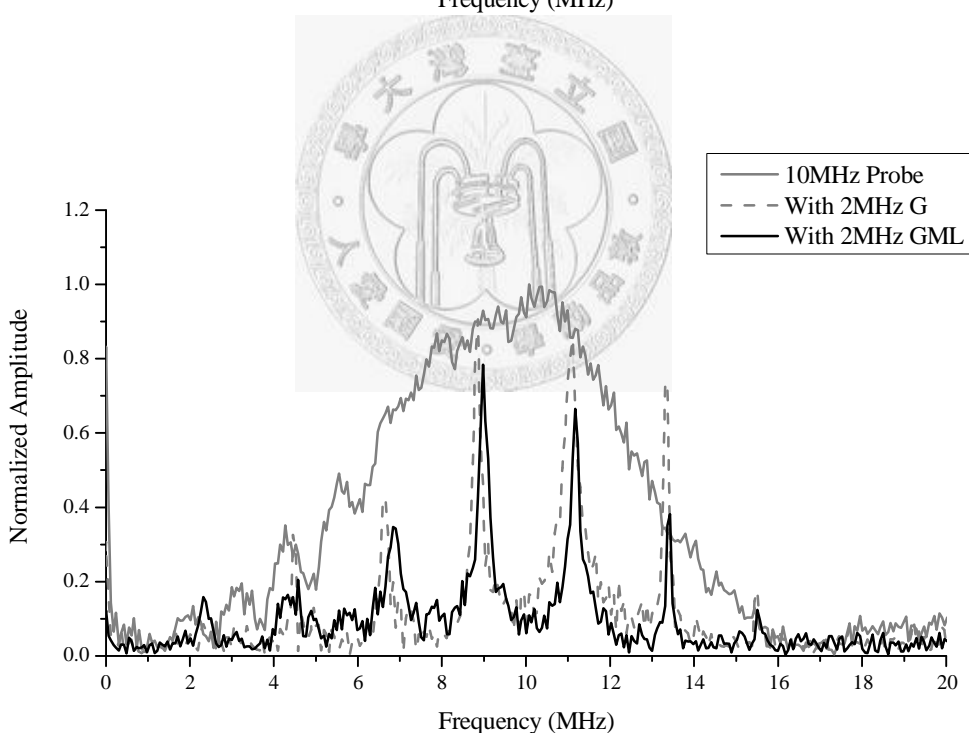
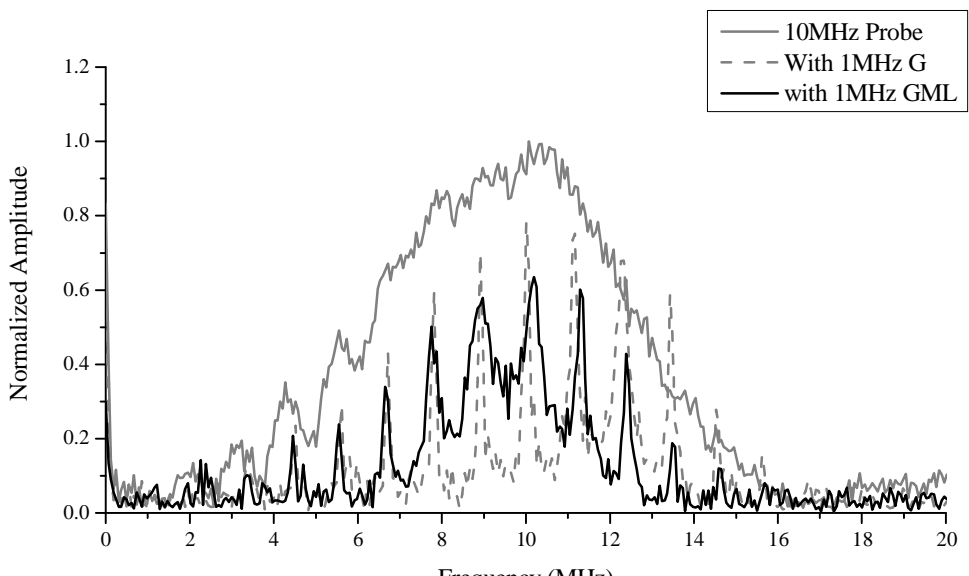


Figure 4.19 Unpoled PZT plates without electrodes (UN) characterized by the 1 MHz transducer, compared with unpoled PZT plates (U).



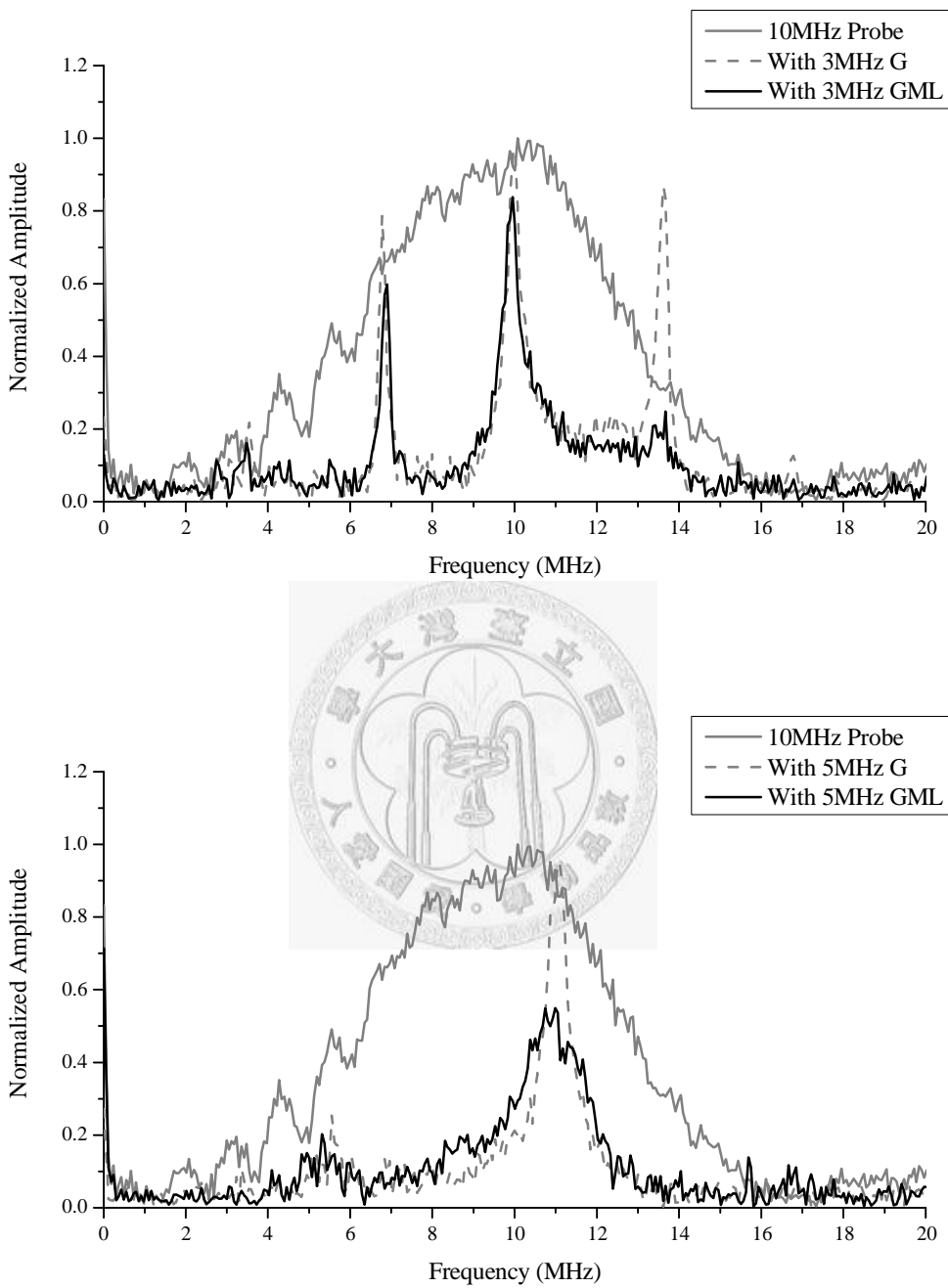
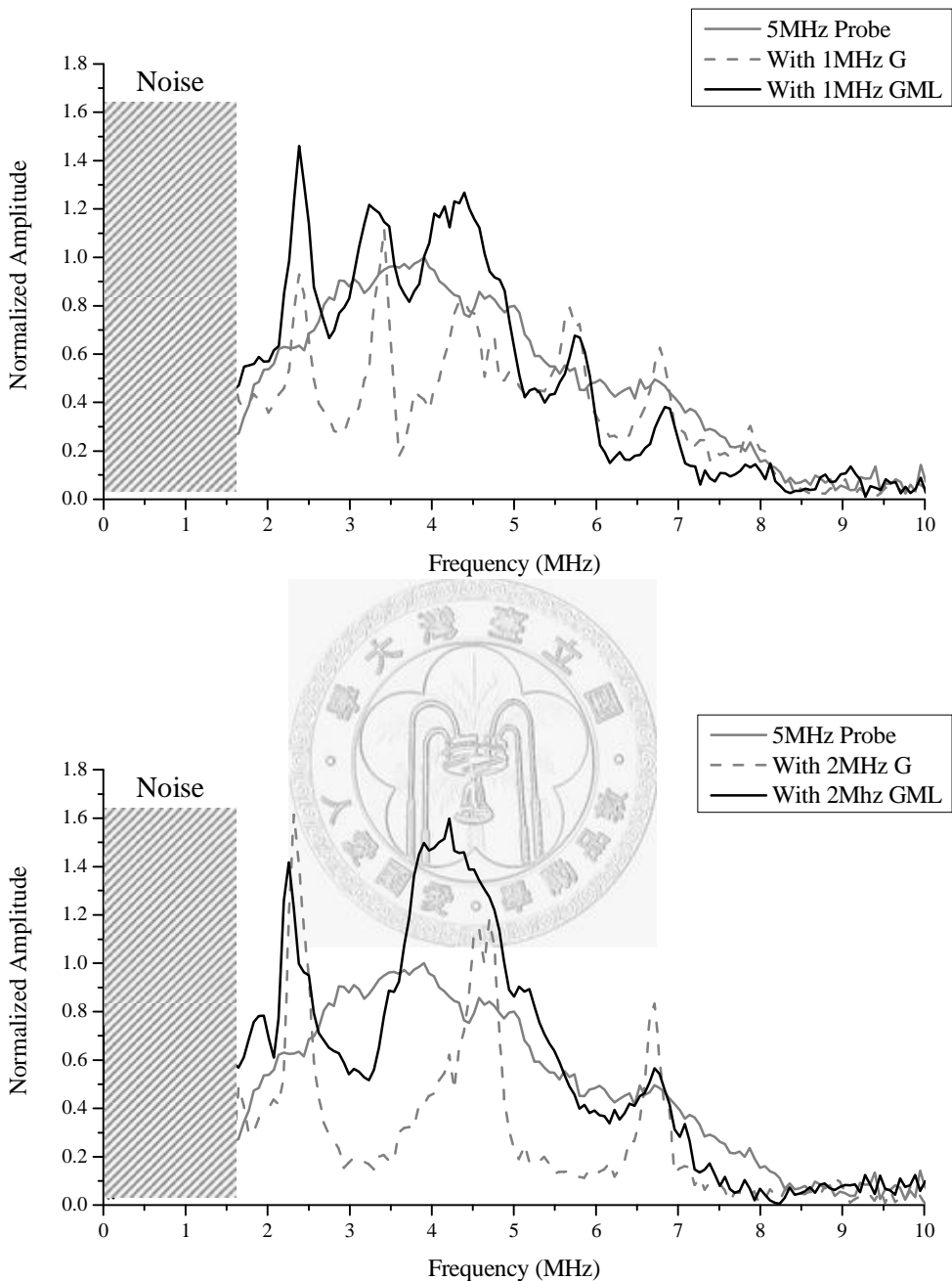


Figure 4.20 Electroded poled PZT plates with matching layer (GML) characterized by the 10 MHz transducer, compared with electroded poled PZT plates (G).



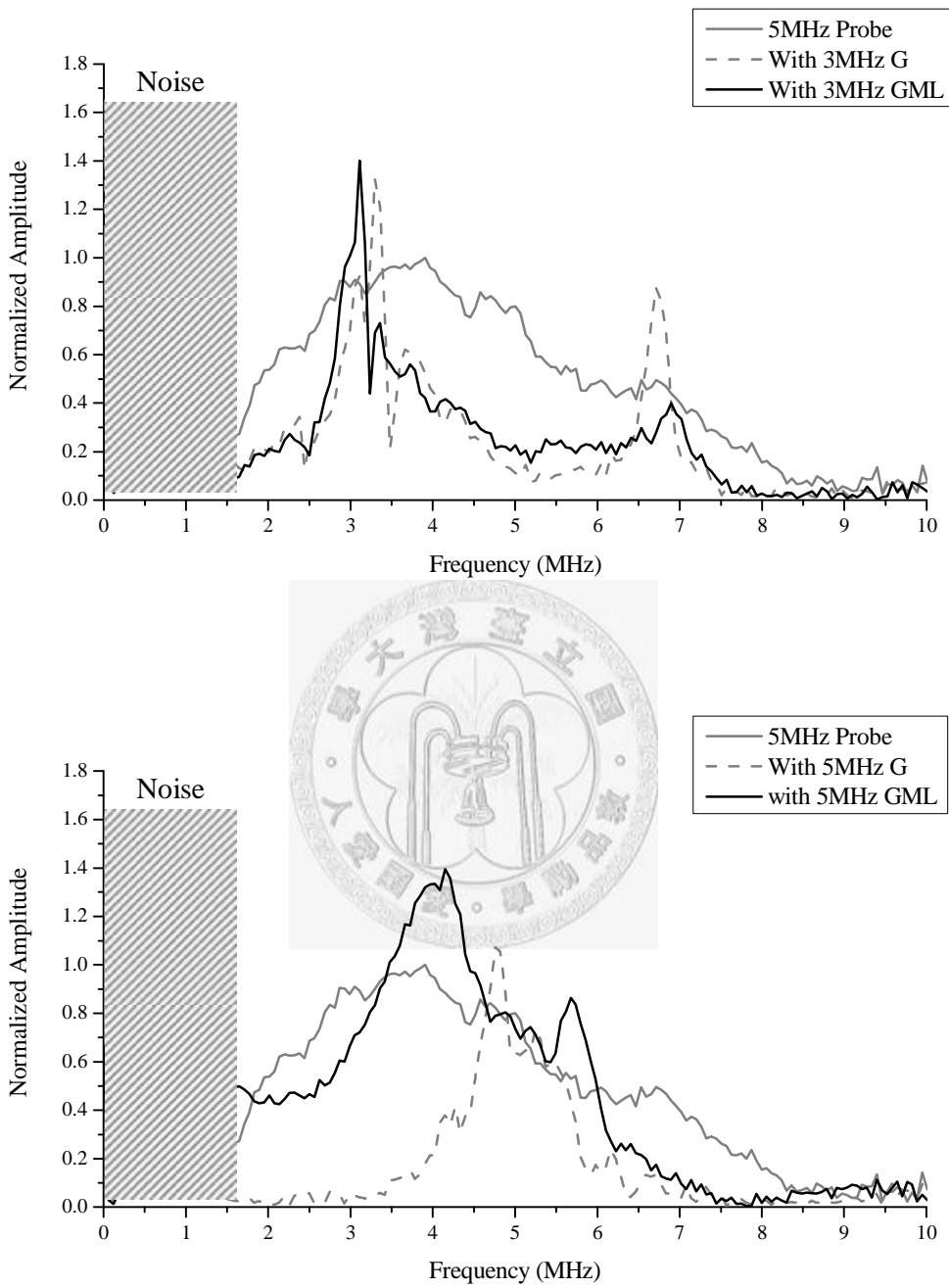
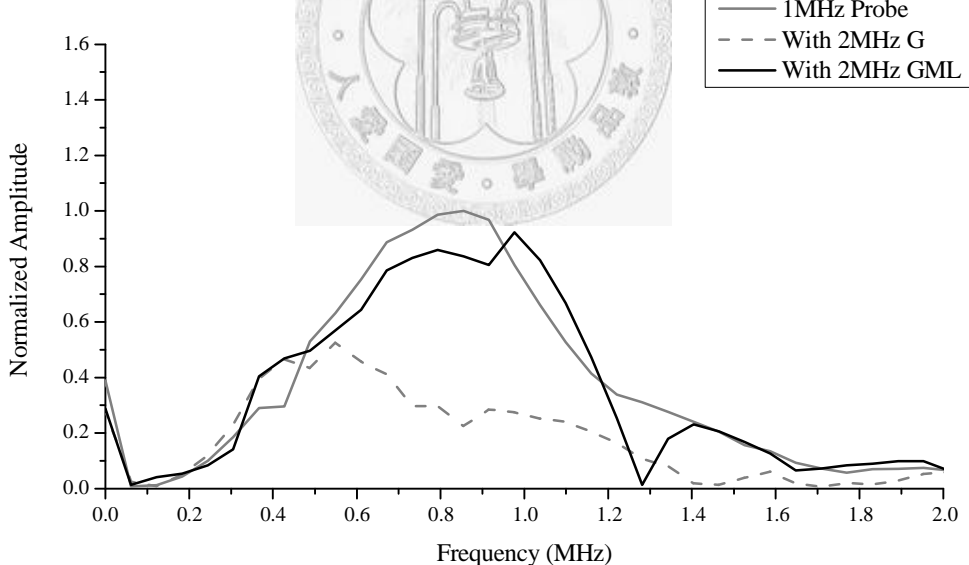
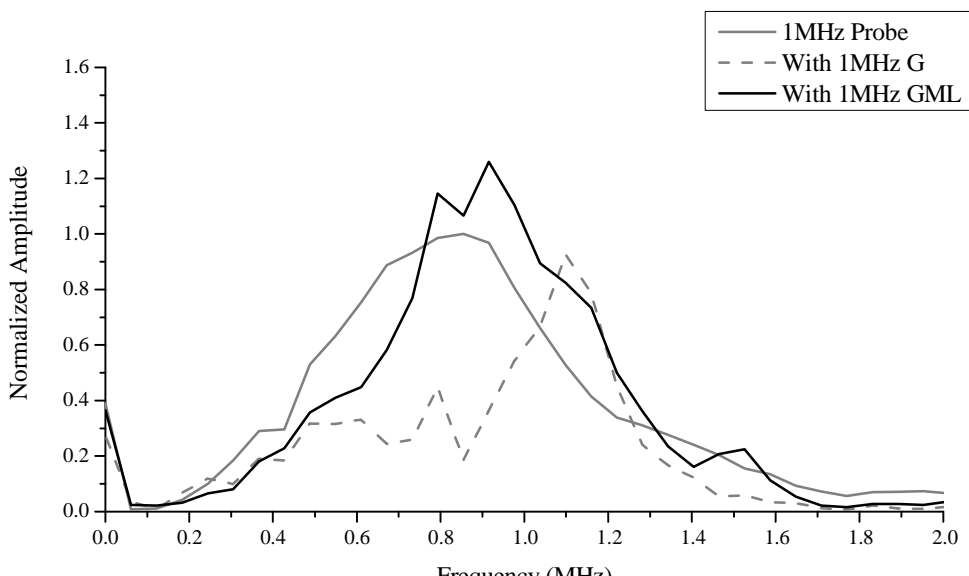


Figure 4.21 Electroded poled PZT plates with matching layer (GML) characterized by the 5 MHz transducer, compared with electroded poled PZT plates (G).



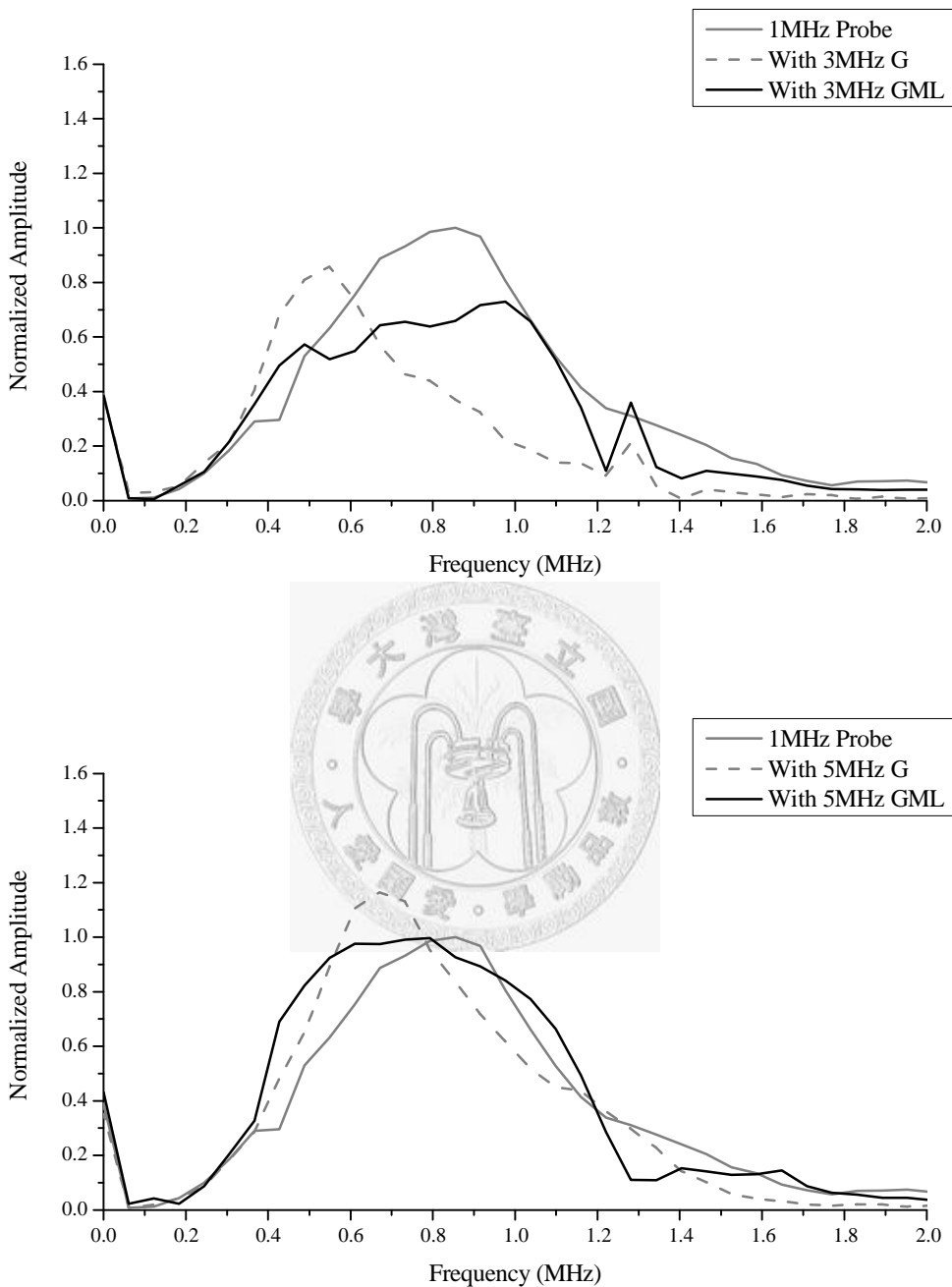
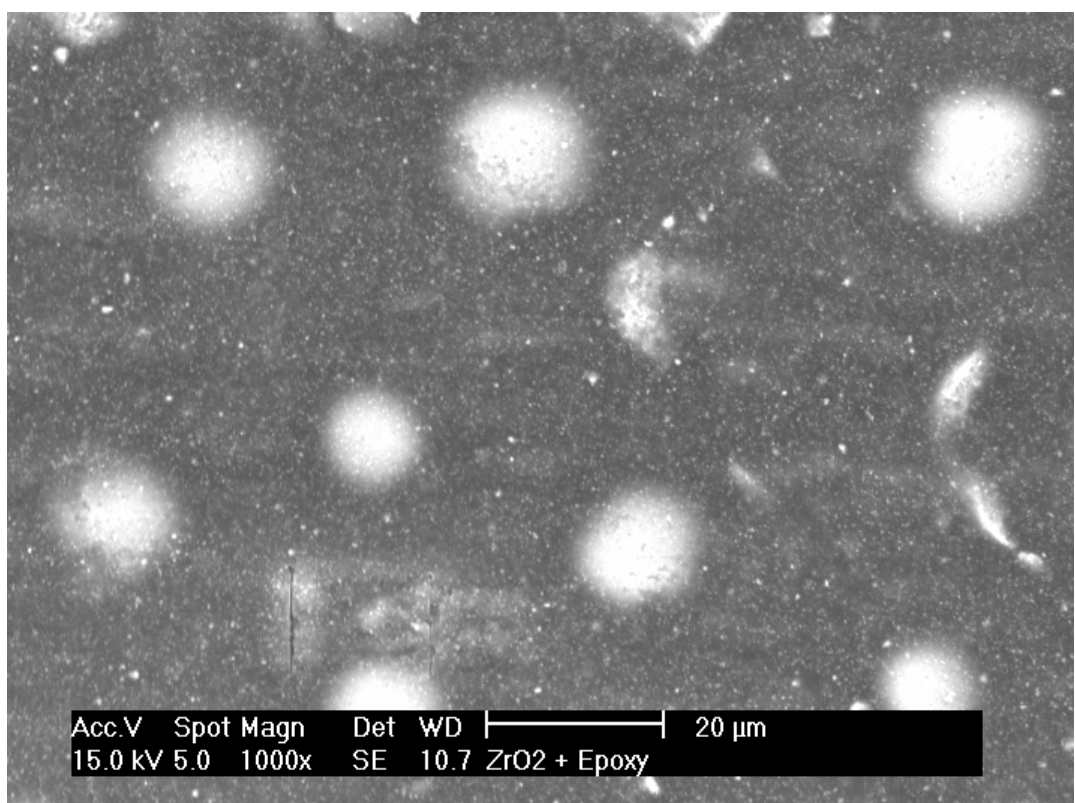
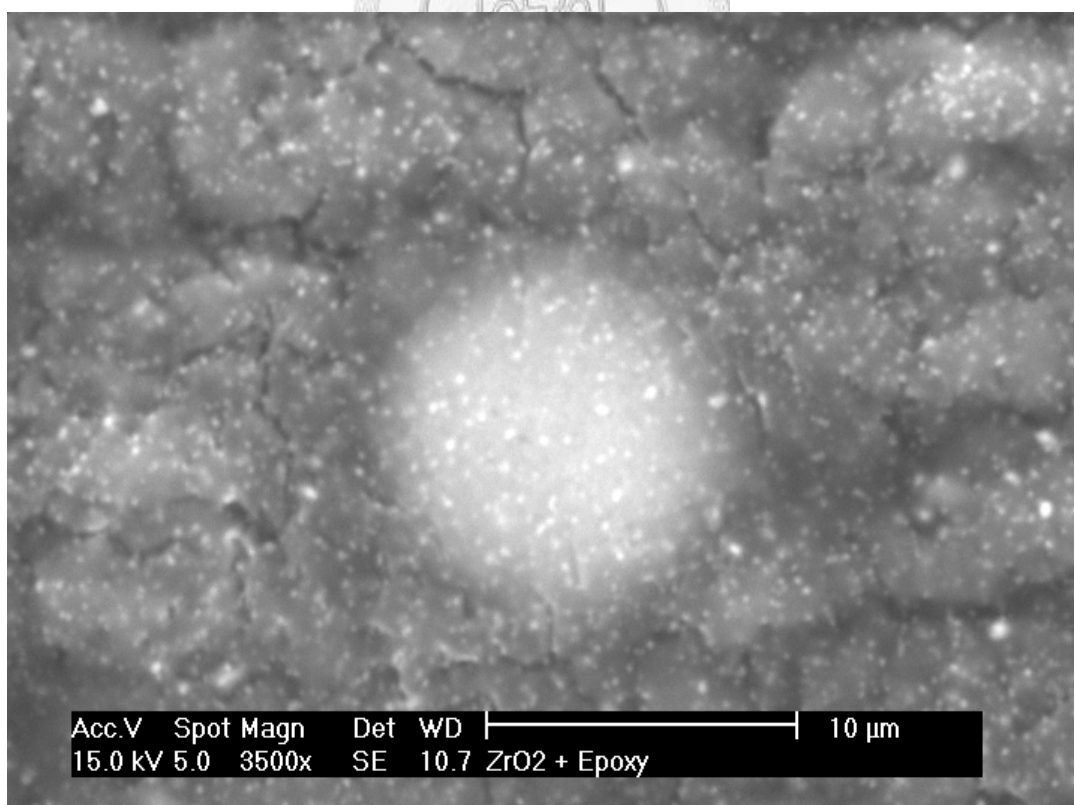


Figure 4.22 Electroded poled PZT plates with matching layer (GML) characterized by the 1 MHz transducer, compared with electroded poled PZT plates (G).



Acc.V Spot Magn Det WD 20 µm
15.0 kV 5.0 1000x SE 10.7 ZrO₂ + Epoxy



Acc.V Spot Magn Det WD 10 µm
15.0 kV 5.0 3500x SE 10.7 ZrO₂ + Epoxy

Figure 4.23 Micro-bubbles resided inside Zirconium dioxide-epoxy matching layer.

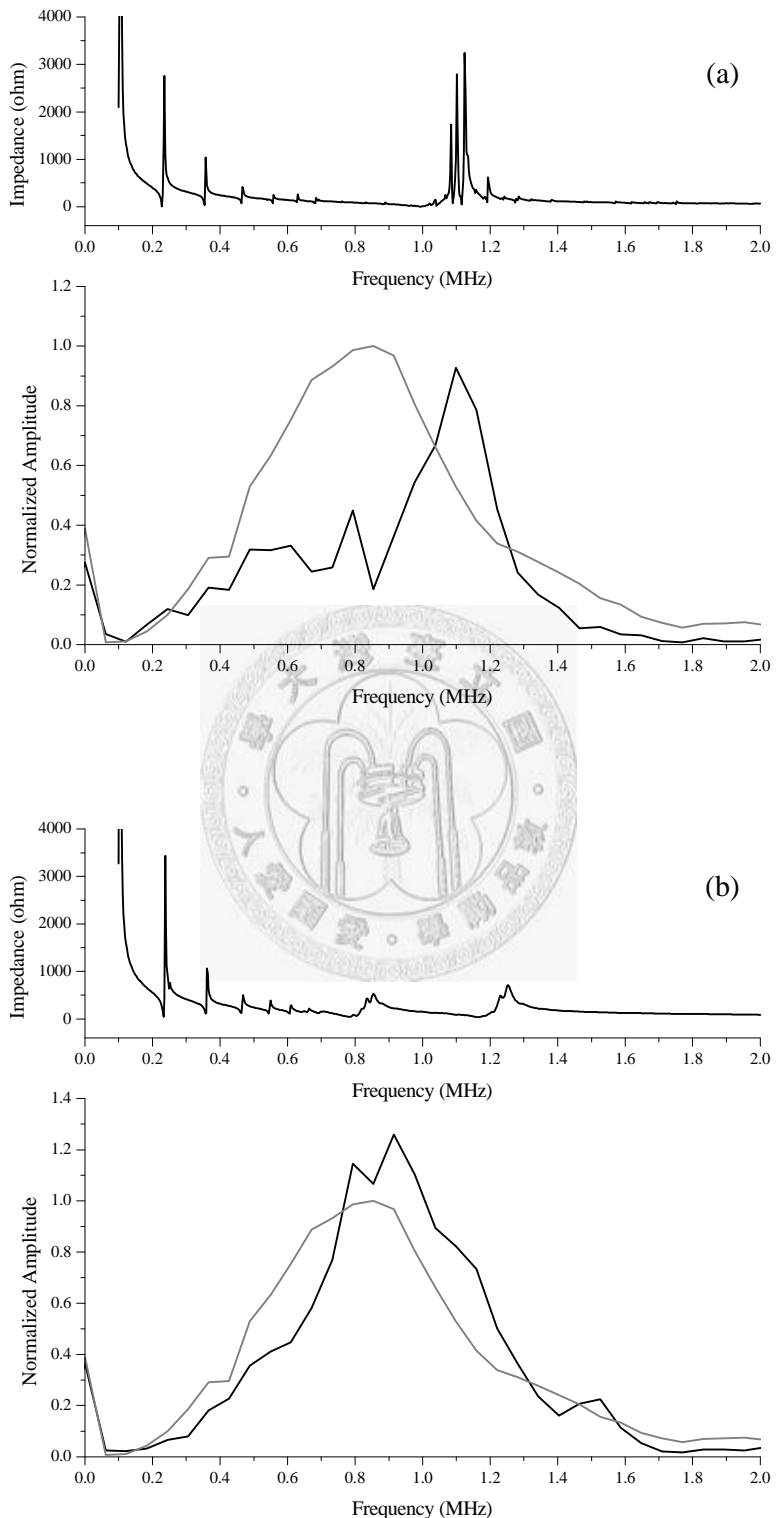
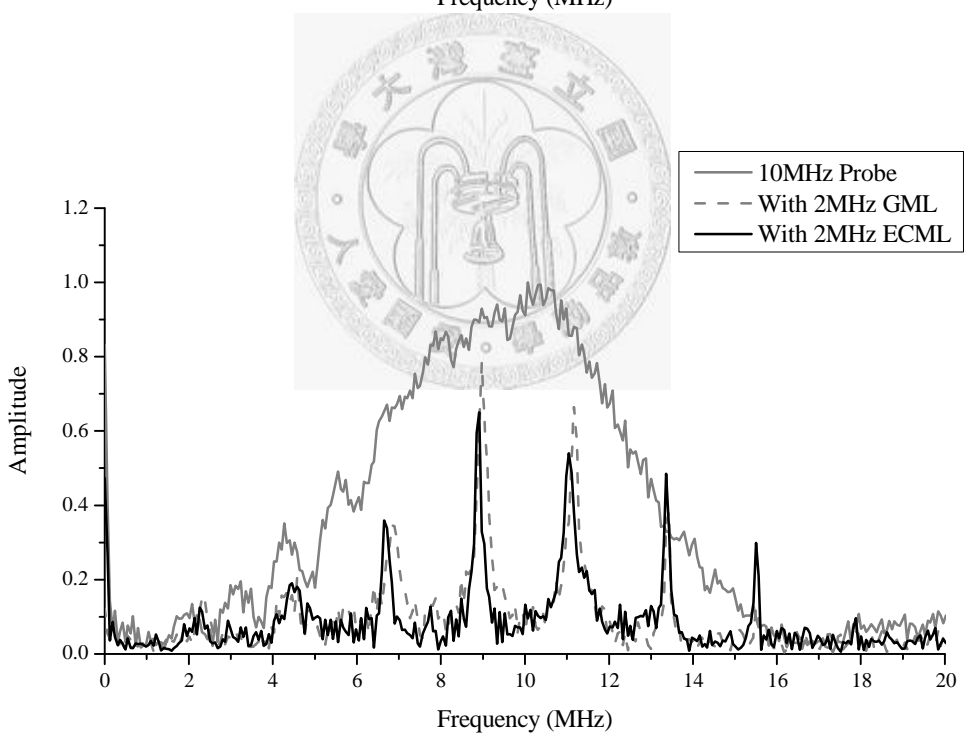
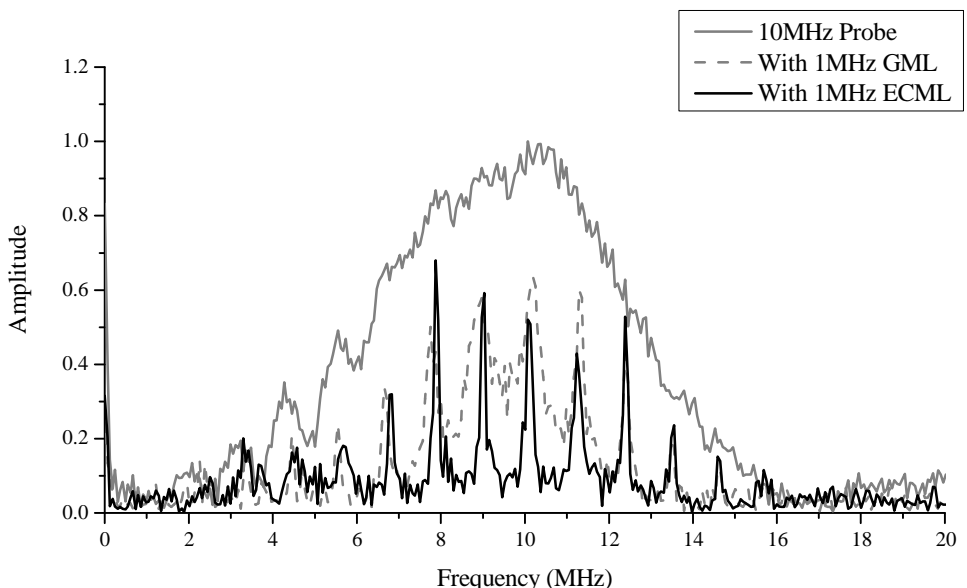


Figure 4.24 Shift of resonant frequency by integration of matching layer.



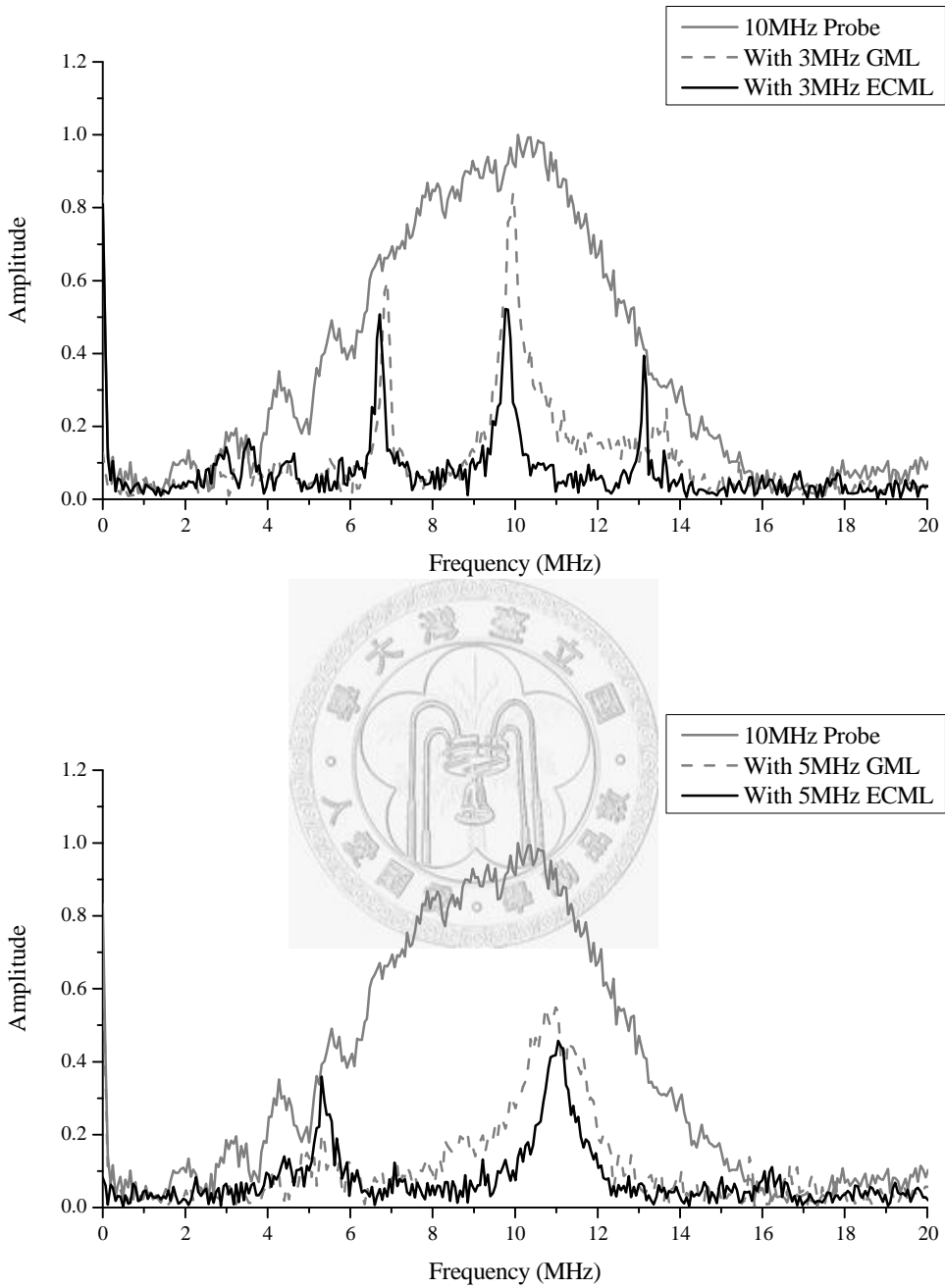


Figure 4.25 Short-circuited poled PZT with composite matching layer (ECML)

characterized by the 10 MHz transducer, compared with electroded poled PZT with composite matching layer (GML).

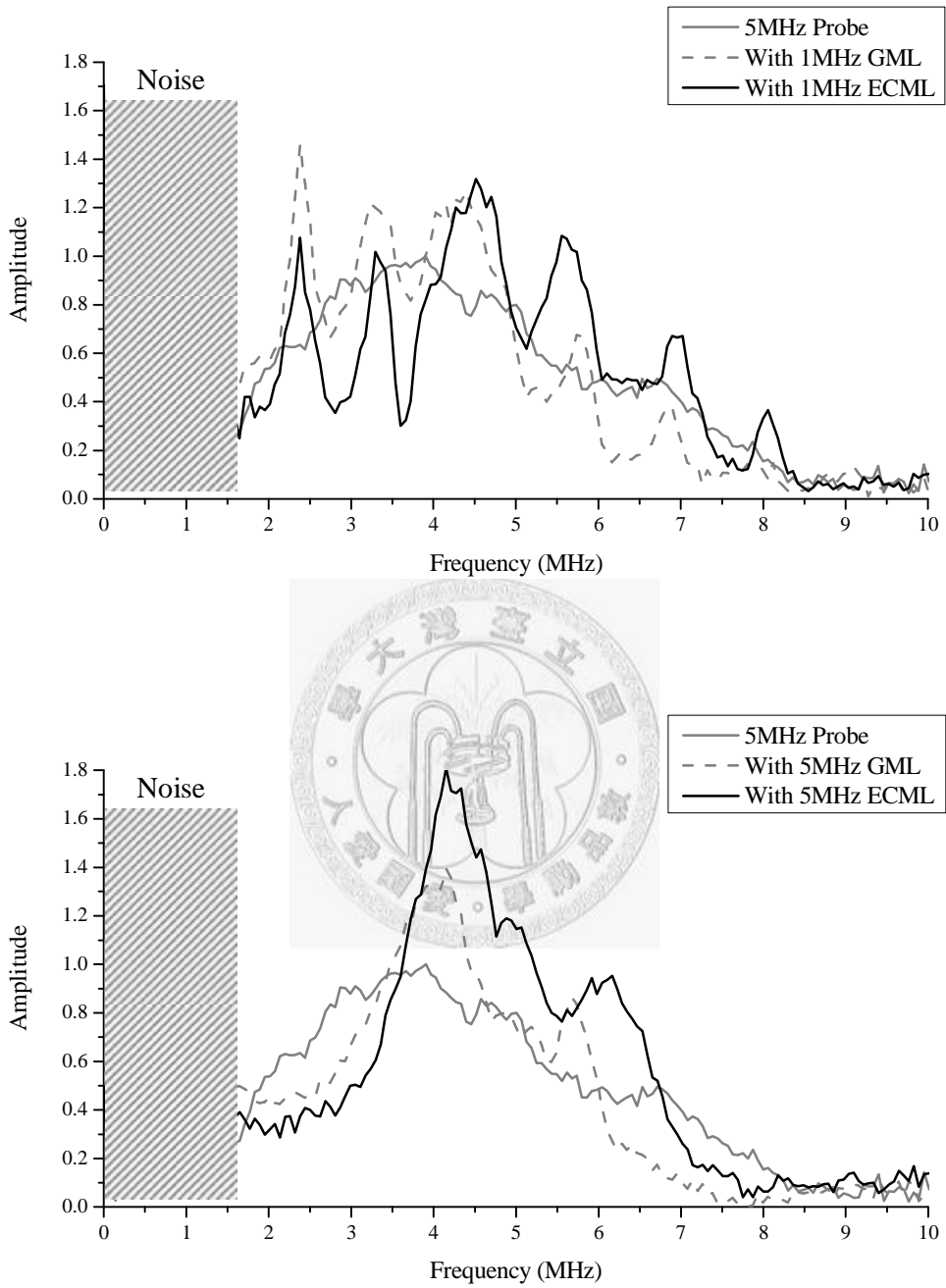


Figure 4.26 Short-circuited poled PZT with composite matching layer (ECML)

characterized by the 5 MHz transducer, compared with electroded poled PZT with composite matching layer (GML).

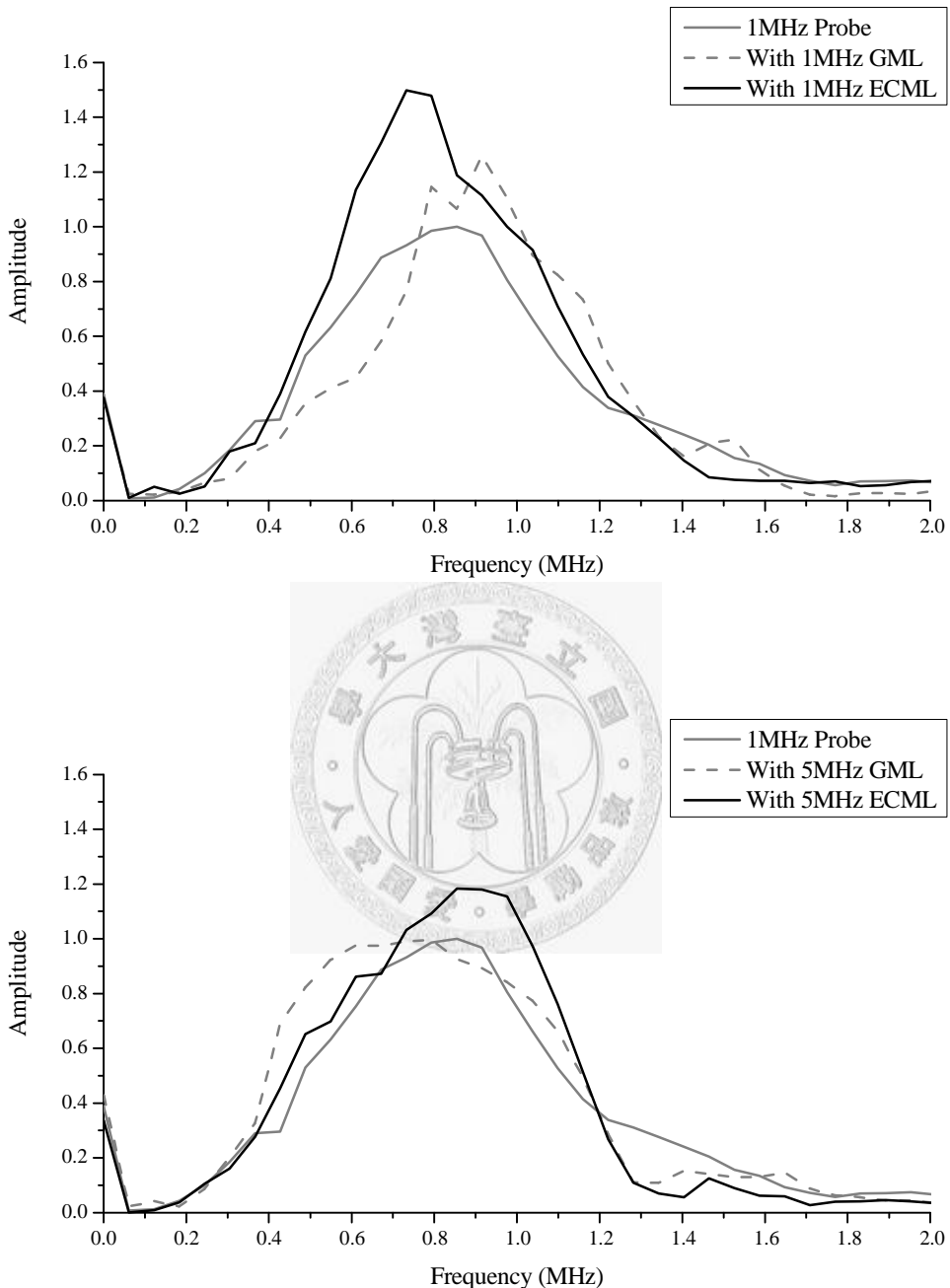
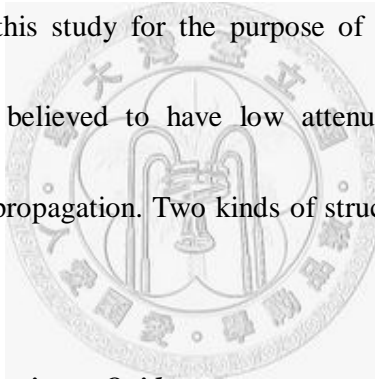


Figure 4.27 Short-circuited poled PZT with composite matching layer (ECML)

characterized by the 1 MHz transducer, compared with electroded poled PZT with composite matching layer (GML).

4.3 Structured Materials

For impedance matching, materials with impedances between PZT and water/human tissue are applied to reduce the large impedance mismatch. Traditionally, composites composed of high and low impedance materials, such as ceramic-loaded epoxy, are good choices. However, it is believed that the attenuation is relatively high because of the great amount of ceramic-epoxy interfaces and the high attenuation of epoxy. Structured ceramics such as porous ceramics and structured ceramics-epoxy composites are therefore produced in this study for the purpose of diminishing the attenuation. Structured composites are believed to have low attenuations due to the available continuous paths for wave propagation. Two kinds of structured materials are prepared in this study.



4.3.1 Structured Porous Aluminum Oxides

In order to resolve high attenuation due the large numbers of interfaces, porous ceramics internal structures are prepared. Five porous aluminum oxides are prepared with different porosities. The values of density, wave velocity inside, impedance and attenuation for the five porous aluminum oxides are listed in Table 4.4. The attenuations of the porous aluminum oxides are characterized by the 10 MHz transducers due to its short wavelength output, which in turn provides a high sensitivity.

The oxides are considered as the composites of air and ceramic, and Table 4.4 shows

that the impedance decreases with increasing pore volume percent. Internal structures of the porous aluminum oxides are shown in Fig. 4.28. The oxides were sintered and therefore small pores among the ceramics structure can be seen. With increasing the amount of pore-forming agent additive, larger pores are formed, and the attenuation is increased due to these big pores.

4.3.2 Epoxy-Loaded Structured Porous Aluminum Oxides

The air within the porous Al_2O_3 structures are removed by filling the pores with epoxies. The density, internal wave velocity, impedance and attenuation of the epoxy-load porous Al_2O_3 are listed at Table 4.5.

For the Al_2O_3 structures mentioned in Section 4.2.2, the measurement of transmission under water is difficult due to the release of air within the air pores. When the pores are filled with epoxies, the wave transmission efficiency is improved. The impedance of the structured porous Al_2O_3 is increased by the epoxy loading, and the attenuation level can be controlled by the amount of air pores filled. A tunable acoustic matching layer is therefore produced, and has potential applications in a system when multiple matching layers are required.

Based on the mechanical (thickness) dominant effect as mentioned in Section 4.2.3, epoxy-loaded Al_2O_3 plates are produced to mimic the 2 MHz unpoled PZT plates, i.e., the thickness of the porous plates is half the 2 MHz wavelength traveling within them.

Fig. 4.29 shows that frequency distributions of the 10 MHz transducer with the epoxy-loaded porous Al_2O_3 plates are similar to the ones with the 2 MHz unpoled PZT plate. The frequency peaks are very sensitivity to the plate thickness, and are broader and less sharper when compared to the ones with the 2 MHz unpolesd PZT plate. This is believed to be caused by a lower level of plate vibration due to the high compliance of the epoxy pores.

4.4 Experimental Errors

In order to reduce the number of experimental variables, the distance between the ultrasonic transducer and the hydrophone during the measurement of frequency distribution was fixed. However, the focal point of the transducer system can be shifted by different amounts when PZT matching layers of different thicknesses are integrated. Therefore, small errors in the measured amplitudes of the frequency peaks are expected.

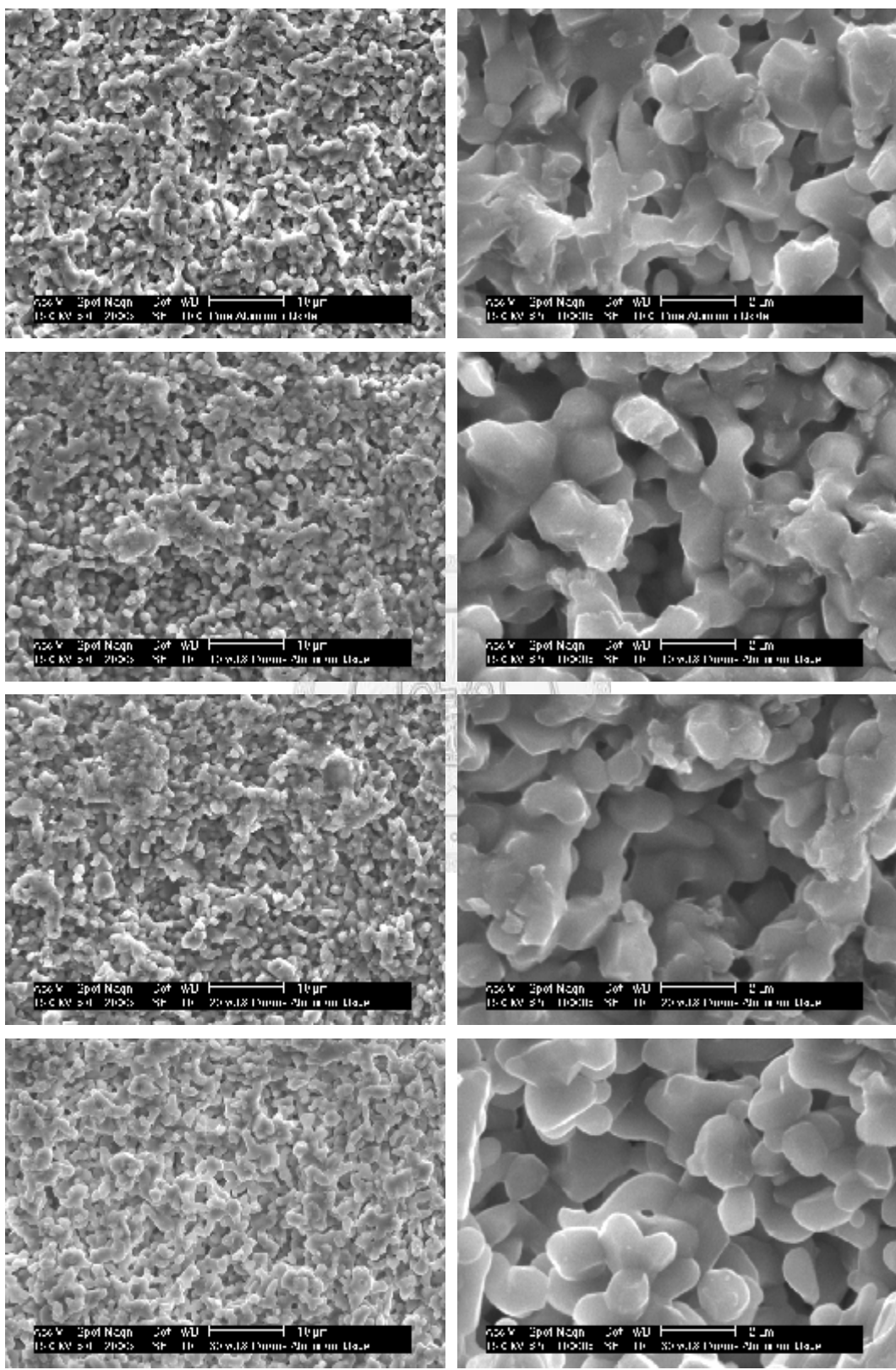
The manufaturings of the structured porous Al_2O_3 and epoxy-loaded structured porous Al_2O_3 matching layers of required thicknesses (e.g. $\lambda/2$) for the 1 MHz and 10 MHz transducers are difficult. This is because that the required half-wavelength thickness for the 1 MHz transducer is too thick to be produced by the traditional powder compaction process, and the required half-wavelength thickness for the 10 MHz transducer is too thin to be machined by conventional grinding.

Table 4.4 Parameters of the structured porous aluminum oxides.

Pore agent vol%	Density (g/cm ³)	Velocity (m/s)	Impedance (MRayl)	Attenuation (Np/cm)
0	2.818	7955.963	22.419	0.066
10	2.616	7357.466	19.247	0.280
20	2.351	7111.309	16.722	0.452
30	2.107	6126.923	12.911	0.852
40	1.979	5682.935	11.245	1.194

Table 4.5 Parameters of the epoxy-loaded structured aluminum oxides.

Pore agent vol%	Density (g/cm ³)	Velocity (m/s)	Impedance (MRayl)	Attenuation (Np/cm)
0	3.128	8204.819	25.665	0.376
10	2.836	8052.819	22.838	6.594
20	2.798	6872.297	19.229	0.795
30	2.724	6113.519	16.653	1.659
40	2.701	6121.702	16.534	2.663



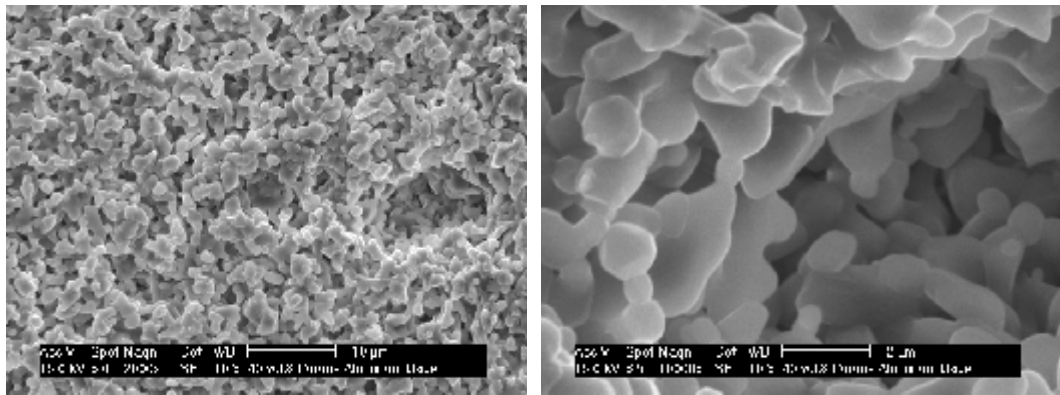


Figure 4.28 SEM pictures of porous aluminum oxides.

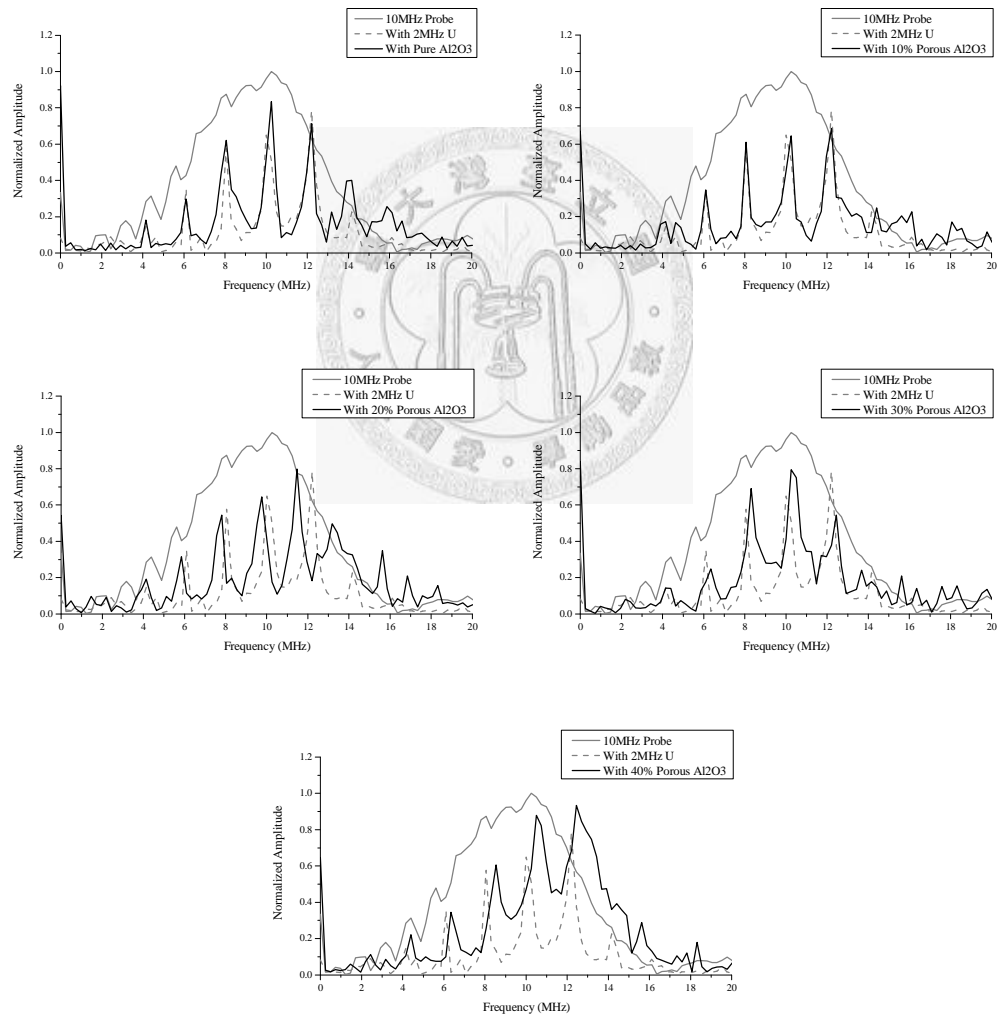


Figure 4.29 Frequency distribution of composites of porous aluminum oxides loaded with epoxy as 2 MHz unpoled PZT.

5. Design of HIFU Transducer

Although commercial HIFU transducers are available, production of a HIFU system is still a daunting challenge. Two issues related to the materials of the HIFU transducer stand out :

1. Selection of a suitable matching layer material with an optimum acoustic impedance and a tolerable attenuation level.
2. A bowl-shape matching layer with a large surface area is hard to produce.

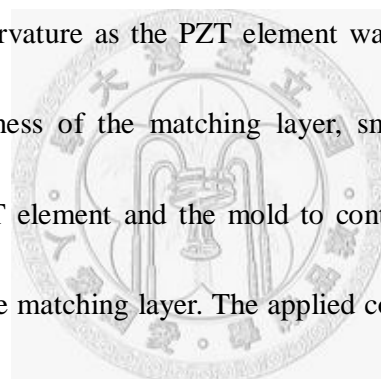
In this study, it is difficult to identify what materials are suitable for acoustic matching purposes in commercial HIFU device. For the home-made HIFU, a ceramic-polymer composite is chosen for the matching layer. Two main advantages of the ceramic-polymer composite are its variable viscosity and adhesive properties. These characteristics ease the integration of the composite onto the bowl-shape piezoelectric element. The manufacture of the home-made HIFU is discussed in Section 5.1. The ZrO₂-epoxy composite is chosen for the matching layer due to its tolerable attenuation and optimum impedance.

The home-made HIFU transducer, shown in Fig. 5.1, is produced to work at 1.5 MHz with a quarter wavelength composite matching layer. The impedance spectrum and phase angle of the transducer are shown in Fig. 5.2.

5.1 Manufacture of a Home-Made HIFU Transducer

The home-made HIFU transducer was designed to resonate at 1.5 MHz and the PZT bowl-shape element with diameter 10 centimeter and curvature radius 20 cm was purchased from FUJI Ceramics Corporation. The HIFU transducer was acoustically matched with a ZrO₂-epoxy composite matching layer and electrically matched with a electronic box made by Broadsound Co., Taiwan.

Preparation of the ZrO₂-epoxy composition is mentioned in Section 3.1 ; A curve-shape mold of identical curvature as the PZT element was used in this case (see Fig. 5.3). To control the thickness of the matching layer, small ZrO₂-epoxy bulks were placed in between the PZT element and the mold to control the available space (i.e., thickness) for the composite matching layer. The applied composite matching layer was cured at room temperature for 24 hr and then aged in the oven at 80°C for 5 hr.



5.2 Characterization of HIFU Transducer Beam Profiles

To characterize the ultrasonic beam profile of a HIFU transducer, such as the axial and lateral pressure distributions, a measuring system was set up under water (see Fig. 5.4). Because of the larger area and thicker thickness of the HIFU transducer, a voltage amplifier (Amplifier Research, Kandel Electronics Inc.) controlled by a function generator (Agilent Technologies) was used as a power source. A power sensor (Bird Electronic Co.) was connected in between the amplifier and the HIFU transducer to

measure the percentages of the transmitted and reflected powers. An accurately tuned electrical matching for the HIFU transducer would greatly increase the transmitted power.

A hydrophone, acted as a wave receiver, was moved incrementally along the axial axis of the HIFU transducer by a step motor to record the axial pressure distribution. The received waves were analyzed by the oscilloscope and the pressure amplitude of each position was averaged over 100 times to minimize the influence of signal noise..

5.3 Characterization with In-vivo Experiment

At the focus point of the HIFU transducer, a great quantity of heat was generated, resulting in a high level of friction between molecules due to thermal vibrations. For the in-vivo experiment, continuous voltage signals were sent to the home-made HIFU transducer from the voltage amplifier. The power sensor monitored the quantity of power transmitted. A bulk of pork was placed at the focal spot of HIFU (see Fig 5.5), and the size and shape of the lesion inside recorded after 80 sec of HIFU treatment at a power of 105 watts. Notice that the pork bulk was sliced into several pieces to aid the observation of the lesion.

5.4 Beam Profiles of HIFU Transducer

The home-made HIFU transducer is driven at 8.7 watts, and the axial and lateral beam profiles are characterized by a hydrophone, shown in Fig 5.6 (a). The point of

maximum amplitude on the axial beam profile is the focal point, and the lateral base on the focal point shown. The amplitudes of the beam profiles are normalized by the amplitude at the focal point.

To determine the focal point size, the amplitude is transformed into logarithm to show the -3 dB points (see Fig 5.6(b)). The distance between two axial -3 dB points is 48 mm, while the two lateral -3 dB points is 2.8 mm.

5.5 In-vivo Experiment on HIFU Transducer

The in-vivo experiment is carried out on the pork bulk to test the performance of the home-made HIFU. The experimental setup is shown in Fig 5.7 and is discussed in Section 5.3. The pork bulk is pre-heated to 37°C to model the temperature of a human body. The HIFU transducer is driven at 105 watts with less than 2% power reflection. The low level of power reflection demonstrates the high efficiencies of the acoustic and electric matching. After the hyperthermia treatment for 80 sec, pork bulk is sliced into several pieces to measure the lesion size, as shown in Fig. 5.8. The length and width of the lesion at the focal point are about 4.7 cm and 1.6 cm, respectively.

The power output of the home-made HIFU is still low compared to the commercial HIFU transducers. This might due to the roughness of the composite matching layer or the undesirable piezoelectric properties of the piezoelectric element. These two factors would enlarge the focal point, and as a result, “dilute” the power at the focal point.



Figure 5.1 The home-made HIFU transducer.

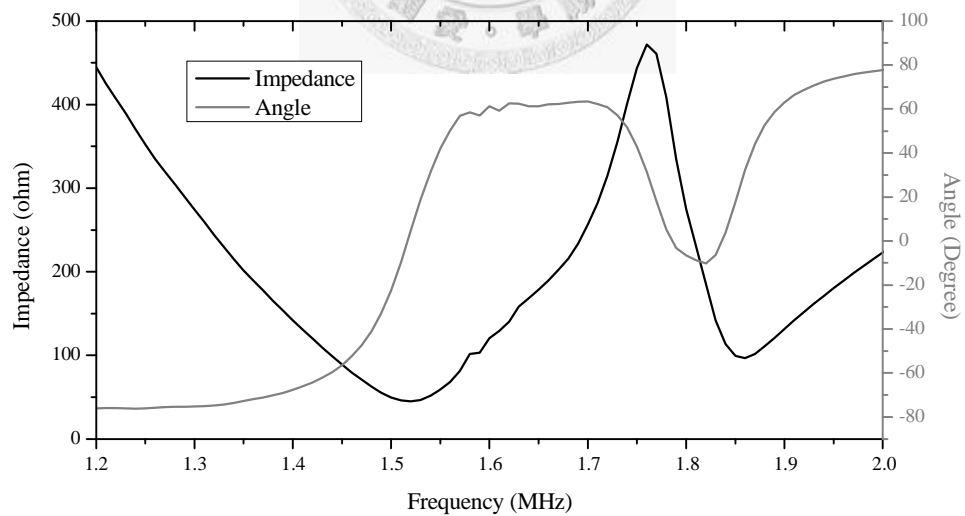


Figure 5.2 Impedance spectrum of the home-made HIFU transducer.

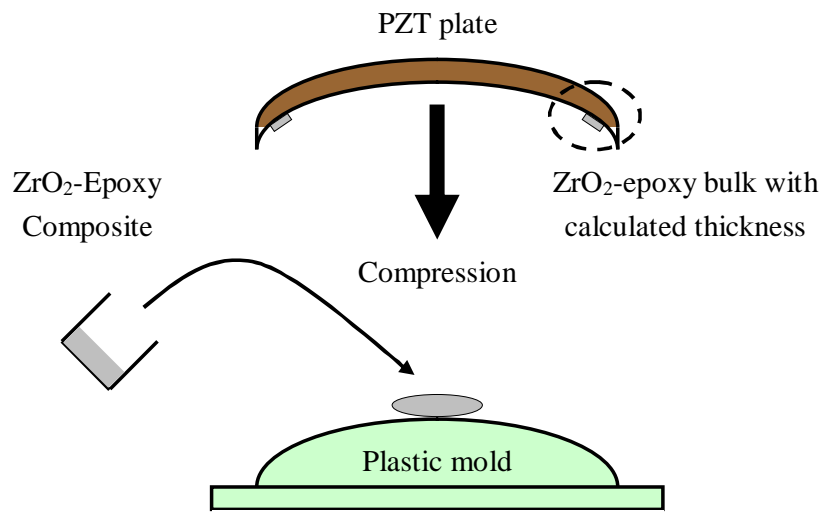


Figure 5.3 Manufacture of acoustic matching layer for the home-made HIFU transducer.

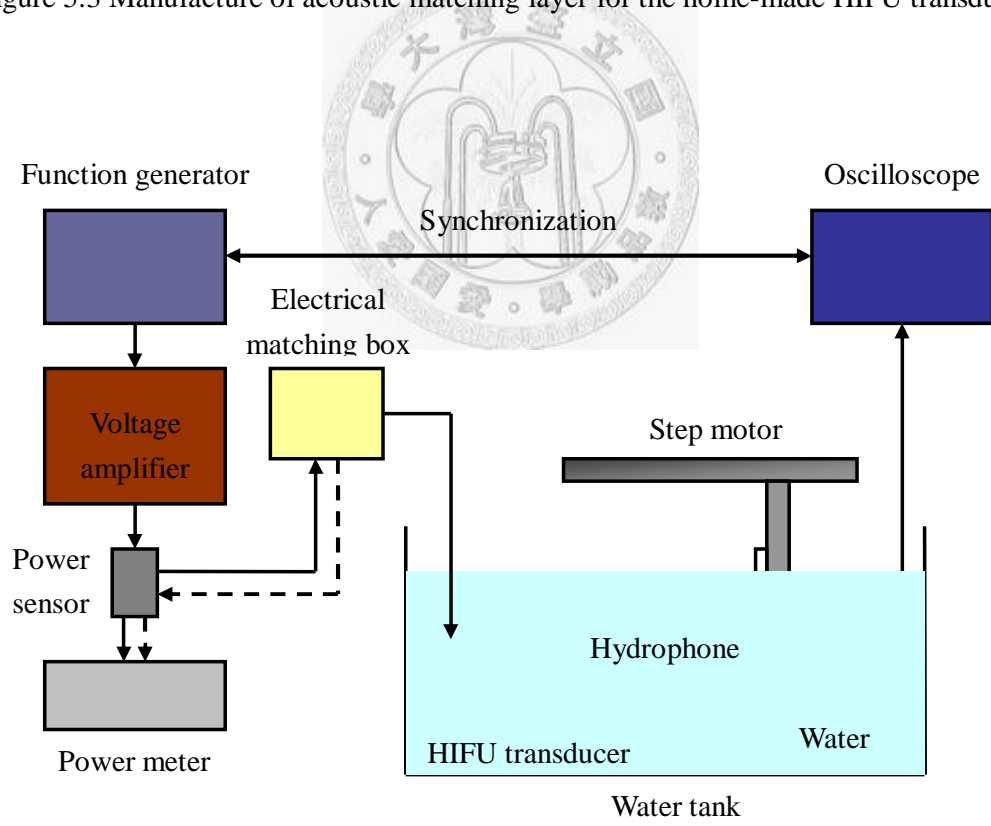


Figure 5.4 Schematic of the beam profile measurement system for the home-made HIFU transducer.

Function generator

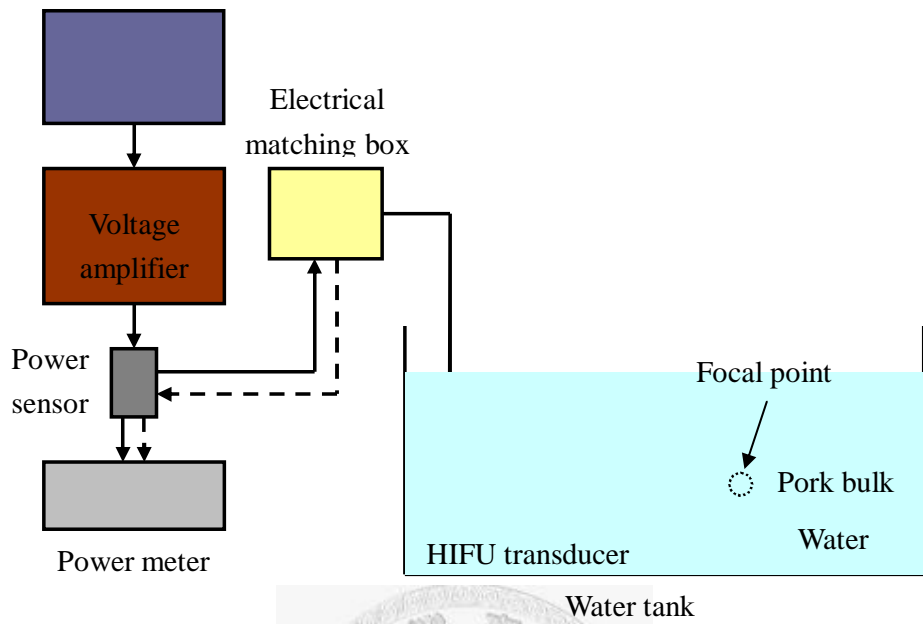
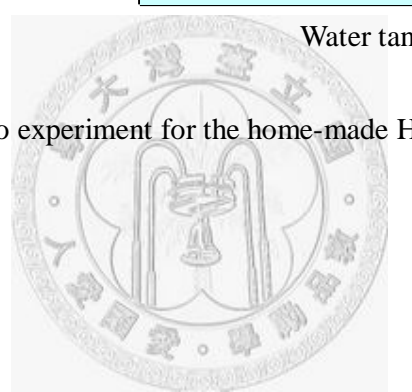


Figure 5.5 In-vivo experiment for the home-made HIFU transducer.



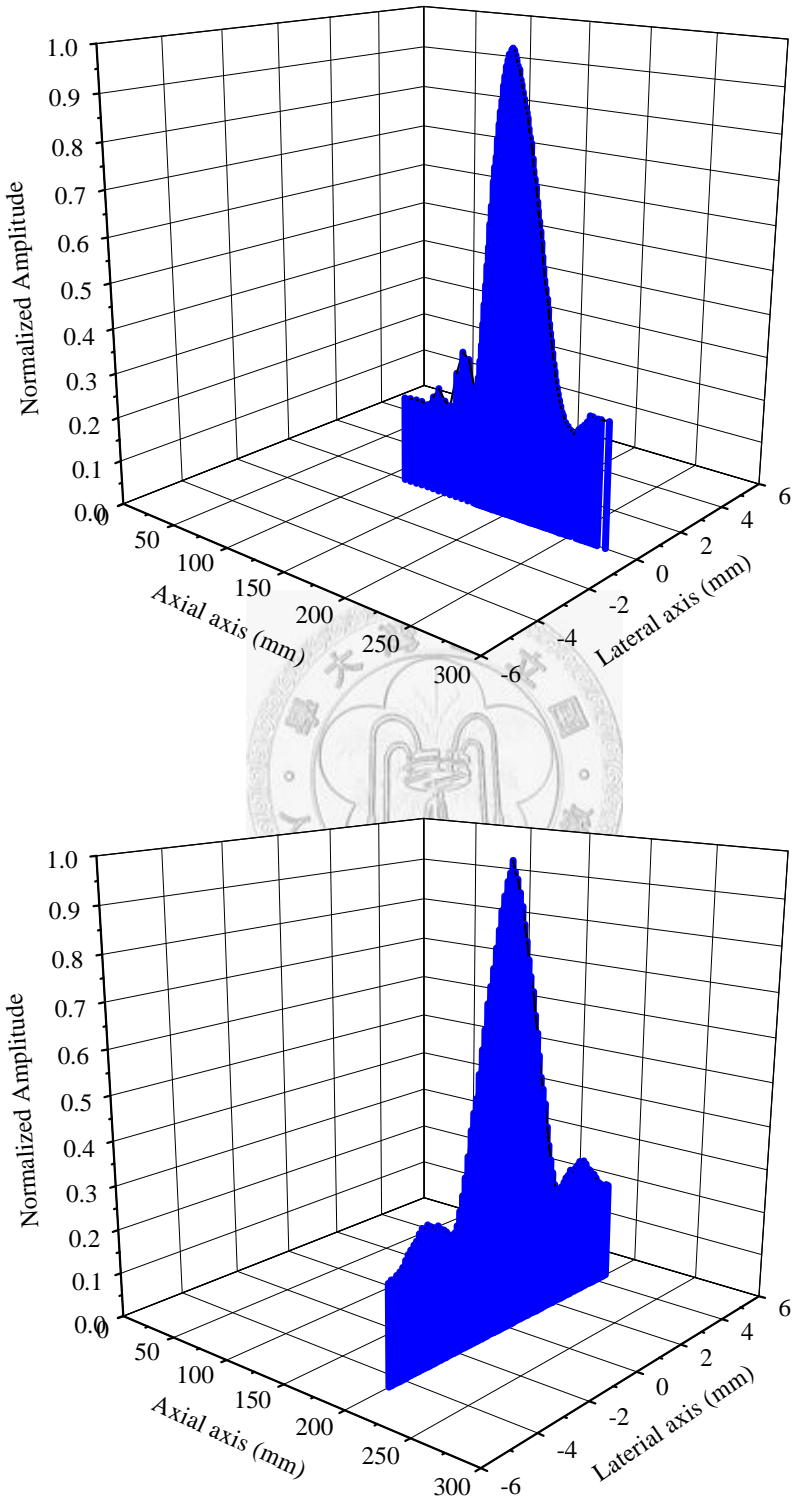


Figure 5.6 (a) Axial and lateral beam profiles of the home-made HIFU transducer.

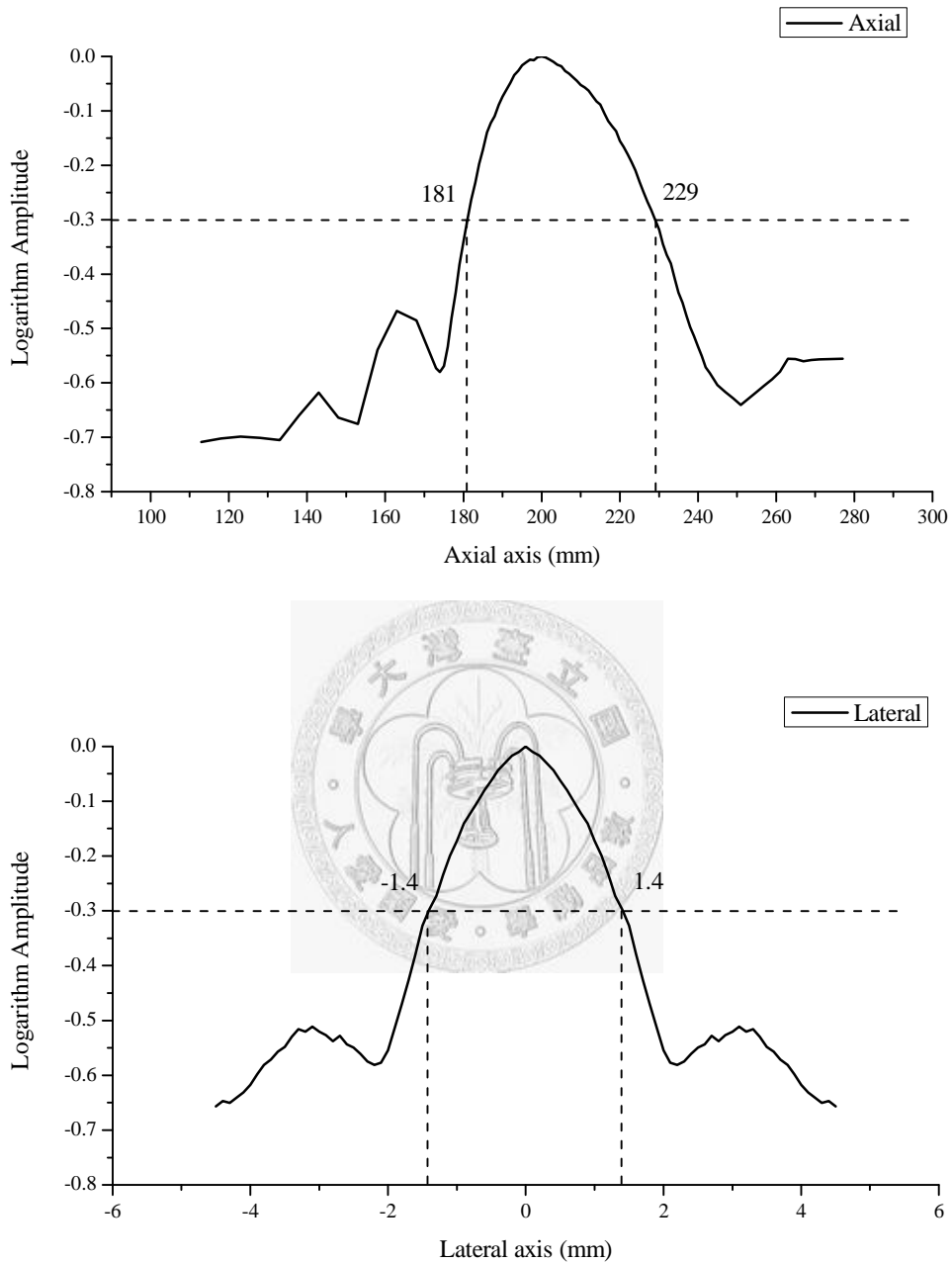


Figure 5.6 (b) Determination of the focal point size of the home-made HIFU transducer.



Figure 5.7 In-vivo experiment setup.

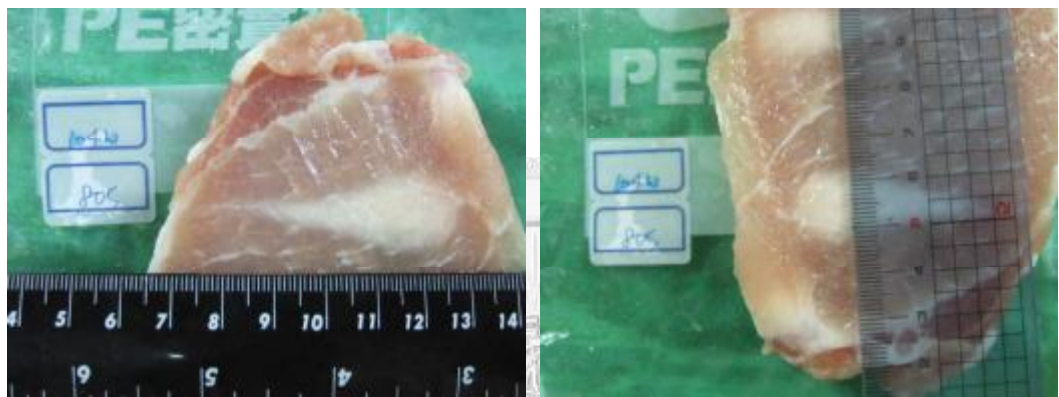


Figure 5.8 The lesion inside the pork bulk after in-vivo experiment.

6. Conclusion

The active PZT matching layers redistribute the frequency spectrums of the commercial ultrasonic transducers and behave like a frequency filter. Instead of bridging the acoustic impedance mismatch, they are designed to manipulate the input frequency distribution. Their filtration behavior is considered as either an electromechanical dominant effect or a mechanical dominant effect. Piezoelectric resonant modes and mechanical quality (Q) govern the electromechanical effect, while dimensions and natural frequencies govern the mechanical effect.

The electroded poled PZT matching layer is designed to filter the frequency spectrum of the ultrasonic transducer. The short-circuited poled PZT layer induces sharper and cleaner frequency peaks, in comparison to those induced by the electroded poled PZT matching layer. The unpoled PZT matching layers with and without the electrodes have the similar behavior as that of the electroded poled PZT matching layers. The electroded poled and short-circuited poled PZT matching layers can increase the amplitude of the frequency distribution when integrated with the second ZrO₂-epoxy composite matching layers. Based on the behaviors of various designs, it is concluded that :

1. For the short-circuited poled PZT plates, the electromechanical effect is dominant.
2. If the thickness mode resonant frequencies of the PZT plates are lower than that of the transducer, the electromechanical effect is dominant.

3. If the thickness mode resonant frequencies of the PZT plates are higher than that of the transducers or if the PZT plates are unpoled, the mechanical effect is dominant.

The frequency filtration behavior of an active PZT matching layer has a significant advantage on the HIFU transducer applications. An acoustic wave of frequency below 1.5 MHz can cause the cavitation effect within a water-based medium (e.g. human tissues). The micro-bubbles generated from the cavitation effect assist the dissipation of acoustic energy, accelerating the generation of heat.

For example, if a 2 MHz broadband HIFU transducer is matched with a 1.3 MHz active PZT matching layer, the broad frequency distribution of the transducer will be filtered into two dominant frequency peaks, located at 1.3 MHz and 2.6 MHz. The 1.3 MHz acoustic wave is then used to generate micro-bubbles within the human tissues while the 2.6 MHz acoustic wave is used to heat up the cells. The heating efficiency of a HIFU transducer is therefore promoted due to the twin-frequency operation. Furthermore, active PZT matchings with short-circuited electrodes and/or additional composite layer designs can be adopted to produce stronger, sharper, and cleaner output frequency peaks.

For acoustic impedance considerations, three different ceramic-epoxy composites are prepared and compared. Among them, ZrO₂-epoxy is the most suitable material with a tolerable attenuation level and an optimum acoustic impedance for bridging the

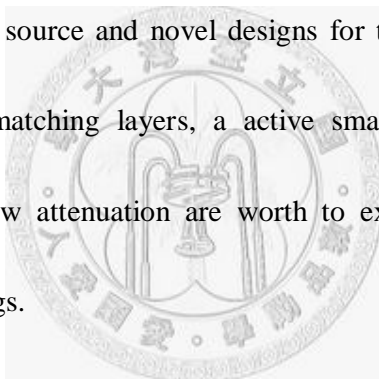
impedance mismatch between the piezoelectric element and water/human tissues.

Furthermore, structured porous aluminum oxides and epoxy-loaded porous aluminum oxides are proposed as matching layers in the multi-layer design.

Finally, a home-made HIFU transducer with a single ZrO₂-epoxy composite matching layer is manufactured. Its performance is examined by an in-vivo experiment.

6.1 Future Research

There are still many challenges in the development of HIFU. New piezoelectric materials for the ultrasonic source and novel designs for the transducer are important topics now. In terms of matching layers, active smart materials with continuous impedance gradient and low attenuation are worth to explore for smart active and passive impedance matchings.



Reference

- [1] D. McKIE, C. McKIE, “Essential of Crystallography,” Blackwell Scientific Publications, 1990.
- [2] G. H. Haertling, “Ferroelectric Ceramics : History and Technology,” Journal of the American Ceramic Society, Vol. 82, No. 4, pp. 797-818, 1999.
- [3] A. J. Moulson, J. M. Herbert, “ Electroceramics,” Second Edition, John Wiley & Sons Ltd, 2003.
- [4] B. Noheda, J. A. Gonzalo, L. E. Cross, R. Guo, S. E. Park, E. D. Cox, G. Shirane, “Tetragonal-to-Monoclinic Phase Transition in a Ferroelectric Perovskite : The Structure of $\text{PbZr}_{0.52}\text{Ti}_{0.48}\text{O}_3$,” Physical Review B, Vol. 61, No. 13, pp.8687-8695, 2000.
- [5]Y. Xu, “Ferroelectric Materials and Their Application,” North-Holland Publishing Co, 1991.
- [6] Y. M. Chiang, B. P. Birnie, III, W. D. Kingery, “Physical Ceramics : Principles for Ceramic Science and Engineering,” John Wiley & Sons Inc, 1997.
- [7] B. Jaffe, W. R. Cook Jr., H. Jaffe, “Piezoelectric Ceramics,” Academic Press, New York, 1971.
- [8] J. F. Nye, “Physical Properties of Crystals : Their Representation by Tensors and Matrices,” Oxford University Press, 1985.
- [9] T. L. Jordan, Z. Qunaias, “Piezoelectric Ceramics Characterization,” ICASE, NASA

Langley Research Center, 2001.

- [10] W. R. Hedrick, D. L. Hykes, D. E. Starchman, "Ultrasound Physics and Instrumentation—3rd edition," Mosby, 1992.
- [11] D. Royer, E. Dieulesaint, "Elastic Waves in Solid," Springer, 2000
- [12] L. E. Kinsler, A. R. Frey, A. B. Coppens, J. V. Sanders, "Fundamentals of Acoustics, 3rd Ed," John Wiley, New York, 1982.
- [13] T. E. Gomez Alvarez-Arenas, "Acoustic Impedance Matching of Piezoelectric Transducers to the Air," IEEE Transactions on Ultrasonics, Ferroelectrics, and Frequency Control, Vol. 51, No. 5, pp. 624-633, 2004.
- [14] S. Temkin, "Elements of Acoustics," Wiley, New York, 1981
- [15] M. N. Jackson, " Simulation and Control of Thickness Mode Piezoelectric Transducers," Ph. D. Dissertation, University of Strathclyde, Glasgow, Scotland, 1984.
- [16] C. S. Desilets, J. D. Fraser, G. S. Kino, " The Design of Efficient Broad-Band Piezoelectric Transducers," IEEE Transactions on Sonics and Ultrasonics, Vol. 25, pp. 633, 2004.
- [17] G. Hayward, J Hossack, "Unidimensional Modeling of 1-3 Composite Transducer," Journal of the Acoustical Society of America, Vol.88, No.2, pp. 618-629, 1990.
- [18] H. W. Persson, C. H. Hertz, "Acoustic Impedance Matching of Medical Ultrasonic Transducers," Utrasonics, Vol. 23, pp. 83-89, 1985.

- [19] Q. Zhou, J. M. Cannata, H. Guo, C. Huang, V. Z. Marmarelis, K. K. Shung, "Half-Thickness Inversion Layer High-Frequency ultrasonic Transducers Using LiNbO₃ Single Crystal," IEEE Transactions on Ultrasonics, Ferroelectrics, and Frequency Control, Vol. 52, No. 1, pp. 127-133, 2005.
- [20] K. K. Shung, M. Zippardo, "Ultrasonic Transducers and arrays," IEEE Engineering in Medicine and Biology, vol. 15, no. 6, pp. 20-30, 1996.
- [21] S. Thiagarajan, I. Jayawyrdena, R. W. Martin, "Design of 20 MHz Wideband Piezoelectric Transducer for Close-Proximity Imaging," Biomedical Sciences Instrumentation, Vol. 27, pp. 57, 1991.
- [22] A. R. Selfridge, "Approximate Material Properties in Isotropic Materials," IEEE Transactions on Sonics and Ultrasonics, Vol. 32, pp. 381, 1985.
- [23] T. R. Gururaja, "Piezoelectric Composite Materials for Ultrasonic Transducer Applications. Part I : Resonant Modes of Vibration of PZT Rod-Polymer Composites," IEEE Transactions on Sonics and Ultrasonics, Vol. 32, pp. 481, 1985.
- [24] T. Yano, M. Tone, A. Fukumoto, "Range Finding and Surface Characterization Using High-Frequency Air Transducers," IEEE Transactions on Ultrasonics, Ferroelectrics, and Frequency Control, Vol. 34, No. 2, pp. 232-236, 1987.
- [25] G. Hayward, A. Gachagan, "An Evaluation of 1-3 Connectivity Composite Transducers for Air-Coupled Ultrasonic Applications," Journal of the Acoustical Society

of America, Vol.99, No.4, pp. 2148-2157, 1996.

[26] S. P. Kelly, T. E. Gomez, G. Hayward, "Characterization and Assessment of An Integrated Matching Layer for Air-Coupled Ultrasonic Applications," IEEE Transactions on Ultrasonics, Ferroelectrics, and Frequency Control, Vol. 52, No. 10, pp. 1314-1323, 2004.

[27] E. Yogeswaren, "Matching Layer Assembly for a Downhole Acoustic Sensor," United State Patent, No. 7075215.

[28] K. Hashimoto, T Hashida, M. Suzuki, M. Hashimoto, H. Nagahara, S. Shiraishi, N. Takahara, "Acoustic Matching Layer and Ultrasonic Transducer," United State Patent, No. 6969943.

[29] H. Wang, W. Cao, Q. F. Zhou, K. K. Shung, Y. H. Hung, "Silicon Oxide Colloidal/Polymer Nanocomposite Films," Applied Physics Letters, Vol. 85, No. 24, pp. 5998-6000, 2004.

[30] W. Roy, D. Mark, H. Andrew, "Apparatus and Method for Producing High Intensity Focused Ultrasonic Energy for Medical Applications," United State Patent, No. 6500133.

[31] R. Geoffrey, E. Christine, "Ultrasound Transducer Array," United State Patent, No. 6974417.

[32] S. Ulrich, S. Todor, L. Riengard, "Ultrasound Transducer for Diagnostic and

Therapeutic Use," United State Patent, No. 5823962.

[33] Y. Yamashita, Y. Hosono, K. Itsumi, "effects of Metal Particle Dopant on Acoustic Attenuation Properties of Silicon Rubber Lens Medical Echo Array Probe," Japanese Journal of Applied Physics, Vol.44, No. 6B, pp. 4558-4560, 2005.

[34] M. Ahmed, S. N. Goldberd, "Thermal Ablation for Hepatocellular Carcinoma," Journal of Vascular and Interventional Radiology, Vol. 13, pp. 231-244, 2002.

[35] H. W. Head, G. D. Dodd III, "Thermal Ablation for Hepatocellular Carcinoma," Gastroenterology, Vol. 127, pp. 167-178, 2004.

[36] W. Y. Lau, T. W. Leung, S. C. Yu, S. K. Ho, "Percutaneous Local Ablative Therapy for Hepatocellular Carcinoma : A Review and Look into the Future," Annals of Surgery, Vol. 237, pp. 171-179, 2003.

[37] J. E. Kennedy, F. Wu, G. R. ter Haar, F. V. Glesson, R. R. Philips, M. R. Middleton, D. Cranston, "High-Intensity Focused Ultrasound for the Treatment of Liver Tumors," Ultrasonics, Vol. 42, pp. 931-935, 2004.

[38] N. T. Saghvi, R. S. Foster, R. Bahrle, R. Casey, T. Uchida, M. H. Phillips, J. Syrus, A. V. Zaitsev, K. W. Marich, F. J. Fry, "Noninvasive Surgery of Prostate Tissue by High Intensity Focused Ultrasound : An Updated Report," European Journal of Ultrasound, Vol. 9, pp. 19-29, 1999.

[39] J. Y. Chapelon, M. Ribault, A. Birer, F. Vernier, R. Souchon, A. Gelet, "Treatment

of Localised Prostate Cancer with Transrectal High Intensity Focused Ultrasound,”

European Journal of Ultrasound, Vol. 9, pp. 31-38, 1999.

[40] W. S. Chen, C. C. Wu, H. Y. Fang, H. L. Liu, “Differences in the lesion formation process between focused ultrasound and microwave ablations,” Medical Phisics, vol. 33, no. 5, pp. 1346-1351, 2006.

[41] J. Kubota, T. Azuma, K. Ishida, M. Motoyama, Y. Sato, K. Sasaki, K. I. Kawabata, N. T. Sanghvi, S. I. Umemura, “Effect of Matching Layer on Acoustic Lens on Suppressing Lamb Wave Formation,” IEEE Ultrasonics Symposium, pp. 1044-1047, 2003.

[42] C. J. Diederich, K. Hyynyne, “Ultrasound Technology for Hyperthermia,” Ultrasound in Medicine and Biology, Vol. 25, No. 6, pp. 871-887, 1999.

[43] W. C. Young, “Roark's formulas for stress and strain,” McGraw-Hill, New York, 1989.